ADA022146

ACTIVE SHIMMY CONTROL SYSTEM

LOCKHEED-CALIFORNIA COMPANY
BURBANK, CALIFORNIA

D D C

MAR 29 1976

C

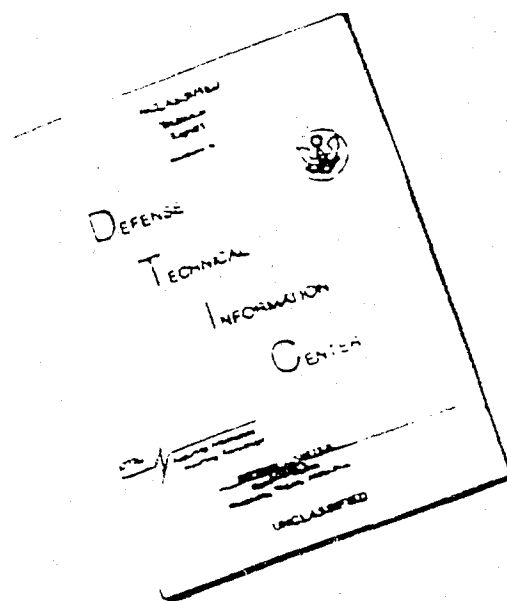DECEMBER 1975

AIR FORCE FLIGHT DYNAMICS LABORATORY
AIR FORCE WRIGHT AERONAUTICAL LABORATORIES
Air Force Systems Command
Wright-Patterson Air Force Base, Ohio 45433

DISCLAIMER NOTICE

THIS DOCUMENT IS BEST QUALITY AVAILABLE. THE COPY FURNISHED TO DTIC CONTAINED A SIGNIFICANT NUMBER OF PAGES WHICH DO NOT REPRODUCE LEGIBLY.

HOWELL K. BREWER
Actg Chief, Mechanical Branch
Vehicle Equipment Division
Air Force Flight Dynamics Laboratory

PETERS SKELE
Project Engineer
Vehicle Equipment Division
Air Force Flight Dynamics Laboratory

REPORT DOCUMENTATION PAGE		READ INSTRUCTIONS BEFORE COMPLETING FORM
1. REPORT NUMBER AFFDL-TR-75-136	2. GOVT ACCESSION NO.	3. RECIPIENT'S CATALOG NUMBER
4. TITLE (and Subtitle) ACTIVE SHIMMY CONTROL SYSTEM.		5. TYPE OF REPORT & PERIOD COVERED Final Oct 1974 — Dec 1975
		6. PERFORMING ORG. REPORT NUMBER
7. AUTHOR(s) Max Gamon, Tom Mahone		8. CONTRACT OR GRANT NUMBER(s) F33615-75-C-3005
9. PERFORMING ORGANIZATION NAME AND ADDRESS Lockheed-California Company Burbank, Ca 91503		10. PROGRAM ELEMENT, PROJECT, TASK AREA & WORK UNIT NUMBERS PE 62201F WU AFFDL-1369-01-48
11. CONTROLLING OFFICE NAME AND ADDRESS AFFDL/FEM Mechanical Branch, Vehicle Equipment Division Air Force Flight Dynamics Laboratory Wright-Patterson AFB, Ohio 45433		12. REPORT DATE Dec 75
		13. NUMBER OF PAGES
14. MONITORING AGENCY NAME & ADDRESS(if different from Controlling Office)		15. SECURITY CLASS. (of this report) UNCLASSIFIED
		15a. DECLASSIFICATION/DOWNGRADING SCHEDULE

16. DISTRIBUTION STATEMENT (of this Report)

APPROVED FOR PUBLIC RELEASE; DISTRIBUTION UNLIMITED

17. DISTRIBUTION STATEMENT (of the abstract entered in Block 20, if different from Report)

18. SUPPLEMENTARY NOTES

19. KEY WORDS (Continue on reverse side if necessary and identify by block number)

Shimmy, Shimmy Control, Anti-shimmy System, Active Control System

20. ABSTRACT (Continue on reverse side if necessary and identify by block number)

A T-37 nose gear is modeled as a multiple lumped mass system with four torsional-degrees-of-freedom and one lateral-degree-of-freedom. Fuselage flexibility is incorporated and a Von Schlippe tire model is used. The equations of motion for various input conditions are solved using measured gear properties.

An Active Shimmy Control System is incorporated in the analytical model.

DD FORM 1473 1 JAN 73 EDITION OF 1 NOV 65 IS OBSOLETE

209 970

A feedback signal proportional to angular velocity is used to control the hydraulic actuator pressure. The equations of motion for the gear with active control are solved for the same inputs as for the passive gear and their responses are compared.

System parameter values were varied about the nominal measured values to determine their effects for both active and passive systems.

A breadboard Active Shimmy Control System was built based on the model results. A test program was performed establishing regions of shimmy for the passive gear. The same conditions were repeated with the active system. Substantial improvement was seen.

A comparision with the theoretical predictions showed good correlation.

PREFACE

This report was prepared by the Lockheed-California Company, Burbank, Calif. under U.S. Air Force Contract F33615-75-C-3005, Project 1369, "Mechanical Subsystems for Advanced Military Flight Vehicles", Task No. 01. The work was administered by the Air Force Flight Dynamics Laboratory, Wright-Patterson AFB. The technical monitors were Lt. Joe Mercer and Peters Skele of AFFDL/FEM.

The Lockheed-California Company Project Leader was Paul Durup. The Principal Investigator was Max Gamon. Development of the active control system design was done by Tom Mahone, with the support of Bob Styerwalt and J.R. Potts. This report covers work performed from October 1974 to December 1975.

TABLE OF CONTENTS

LIST OF ILLUSTRATIONS

LIST OF ILLUSTRATIONS (Cont'd)

LIST OF ILLUSTRATIONS (Cont'd)

LIST OF ILLUSTRATIONS   (Concluded)

LIST OF TABLES

INTRODUCTION

The methods used to determine the shimmy characteristics for a landing gear
in the design stage of an airplane can vary from a simple rigid tire repre-
sentation to a detailed nonlinear representation including variations in tire
characteristics as a function of fluid pressure, and variation in strut
friction as a function of gear load and strut stroking velocity. Testing
varies from running over a two by four placed on the runway for the purpose
of exciting the nose gear in a shimmy mode to dynamomenter testing using a
feedback control oscillatory drive system to excite the gear at various
controlled torsional frequencies and amplitudes. The latter test technique
provides data for determining shimmy margins under test conditions used to
simulate gear degradation with age. There are various analytical and test
techniques whose capabilities lie between the aforementioned extremes.

Even though gears have performed satisfactorily early in their service life,
some have become chronic shimmiers as they age. This change is usually
attributed to wear in the gear which causes an increase in backlash. Inas-
much as most shimmy evaluation techniques do not provide a means of assess-
ing margins, and adequate estimates of the degradation of gear parameters
affecting shimmy may not be made, a clear understanding of the susceptibil-
ity of gears to shimmy is not established.

Therefore, the performance of an ideal shimmy suppression system should not
be affected by the gear aging process. Some of the parameters that can
change during operation from the values originally expected include:

o Backlash increase from wear of torque arm attachments,
   trunnions, steering collar, and steering actuator linkages.

o Increase in damper fluid air entrapment.

1

o Reduction in strut bearing friction caused by reduced nose gear load attributed to an aft shift in operational center-of-gravity position.

o Change in tire stiffness characteristics to accommodate airplane growth and/or changes in the operational center-of-gravity position.

Unless adequate allowance is made for these parameter changes, which may not be practical in the development of a passive damper, eventually shimmy may occur.

The nature of active control systems is such that they may be independent of some of the aforementioned parameter changes and it may be practical to provide means of adjusting the system to accommodate the more permanent parameter changes. Accordingly, while an active antishimmy system may yield a more complex gear, the potential for providing shimmy free operations throughout the lifetime of the airplane makes development and evaluation of such a system quite attractive.

In order to assess the practicality and performance potential of active shimmy control, the present research program was initiated. The objective of this program is to develop a breadboard version of an active shimmy control system for the T-37 nose gear. This particular gear was chosen because of its long history of shimmy problems in service. The program is conducted in four phases. Phase I consists of obtaining a T-37 nose gear from the Air Force Flight Dynamics Laboratory (AFFDL) and measuring certain gear characteristics pertinent to shimmy behavior. During Phase II, an analytical model of an active shimmy control system is developed, and analyses are performed to determine a specific control scheme. In Phase III, a breadboard version of the control system is designed and built. The landing gear is also instrumented for shimmy testing. During Phase IV, the active shimmy control system is tested on the 192 inch dynamomenter at AFFDL's Landing Gear Test Facility.

ANALYTICAL MODEL DESCRIPTION

General

Both the passive and active nose gear shimmy models are incorporated into
one Continuous System Modeling Program (CSMP) digital computer program
utilizing computer graphics display and interactive operation. The T-37
nose landing gear is modeled as a multiple lumped mass system with four
torsional degrees of freedom (about the strut axis) and one lateral degree
of freedom with a Von Schlippe tire model (Reference 1). The active
shimmy control system utilizes axle torsional acceleration feedback signals
to control the steering actuator displacement. Figure 1 shows a
drawing of the T-37 nose gear with the essential mechanical elements identi-
fied. When the axle rotates about the strut axis, the wheel fork transmits
this motion via the torque arms to the bottom of the outer cylinder. The
outer cylinder rotates inside the trunnion yoke, which attaches to the air-
plane at the trunnions. The top of the outer cylinder is attached to the
steering actuator housing (cylinder) while the steering actuator piston is
attached to the trunnion yoke.

Torsional Degrees of Freedom

The analytical model for the torsional degrees of freedom is shown in
Figure 2. The unsprung mass ITH is connected to the ground via the tire
(described later) and is connected to the outer cylinder ITH1 through the
torque arms of stiffness KTH with backlash DTH. Piston-outer cylinder
friction CP damps motion across the torque arm backlash DTH and stiffness KTH.
The outer cylinder ITH1 is connected to the actuator housing IAL with spring KOC,
representing the stiffness of the outer cylinder, in series with backlash
DAL, representing the deadband at the actuator housing to outer cylinder con-
nection. Friction CF is the friction between the outer cylinder and the
trunnion yoke in which it rotates. The trunnion yoke is connected to the
fuselage. ITH2 represents local fuselage structure which is connected to
the "rigid" airplane through the fuselage stiffness KF. BF is a linear
damper representing fuselage structural damping.

3

Steering Actuator

Trunnion

Outer Cylinder

Piston

Trunnion Yoke

Torque Arms

Wheel Fork

Axle
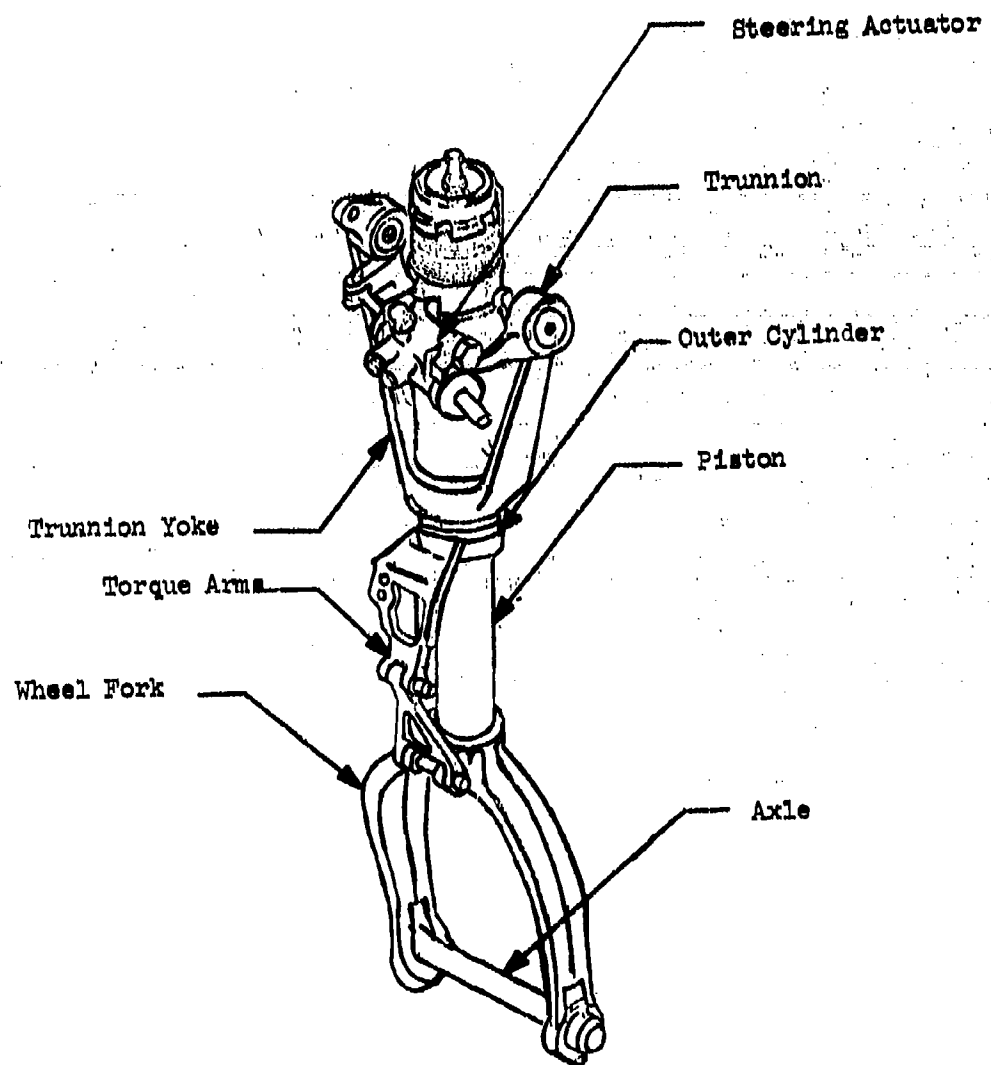
FIGURE 1 - T-37 NOSE LANDING GEAR

4
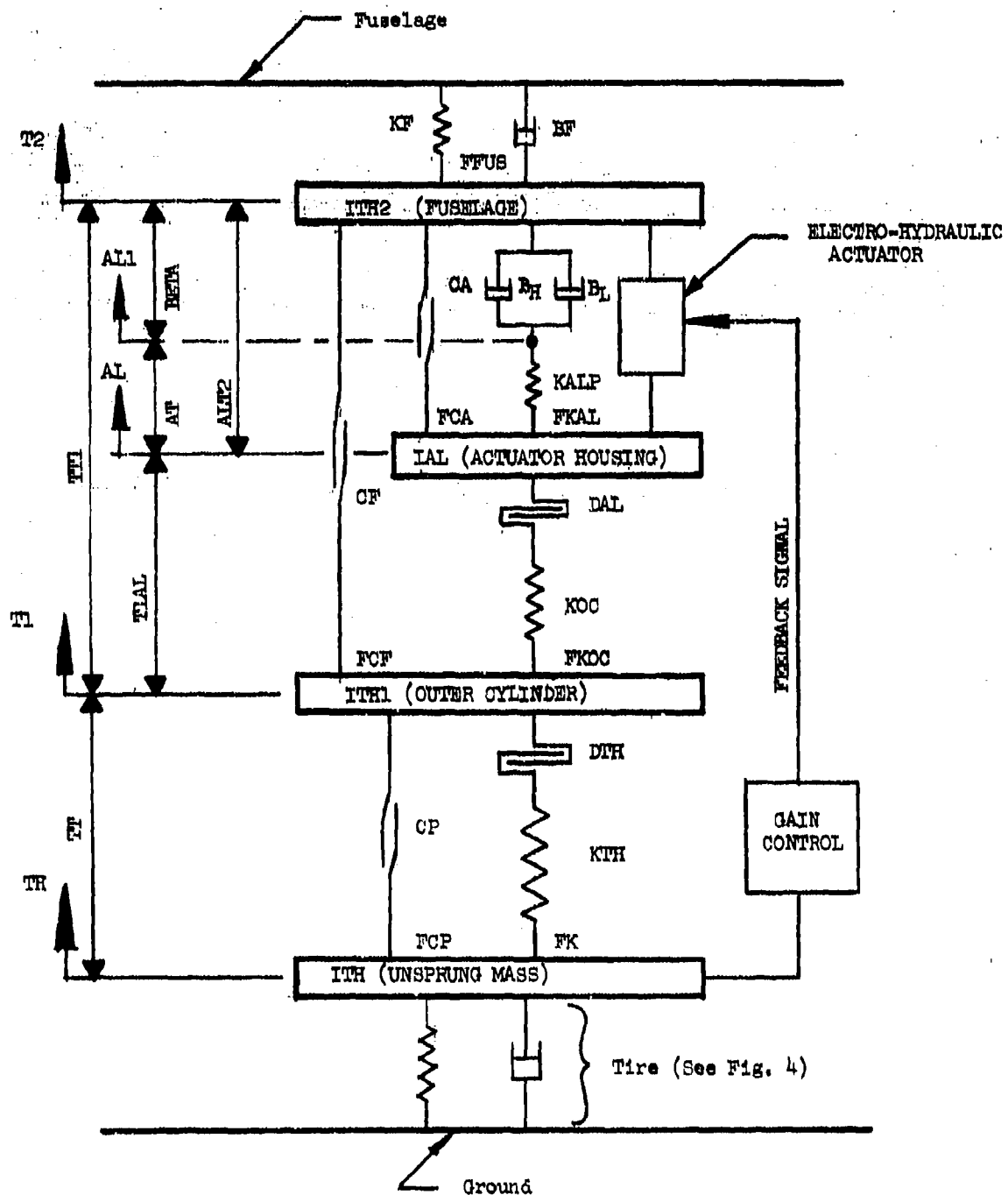
FIGURE 2 - TORSIONAL RESPONSE MODEL

CA is the steering actuator friction. BH, BL and KALP, shown in Figure 2, are used only for the passive system. BH and BL are hydraulic (velocity squared) and linear shimmy damper constants, and KALP is the stiffness of the hydraulic fluid column in the actuator. For the active system, the force generated in the steering actuator is computed from a detailed servo-valve/actuator model shown only as a box in Figure 2. In the active model, the feedback signal, after passing through a gain control circuit, is sent to the actuator which generates the steering actuator force FKAL. The active system controls the actuator displacement ALT2 shown in Figure 2.

Lateral Degree of Freedom

The analytical model for the lateral degree of freedom is shown in Figure 3. Laterally, the gear is assumed to be a rigid "pendulum" rotating about a fore-aft axis located H inches above the axle centerline. This lateral rotation is resisted by a linear torsional spring KPH, representing combined gear lateral flexibility and local fuselage flexibility. Acting in parallel with KPH is a linear damper BPH representing the structural damping in the gear and local fuselage structure. The torsional backlash DPH is in series with the spring and damper and depicts rotational deadband from the lateral piston-cylinder, cylinder-trunnion yoke, and trunnion-fuselage joints. The landing gear's lateral rotational inertia is IPH.

The axle centerline is located aft of the strut centerline by the mechanical trail L. If the strut is inclined (forward at the bottom), then the tire forces at the ground contact points are located aft of the axle center-line by the geometric trail LG. The geometric trail is related to the rolling radius R and the strut inclination angle β by the relation

$$LG = R \sin \beta \tag{1}$$

Also shown in Figure 3 are the positive sign conventions (right hand rule for rotations) for axle torsional rotation TH, gear lateral rotation PH,

KPH

TORSIONAL SPRING

IPH

PH

BPH

DPH

TORSIONAL BACKLASH
FOR PH ROTATIONS

TORSIONAL DAMPER

FK

FCP

H

L

TH

R

(FORWARD)

V

FT

LG

GROUND

MF
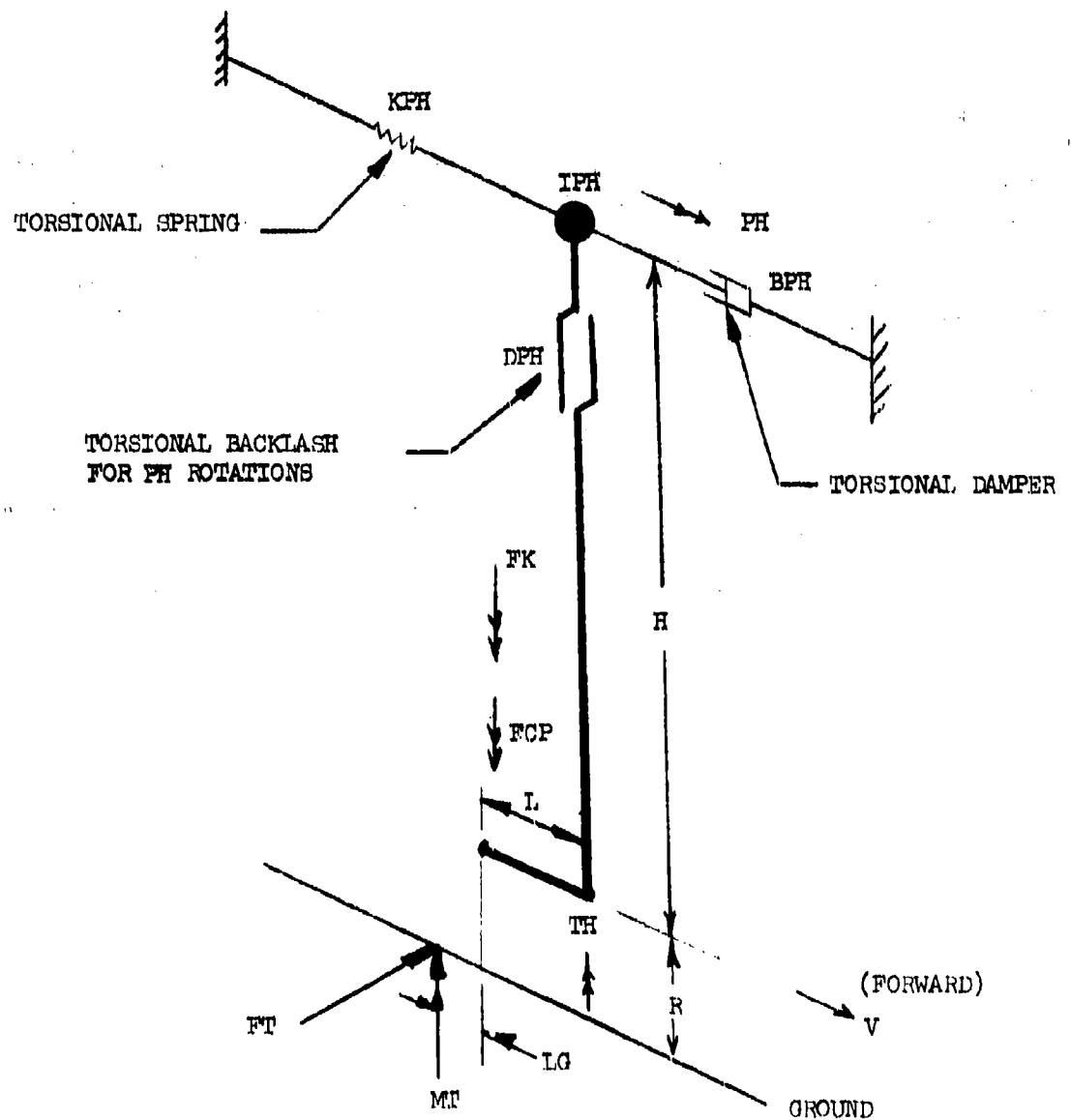
FIGURE 3 - LATERAL MODE MODEL

7

tire force and moment FT and MT, gear moments FK and FCP and airplane forward velocity V. Gyroscopic and inertia coupling terms between the lateral and torsional modes through L are included in the model. The coupled dynamic equations of motion for the lateral and torsional degrees-of-freedom are shown below. In each equation, the second term represents inertia coupling and the third term represents gyroscopic coupling.

$$IPH \, (PHDD) - M \, (L)(H) \, (THDD) - I \, \frac{V}{R} \, THD + L \, \{FZ - M(G)\} \, TH + BPH \, (PHD) + KPH(PH)$$
$$+ \{W(H) - (H+R) \, FZ\} \, PH = (H+R) \, FT \qquad (2)*$$
$$ITH \, (THDD) - M(L)(H) \, (PHDD) + I \, \frac{V}{R} \, PHD + L(FT) - MT + FCP + FK = 0 \qquad (3)*$$

Tire Model

The tire lateral force and moment are calculated according to a dynamic model developed by Von Schlippe (Reference 1). This employs the "stretched string" representation for the tire equator, which takes on the deflected shape shown in Figure 4. Figure 4 shows a view looking down on the tire contact patch, with forward airplane motion to the right. Z and $\bar{Z}$ are the tire equator lateral deflections at the forward and aft ends of the contact patch. Referring to Figure 4, the tire force and moment are given simply by

$$FT = KT \, (Z + \bar{Z}) \qquad (4)$$
$$MT = KM \, (Z - \bar{Z}) \qquad (5)$$
$$\text{where} \quad KT = \frac{K \text{ lateral}}{2} \qquad (6)$$
$$\text{and} \quad KM = \frac{K \text{ torsional}}{2 \, (HS)} \qquad (7)$$

K lateral and K torsional are the lateral and torsional tire stiffnesses, while KT and KM are the corresponding input parameters to the computer program. For this study, K lateral and K torsional are determined by using empirical equations from Reference (2).

The tire deflections Z and $\bar{Z}$ are determined from the tire equator coordinates Y and $\bar{Y}$ and the location of the wheel center plane in terms of gear motions PH and TH. The following equations for Z and $\bar{Z}$ can be derived by inspection of Figure 4.

$$Z = Y - (HS - L - LG) \, TH - (H + R) \, PH \qquad (8)$$
$$\bar{Z} = \bar{Y} + (HS + L + LG) \, TH - (H + R) \, PH \qquad (9)$$

$$* \, PHD = \frac{d}{dt}(PH), \quad PHDD = \frac{d}{dt}(PHD), \quad THD = \frac{d}{dt}(TH), \quad THDD = \frac{d}{dt}(THD)$$

8
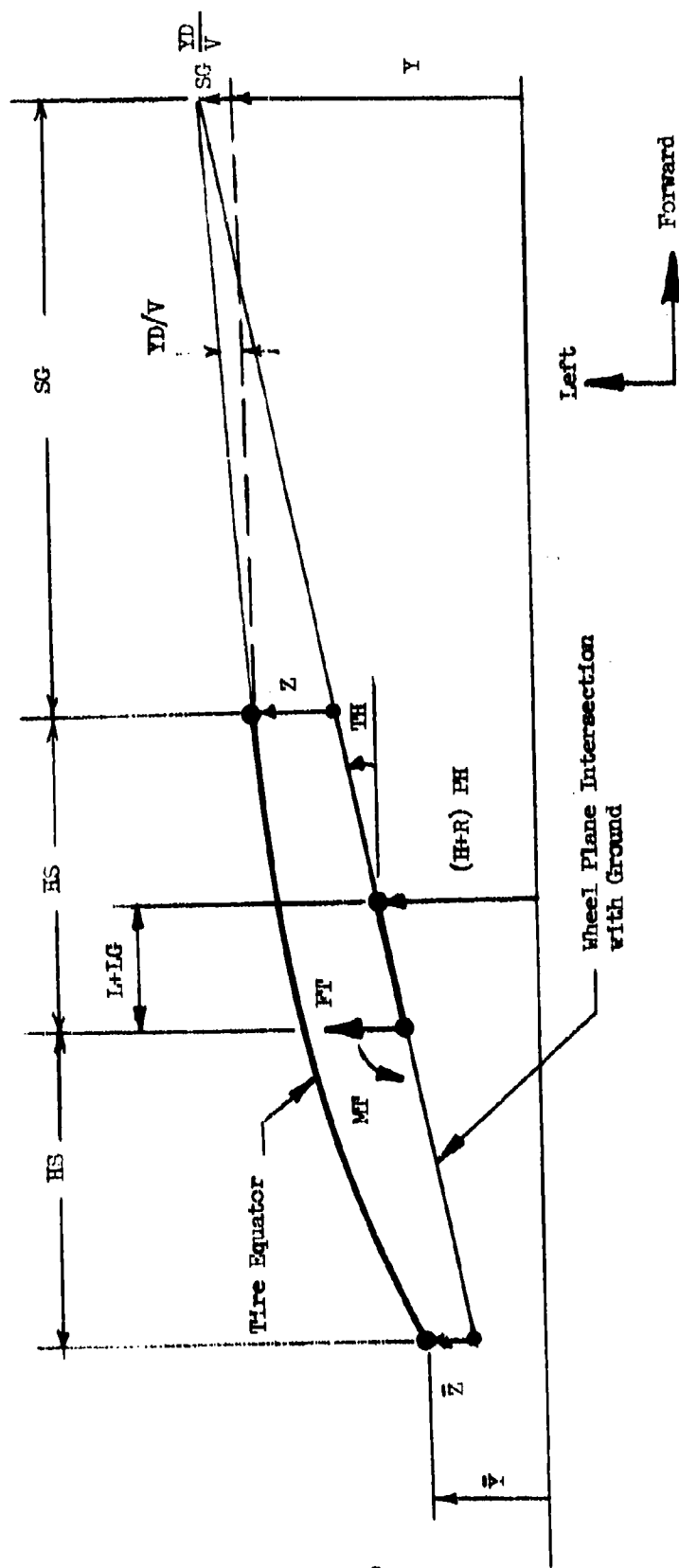
FIGURE 4 - TIRE MODEL

9

The Von Schlippe tire theory (Reference (1)) develops the kinematic constraint equations for Y and $\bar{Y}$. The details are not presented here; however, the resulting differential equations governing Y and $\bar{Y}$ are

$$(SG)\ \frac{YD}{V}\ +\ Y\ =\ (SG + HS-L-LG)\ TH + (H + R)\ PH \qquad (10)$$

and $\qquad \bar{Y}\ (t)\ =\ Y\ (t - \frac{2\ HS}{V}) \qquad\qquad\qquad (11)$

YD is the time derivative of Y. Equations (10) and (11) provide the tire model with its dynamic properties, i.e., the effective tire stiffness and damping vary with velocity and shimmy frequency. The yawed rolling relaxation length SG and half-footprint length HS are determined empirically from Reference (2).

Active System Model

The active shimmy control system for the T-37 nose gear consists of the following major elements:

(1) An electro-hydraulic servovalve attached to the existing steering cylinder

(2) A torsional accelerometer mounted on the wheel fork to measure axle torsional acceleration

(3) An electronic signal shaping and gain control network to convert the accelerometer output into the desired feedback signal for the servovalve.

Figure 5 shows a schematic diagram of the T-37 steering actuator. The servovalve for the active system is connected to the existing steering actuator through a coupling manifold which connects directly to existing ports in the steering cylinder. Figure 5 shows where the coupling manifold connects to the steering cylinder. For the purposes of breadboard system testing, the passive damping orifices are plugged and the existing spool valve is fixed relative to the actuator housing. Nose gear steering

10

INLET

POWER-ON
DAMPING ORIFICE
(DIA = .024 IN)

TO COMPENSATOR
& RETURN

STEERING INPUT
FIXED TO
HOUSING

POWER-OFF
DAMPING ORIFICES
(DIA = .084 IN)

SPOOL VALVE
CENTERING
SPRINGS

$A_{OIL} = 1.081 \text{ IN}^2$

Existing Damping
Orifices Blocked

Connection to Servovalve
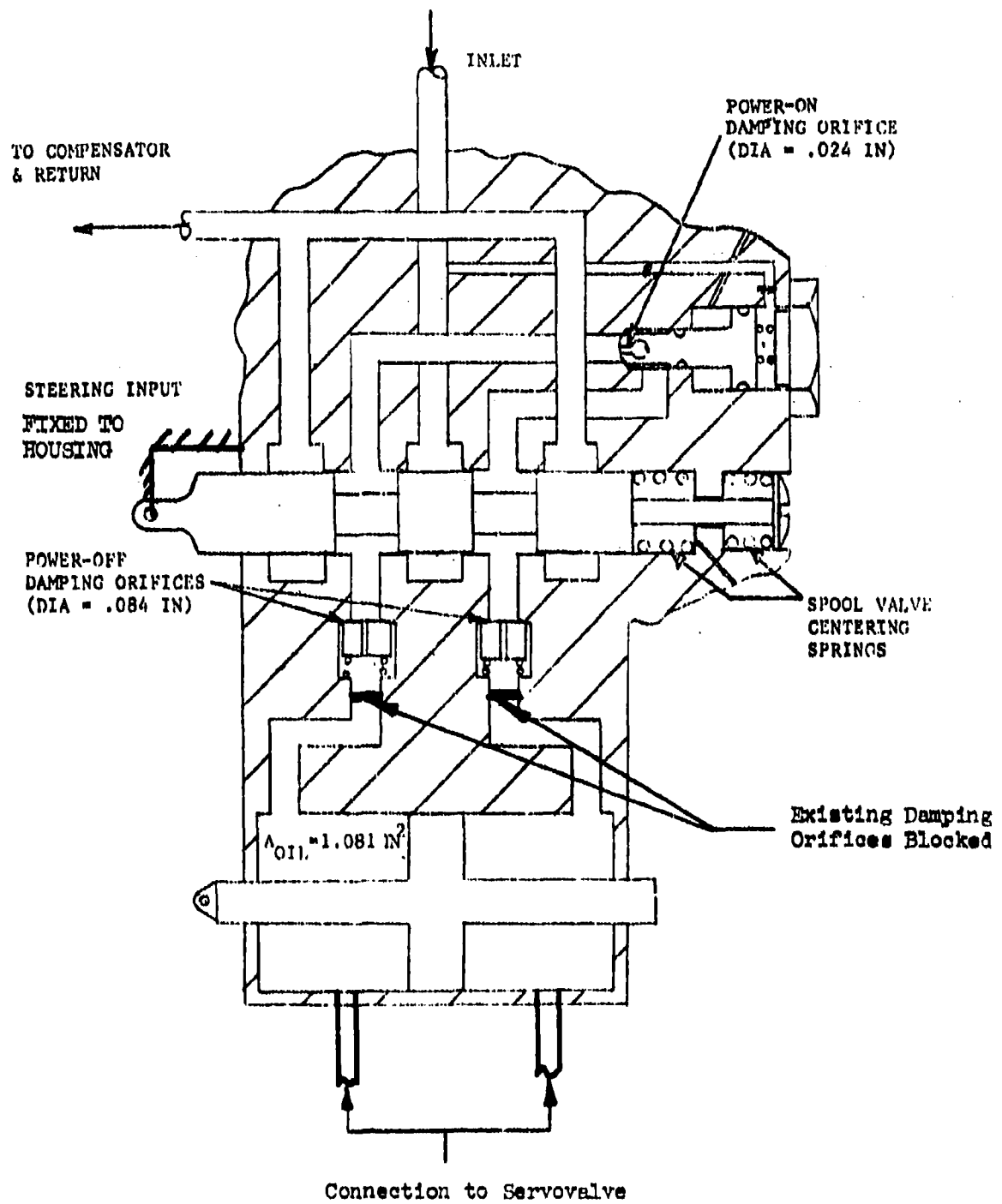
FIGURE 5 - STEERING CYLINDER SCHEMATIC

11.

for the shimmy tests is accomplished through electrical commands to the active system.

The analytical model for the servovalve and steering actuator combination is shown in Figure 6. In this model, the input ALT2C is the electrical feedback control signal obtained from the signal shaping and gain control network. The spool valve electrical input signal X1 is the difference between the control signal ALT2C and the actual measured actuator position response ALT2 (see Figure 2). The spool valve opening X2 is the result of X1 passing through a second order filter representing the spool valve dynamic response. The output of the servovalve is the fluid flow rate which is X9 in Figure 6. This flow rate is proportional to the valve opening X2, as modified by a valve opening amplitude limiter (X3).

Valve flow rate degradation with load pressure is modeled by the following equation which is characteristic for the type of flow control servovalve being used.

$$\frac{Q}{X2} = \sqrt{p_S - p_L} \tag{12}$$

Q is the output flow rate X9, X2 is the spool valve opening, p_s is the system supply pressure and p_L is the load pressure. In Figure 6, p_s is X5 and p_L is X6, which is related directly to the actuator force FKAL. The flow rate, due to piston motion, X10 (directly related to the actuator velocity ALT2D) is subtracted from the servo flow rate X9, yielding the load flow rate X11. This is the flow rate due to fluid compressibility. The integral of this term times a constant K3 yields the actuator force FKAL, which physically feeds back into the system through K5 to yield X6 which is the load pressure p_L. The K6 inner feedback constant represents valve leakage.

The net effect of this system is to control the displacement ALT2 in accordance with the input signal ALT2C, below the cutoff frequency of the actuator model as controlled by K7. The "output" ALT2 is related to the input command ALT2C by a 1st order filter whose time constant is determined by K7, in addition to the 2nd order response of the servovalve (X2/X1).

12

FIGURE 6 - SERVOVALVE - ACTUATOR MODEL

13

Constants K1 through K7 are chosen so as to nondimensionalize the actuator model "internal" response variables X2 through X11. Thus, a value of 1 for X2 represents full scale spool valve travel, 1 for X5 represents system supply pressure p_s and 1 for X9 represents the rated flow capacity of the servovalve.

The analytical model for the active system feedback gain control and signal shaping network is shown in Figure 7. THDD is the calculated axle torsional acceleration (the second derivative of TH shown in Figure 2). This passes through a second order filter representing the dynamic response of the torsional accelerometer, yielding THMDD (measured acceleration). A direct low gain path through the constant G1SMAL provides the primary feedback signal SMGN. An additional nonlinear high gain path yielding BIGGN is provided. This signal path has a gain of G1BIG, which is typically chosen 3-4 times greater than G1SMAL, but its output is of limited magnitude. BIGGN and SMGN are summed to provide the feedback signal XC. The purpose of this network is to provide high effective feedback gain on XC for low magnitude THMDD (when BIGGN dominates SMGN because G1BIG is much greater than G1SMAL), and to yield a low effective gain of G1SMAL for large amplitude THMDD (when the limiter on BIGGN diminishes its magnitude relative to SMGN). The model also provides for a first order filter on THMDD to reduce the signal noise content, and a switch to completely remove the nonlinear high gain path if desired (leaving only the linear feedback gain G1SMAL).

The output XC from the gain control network is then either used directly for the input to the servovalve as ALT2C (See Figure 6), or may be routed through a first order lead-lag signal shaping network whose output is then ALT2CP.

A complete listing of the analytical model equations of motion is contained in Appendix D.
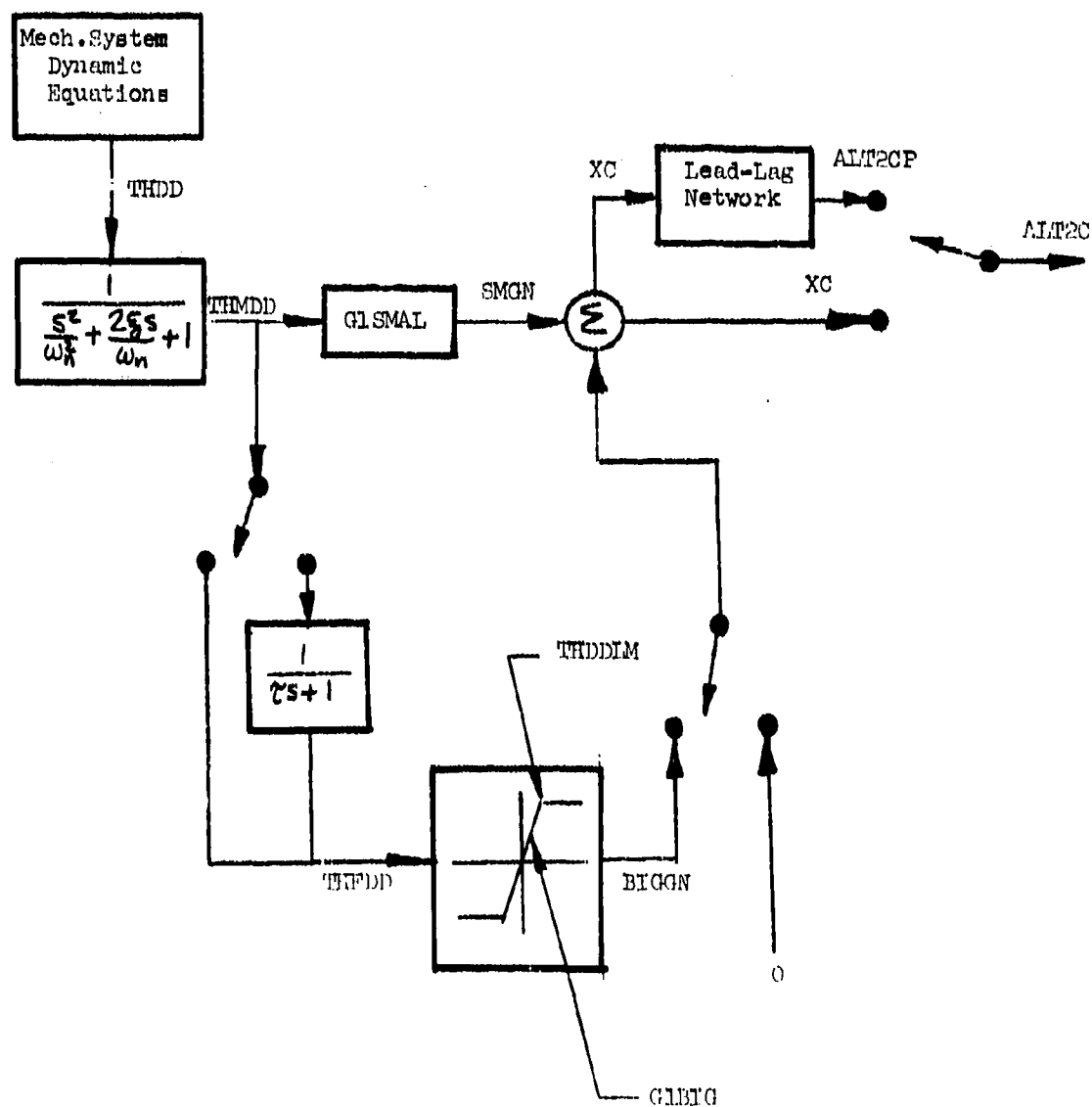
FIGURE 7 — GAIN CONTROL AND SIGNAL SHAPING NETWORK

15

PARAMETER DETERMINATION

General

Parameter measurement tests were performed on the T-37 nose gear to
determine stiffnesses, inertias, frictions, backlashes and passive shimmy
damper performance. Table 1 contains a definition of all the input para-
meters of the analytical model. Table 2 lists the parameter values used in
the analyses, and indicates the sources for the data. A dash in the "EXTEND-
ED" column means the parameter value is the same as for the mid position. An (X) in
the column "DESIGN VAR" in Table 2 means that the parameter is a design
variable for the active control system. The values shown for these para-
meters represent a baseline active system design chosen from a number of
candidate designs. In particular, it should be noted that the lead-lag
signal shaping network is not used in the baseline system. The dynamic
characteristics of the servovalve and torsional accelerometer are taken
from catalogue data for off-the-shelf hardware. The calculations of actuator
constants K3, K4, K5 and K6 utilize geometric data physically measured on
the actuator and gear. In addition, K1 through K6 all involve data peculiar
to the particular servovalve chosen, specifically its rated flow and system
operating pressure.

The following subsections present detailed discussions of the methods of
measuring the physical gear parameters and the passive steering actuator
performance.

1. Lateral and Torsional Stiffness - KPH, KTH and KOC
    The nose gear assembly, including the drag strut, was hung in the
    AFFDL-supplied test fixture and suspended in a structural steel frame-
    work as shown in Figures 8 and 9. The gear was loaded both laterally
    and in torsion by means of weights on a cable passing over a pulley at
    the side of the test framework (not shown in Figures 8 and 9). Dial
    gages mounted to a vertical extension of the gear holding fixture were
    used to measure deflections and rotations. The stiffness measurements
    were made with a solid link replacing the steering actuator.

16

TABLE 1 — INPUT PARAMETER DEFINITION, ACTIVE SHIMMY MODEL

PARAMETER	UNITS	DESCRIPTION
KPH	IN-#/RAD	Lateral rotational stiffness ($= H^2$ K lateral)
KTH	IN-#/RAD	Torsional stiffness - axle to bottom of outer cyl.
KF	IN-#/RAD	Torsional stiffness - fuselage
KOC	In-#/RAD	Torsional stiffness - bottom to top of outer cyl.
KALF	IN-#/RAD	Torsional stiffness - steering actuator
IPH	IN-#-SEC^2	Lateral rotational inertia
ITH	IN-#-SEC^2	Torsional inertia - Wheel,tire,fork,piston, $\frac{1}{2}$ torque arm
ITH1	IN-#-SEC^2	Torsional inertia - Outer cylinder, $\frac{1}{2}$ torque arm
ITH2	IN-#-SEC^2	Torsional inertia - Fuselage
IAL	IN-#-SEC^2	Torsional inertia - Steering actuator cylinder
I	IN-#-SEC^2	Polar moment of inertia of wheel & tire
M	#-SEC^2/IN	Mass of wheel, tire & axle (used w/mech. trail for inertia coupling)
W	#	Total unsprung weight
CP1	IN-#	Piston - cylinder friction - Coulomb
CP2	IN-#/#	Piston - cylinder friction per unit side load
CF1	IN-#	Friction between outer cylinder & trunnion yoke - Coulomb
CF2	IN-#/#	Friction between outer cylinder & trunnion yoke per unit side load
CA	IN-#	Coulomb friction in steering actuator
LTH	RAD	Backlash in torque arms (total freeplay = 2 DTH)
DAL	RAD	Backlash in steering actuator (total freeplay = 2 DAL)
DPH	RAD	Lateral rotational backlash (total freeplay = 2DPH)
BH	IN-#/(RAD/SEC^2)	Passive hydraulic damping in steering actuator
BL	IN-#/(RAD/SEC)	Passive viscous damping in steering actuator
BF	IN-#/(RAD/SEC)	Viscous equivalent of fuselage structural damping in torsion
BPH	IN-#/(RAD/SEC)	Viscous damping of gear lateral rotational mode
GIBIG	——	High gain for THDD
GISMAL	——	Low gain for THDD
THDDLM	RAD/SEC^2	Limit amplitude of THDD for high gain
L	IN	Mechanical trail of axle aft of strut centerline
LG	IN	Geometric trail of tire contact patch center aft of strut centerline intersection with ground plane
H	IN	Height of lateral rotation point of gear above axle
VK	KNOTS	Airplane forward velocity
FZ	#	Vertical load on nose gear

TABLE 1 - INPUT PARAMETER DEFINITION, ACTIVE SHIMMY MODEL (CONT'D)

PARAMETER	UNITS	DESCRIPTION
R	IN	Tire rolling radius
SG	IN	Tire relaxation length
HS	IN	Tire half footprint length
KT	#/IN	(Tire lateral stiffness)/2
KM	#/RAD	(Tire torsional stiffness)/2HS
P1	SEC	Time constant for lead term in signal shaping network
P2	SEC	Time constant for lag term in signal shaping network
TAUFIL	SEC	Time constant for filter on axle acceleration signal
K1	1/RAD	Servovalve constant converting input signal in radians to normalized valve spool position
K2	--	Servovalve pressure gain
K3	IN-LBS	Fluid compressibility constant converting nondimensional compresssed fluid volume to steering actuator moment
K4	$(RAD/SEC)^{-1}$	Steering actuator constant relating actuator velocity to nondimensional flow rate
K5	$(IN\text{-}LBS)^{-1}$	Steering actuator constant relating actuator moment to nondimensional load pressure
K6	$(IN\text{-}LBS)^{-1}$	Steering actuator normalized leakage flow constant
K7	--	Control loop negative feedback gain constant
ZETAA	--	Damping ratio for second order model of accelerometer
OMEGAA	RAD/SEC	Natural frequency for second order model of accelerometer
ZETAS	--	Damping ratio for second order model of servovalve
OMEGAS	RAD/SEC	Natural frequency for second order model of servovalve

TABLE 2 - INPUT PARAMETER VALUES

PARAMETER	GEAR POSITION		DATA SOURCE				NOTES
	MID	EXTENDED	REF (2)	REF (3)	CALAC TESTS	DESIGN VAR.	
KPH	1.63E6	1.403E6			X		
KTH	112000	54000			X		
KF	.124 E6	-		X			
KOC	77270	-			X		
KALP	18000	-			X		
IPH	69.7	83.9			X		
ITH	.68	-			X		
ITH1	.03	-			X		
ITH2	3.49	-		X			1
IAL	.0285	-			X		2
I	.771	-		X			
M	.039	-		X			
W	22.3	-			X		
CP1	22	19.5			X		
CP2	.19	-			X		
CF1	.6	-			X		
CF2	0	-			X		
CA	10.45	-			X		
DTH	.0041	.0081			X		
DAL	.004	-			X		
DPH	.00108	.00148			X		
BH	0	-			X		
BL	186	-			X		
BF	52.6	-					3
BFH	853	935					3
GLBIG	.024	-				X	
GISMAL	.006	-				X	
THDDLM	40	-				X	
P1	0	-				X	
P2	0	-				X	
TAUFIL	0	-				X	

TABLE 2 - INPUT PARAMETER VALUES (CONT'd)

PARAMETER	GEAR POSITION		DATA SOURCE			DESIGN VAR.	NOTES
	MID	EXTENDED	REF (2)	REF (3)	CALAC TESTS		
K1	.114	-				X	
K2	33.3	-				X	
K3	2.62E6	-				X	
K4	.114	-				X	
K5	.000412	-				X	
K6	4.2E-6	-				X	
K7	31.4	-				X	
ZETAA	.7	-				X	
OMEGAA	879.6	-				X	
ZETAS	.6	-				X	
OMEGAS	1000	-				X	
L	.48	-			X		
LG	.164	.473		X			
H	36.875	40.5		X	X		
VK	0 - 100	-				X	
FZ	650	200		X			
R	6.96	7.53	X				
SG	6.649	2.563	X				
HS	3.131	1.961	X				
KT	203	225	X				
KM	845	251	X				

TABLE 2   Footnotes

1 Calculated from fuselage stiffness in Ref. (3) and assumed natural frequency of 30 Hz.

2 Value shown for passive system;   IAL = 0.058 for active system due to added weight of servovalve and manifold
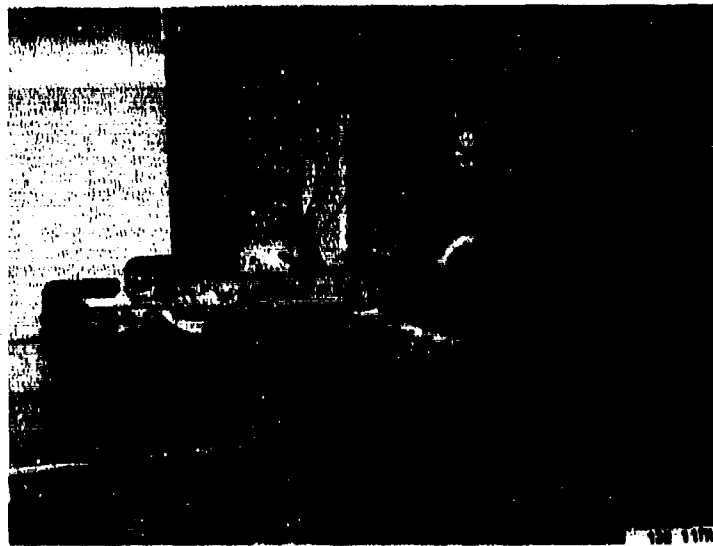
3 Calculated using structural damping ratio of 4%
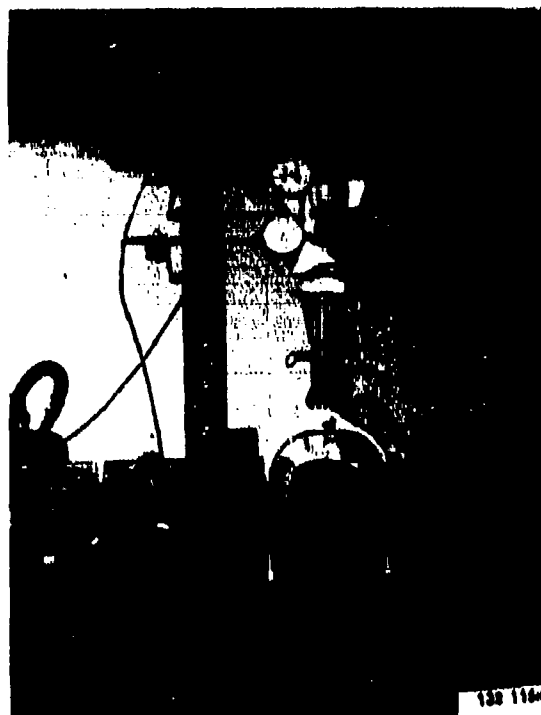
FIGURE 8

TEST FIXTURE FOR MEASURING NOSE GEAR PARAMETERS

FIGURE 9

DETAIL OF GEAR INSTALLATION IN TEST FIXTURE

21

2. Steering Actuator Stiffness - KAL

The steering actuator passive stiffness KALP given in Table 2 was obtained from the Steering Actuator Output Impedance tests described in the subsection of the same title. The value shown represents the actuator stiffness under dynamic conditions with cavitation in the actuator. This is considered the most representative condition for shimmy.

3. Lateral Rotational Inertia - IPH

The lateral rotational inertia was calculated by suspending the gear assembly from a known torsion rod spring and measuring the undamped natural frequency. The gear assembly (minus the drag strut) was suspended with its lateral plane horizontal and its center-of-gravity directly under the torsional spring centerline. The c.g. location was measured relative to the yoke and trunnion axis.

4. Torsional Inertia - ITH and ITHI

The inertia of the rotating assembly (less steering actuator) was calculated from a measured undamped natural frequency and spring rate with the unit suspended from a torsion rod spring with the steering axis directly under the torsion rod axis.

5. Steering Actuator Inertia - IAI

The inertia was calculated using a measured weight of the actuator assembly less a calculated piston rod weight (net weight = 2.86 lb.) and using an effective lever arm from the steering axis of 2.0 in.

6. Total Unsprung Weight - W

The gear assembly was disassembled and the components that move vertically were weighed. (The lower brass bearing was not easily removable so its weight was calculated and subtracted from the total measured.)

7. Piston/Cylinder Friction - CP

The torsional friction of the piston inside the outer cylinder was measured with the gear hanging in the test frame as shown in Figure 9.

The scissor linkage was disconnected by removing the quick release pin. A spring scale was used to measure the force required at the end of the scissor arm (6.5 inch lever) to rotate the fork assembly. The outer cylinder was restrained from turning by replacing the steering actuator with a solid link.

The measurement was repeated at various side loads up to 115 lb. by hanging weights on a cable over a pulley at the side of the test framework. The strut was in midposition. The friction increased nonlinearly with increasing side load. A plot was made and an average slope utilized giving results within ± 15%, with a side load between 0 and 120 lb.

8. **Outer Cylinder Friction - CF**

The outer cylinder friction was measured by removing the steering actuator and centering springs and measuring the torque as above. Side load produced no detectable change in friction. Since the outer cylinder rotates on ball bearings within the trunnion yoke, this friction is very small relative to the piston/cylinder friction.

9. **Steering Actuator Friction - CA**

The actuator friction about the steering axis was calculated from the linear actuator friction and the effective radius.

10. **Backlash in Steering System - DTH and DAL**

The rotary backlash in the various components of the system was measured by mounting dial gages from the test fixture to measure deflection at the end of a lever arm (5.5 inch radius), attached to each of the components. The relative motion at each joint was calculated from the difference in dial gage readings.

Included in the total steering actuator backlash (DAL) were two sources of freeplay: (1) the backlash in the two pins attaching the

actuator, and (2) the backlash in the keyed connection between the outer cylinder and the collar around it to which the steering actuator is mounted.

11. Lateral Backlash at Wheel - DLAT

In addition to the torsional angular backlash as measured above, a linear lateral backlash was measured at the wheel axle location. A dial gage was used to measure position directly. The value shown in Table 2 corresponds to the intersection of the linear load-deflection curve with the deflection (X) axis.

12. Steering Actuator Damping Constants - BH and BL

The damping constants were obtained from the Steering Actuator Output Impedance tests described in the subsection having the same title. The results indicate that a linear damping constant represents the observed results better than a hydraulic (velocity squared) constant.

13. Axle Trail - L

The strut fork positive trail was measured by aligning the steering pivot axis vertically, measuring the horizontal position of the axle relative to the test fixture, and then rotating the axle 180° about the steering axis and repeating the measurement.

Steering Actuator Output Impedance

The T-37 nose landing gear steering actuator was mounted in a test fixture with an electro-hydraulic driving servo, as shown in Figure 10. The instrumentation recorder and supporting electronics for instrumentation and driving servo loop closure are shown in Figure 11. Force and displacement signals for impedance measurements were routed to a central data system for processing and presentation.

The tests consisted of using the drive servo to generate sine waves of steering actuator output piston position at amplitude of $\pm$ 0.05 inches and
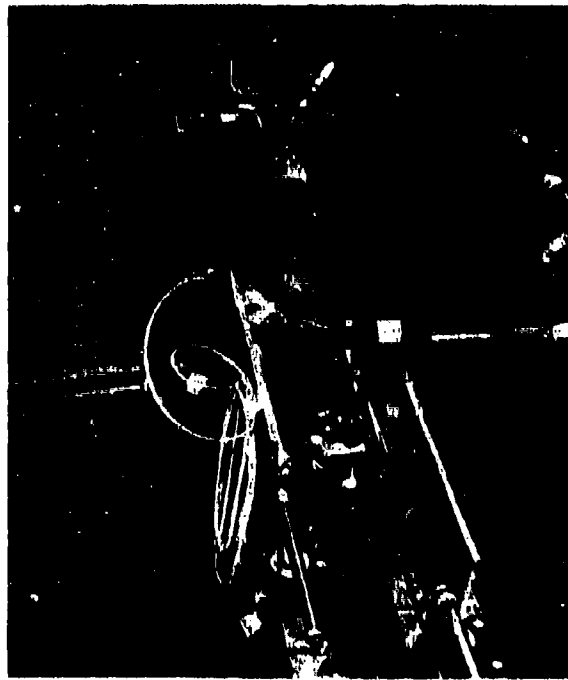
24

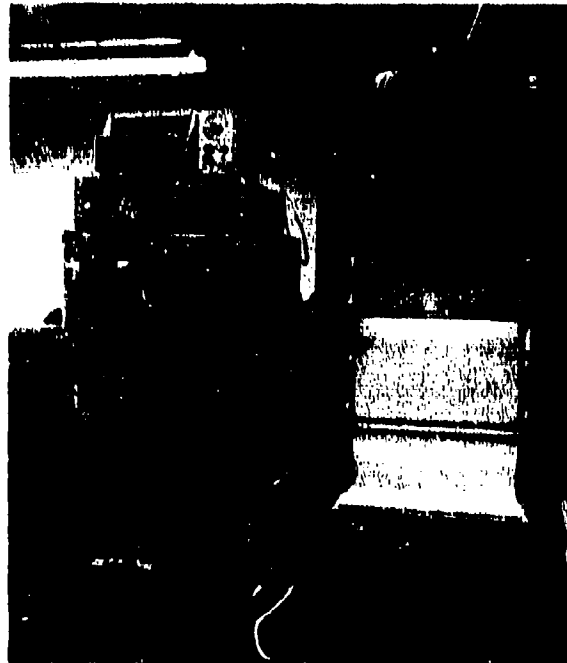FIGURE 10 - STEERING ACTUATOR IMPEDANCE TEST FIXTURE

FIGURE 11 - INSTRUMENTATION ELECTRONICS AND DATA RECORDER

25

± 0.15 in. over a frequency range of 1 to 50 Hz. The steering actuator spool valve was fixed with respect to the actuator body, and the body was mounted in the test fixture with a bracket having a spring rate of approximately 150,000 lb/in. The steering actuator was in the normal "power on" configuration.

For each displacement and drive frequency; position, derived rate, and force data were obtained following signal stabilization. Typical results at 1, 10 and 25 Hz. are shown in Figures 12 to 14. The force and displacement signals were further processed to obtain fundamental sine wave components and effective amplitude ratio and phase shift to produce the Bode plots shown in Figures 15 and 16. The dotted lines on these figures represent a linear approximation to the amplitude ratio data. For these approximate curves, the break frequency is taken at the 45 degree phase lag point, and the slope of the curve below the break frequency is 6 DB per octave.

The test data indicates that very little damping is available from the steering actuator at frequencies above approximately 5 to 10 Hz., depending upon amplitude, because at these frequencies the force approaches an in-phase relationship with displacement, with magnitudes of 2000-5000 lb./in. This low effective spring rate makes it impossible for the actuator to support the internal orifice damping, and the actuator impedance, therefore, levels off, as a function of frequency, at the effective spring rate.

Cavitation was suspected as the cause of the low spring rate characteristic, since the steering actuator does not have anti-cavitation valves. Because of the time delay in the formation of a stable flow through the orifice, there is insufficient hydraulic fluid to fill the cavity created when the piston is pushed away from the fluid on one side of the piston. The pressure on that side instantaneously drops to a sufficiently low pressure to cause the air dissolved in the fluid to come out of solution. Successive cycles of piston motion result in more air coming out of solution until a stabilized hydraulic fluid-air mixture is achieved producing the low effective spring rate.

26

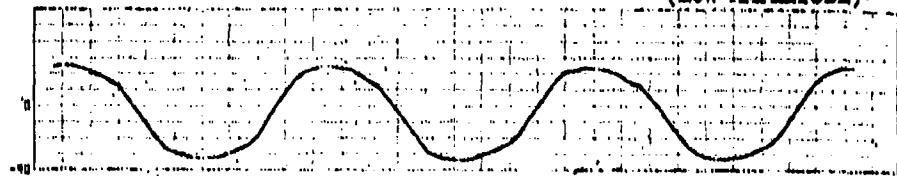ACTIVE SHIMMY CONTROL IMPED TEST
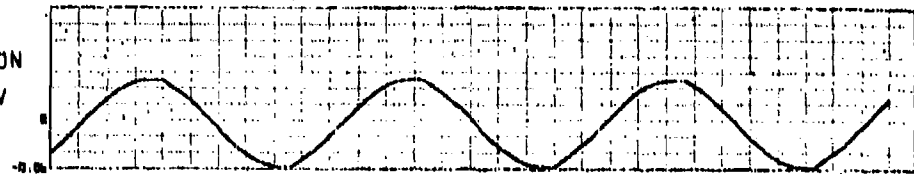INPUT FREQUENCY 1.1 Hz

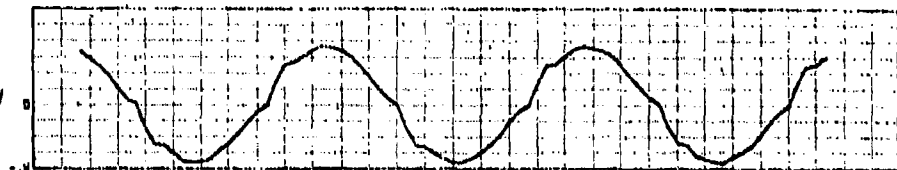TEST 24413   RUN 1   09 DEC 79   (LOW AMPLITUDE)

OUTPUT FORCE
10 LBS./DIV
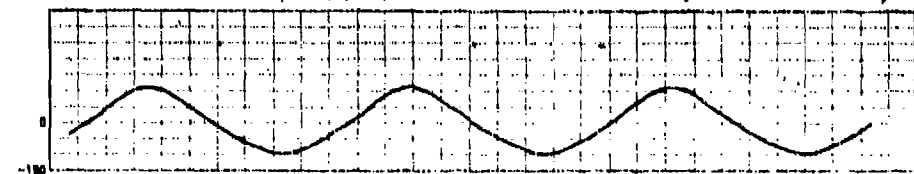
OUTPUT POSITION
0.02 INCH/DIV

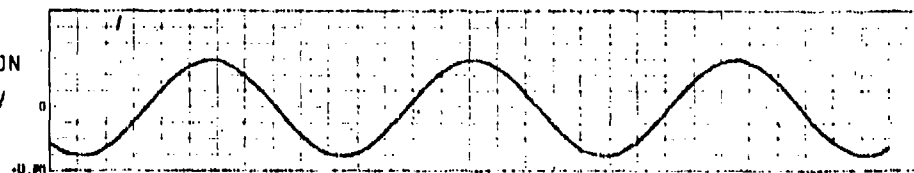DERIVED RATE
.1 INCH/SEC/DIV

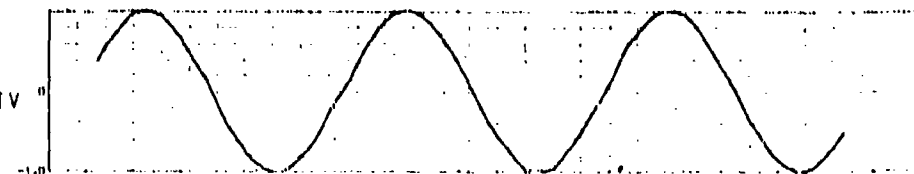RUN 9   (HIGH AMPLITUDE)

OUTPUT FORCE
50 LBS./DIV

OUTPUT POSITION
0.05 INCH/DIV

DERIVED RATE
.2 INCH/SEC/DIV

SECONDS

FIGURE 12 - OUTPUT IMPEDANCE TESTS, 1.1 Hz

27

ACTIVE SHIMMY CONTROL (MPTD) TEST
INPUT FREQUENCY 10.0 HZ

TEST 24413   RUN 4   04 DEC 74   (LOW AMPLITUDE)

OUTPUT FORCE
100 LBS./DIV

OUTPUT POSITION
0.02 INCH/DIV

DERIVED RATE
1 INCH/SEC/DIV

RUN 12   (HIGH AMPLITUDE)

OUTPUT FORCE
200 LBS./DIV

OUTPUT POSITION
0.05 INCH/DIV

DERIVED RATE
5 INCH/SEC/DIV

SECONDS

FIGURE 13 -   OUTPUT IMPEDANCE TESTS, 1C Hz.

28

ACTIVE SHIMMY CONTROL IMPED TEST
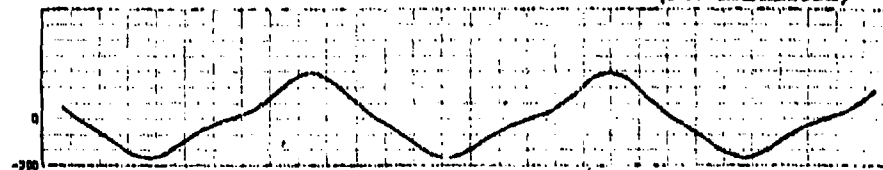INPUT FREQUENCY 25.0 HZ
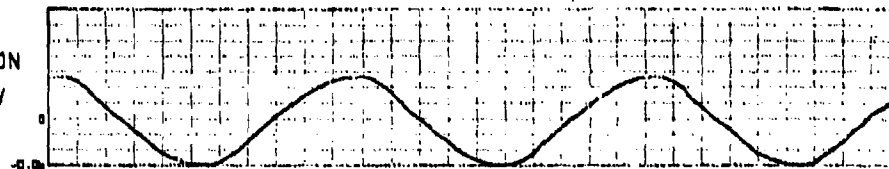
TEST 24413   RUN 6   04 DEC 74   (LOW AMPLITUDE)

OUTPUT FORCE
100 LBS./DIV
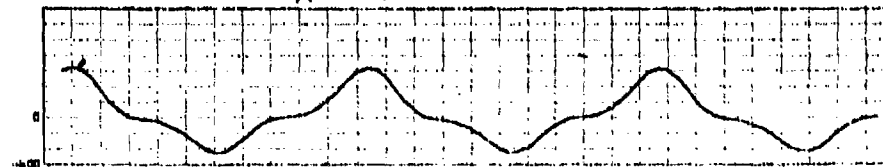
OUTPUT POSITION
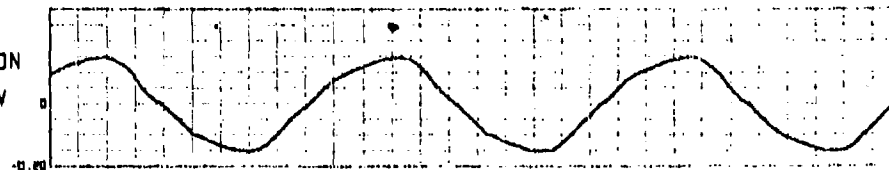0.02 INCH/DIV
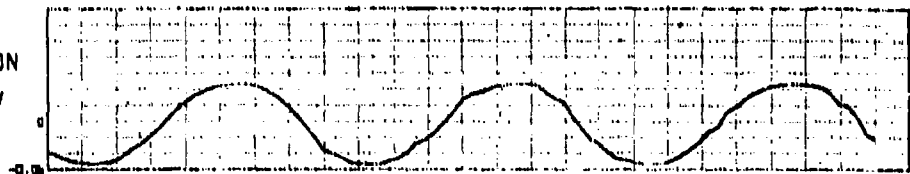
DERIVED RATE
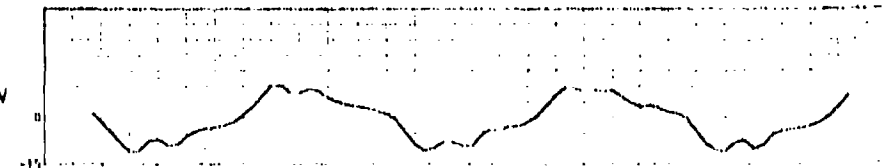5 INCH/SEC/DIV

RUN 14   (HIGH AMPLITUDE)

OUTPUT FORCE
100 LBS./DIV
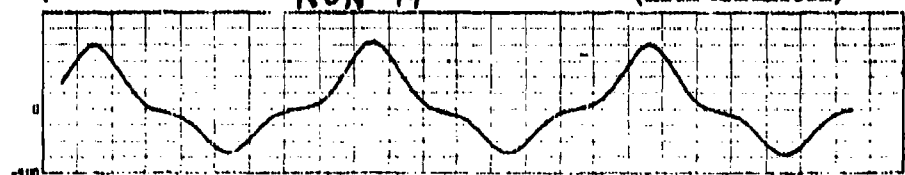
OUTPUT POSITION
0.05 INCH/DIV
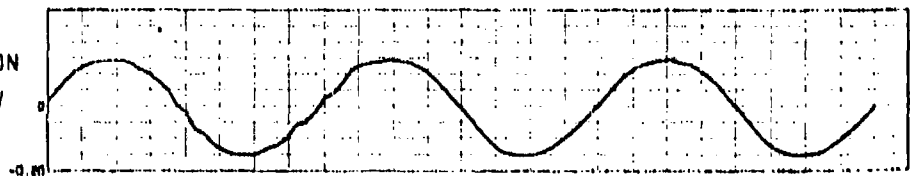
DERIVED RATE
10 INCH/SEC/DIV

SECONDS

FIGURE 14 - OUTPUT IMPEDANCE TESTS, 25 Hz

29

ACTIVE SHIMMY CONTROL IMPED TEST 0.3 INCH PK-PK

TEST 24413

OUTPUT FORCE - LBS. ; 0 DB = 1.0 LB/INCH
OUTPUT POSITION - INCH

FREQUENCY - HZ.

12-09-74

FIGURE 15- BODE PLOT, OUTPUT IMPEDANCE TESTS, HIGH AMPLITUDE

30

ACTIVE SHIMMY CONTROL IMPED TEST   0.1 INCH PK-PK

TEST 29413

$O DB = 1.0 \frac{LB}{INCH}$

OUTPUT FORCE - LBS.
OUTPUT POSITION - INCH

FREQUENCY - HZ.   12-05-74
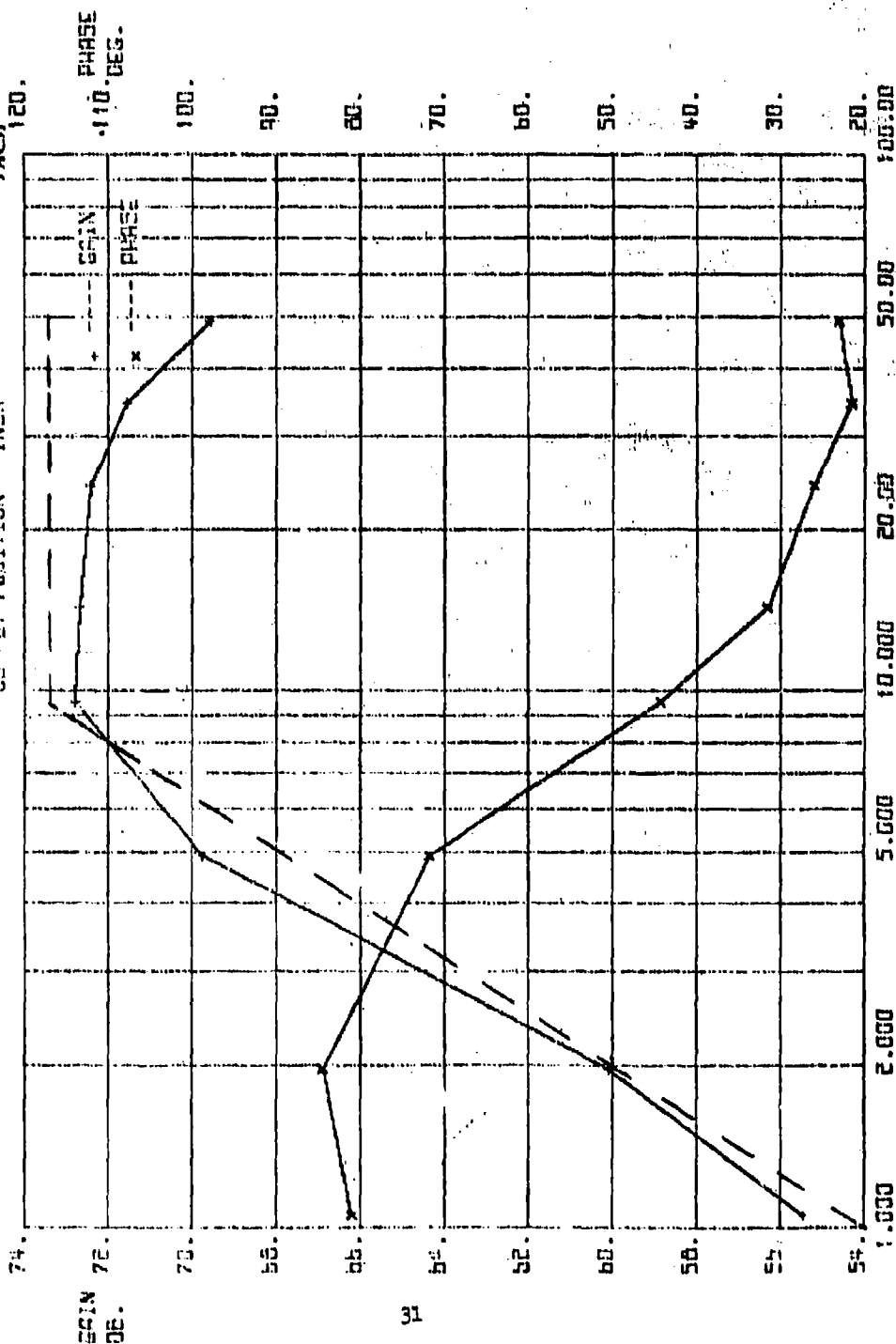
FIGURE 16— BODE PLOT, OUTPUT IMPEDANCE TESTS, LOW AMPLITUDE

31

To investigate the cavitation theory, a transient recording was made starting at the initiation of cycling inputs at 10 Hz. to the steering actuator. The result is shown in Figure 17 which indicates a higher initial impedance decaying to the lower stabilized impedance. The test was then repeated with the steering actuator spool valve biased out of neutral position to create a quiescent load pressure and associated damping orifice flow through the spool valve. The time history for this test, starting with the initiation of cycling inputs, is shown in Figure 18. In this case, the stabilized impedance is higher (approximately 15,000 lb./in.), and the cavitation theory would indicate that the spool valve can now support a portion of the flow requirement to prevent as complete a collapse of spring rate as that observed when the spool valve was in neutral.

Steering Actuator Input Response

The same test fixture and supporting electronics for the impedance tests were used for the response tests. Spool valve input and actuator output signals were routed to the Rye Canyon Central Data System for processing and presentation.

The tests consisted of using the drive servo to generate a sine wave of steering actuator spool valve position with respect to the actuator body and measuring the actuator piston position with respect to the body. The steering actuator was in the normal "power on" configuration and the output load was negligible. For each test condition, spool valve input position, and piston derived rate were obtained. Sample time traces are shown in Figures 19 and 20 for various test conditions.

Run 1 shows the small signal spool overlap region and indicates a deadband of approximately ± 0.008 in. spool travel. Run 4 shows the large signal response characteristic in which a spool valve over-travel condition is reached in one direction with the output rate decreasing to zero for increasing spool valve travel. Run 3 shows an intermediate drive amplitude with 0.19 in. peak-to-peak valve travel producing 20 in./sec. peak-to-peak
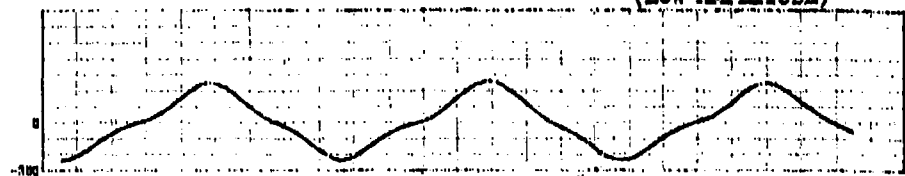
ACTIVE SHIMMY CONTROL ACTUATOR TEST

TEST 24500   RUN 2   13 DEC 74

OUTPUT FORCE
200 LBS/DIV

OUTPUT POSITION
0.02 INCH/DIV

DERIVED RATE
1 INCH/SEC/DIV

0   1.0   2.0   3.0   4.0   5.0
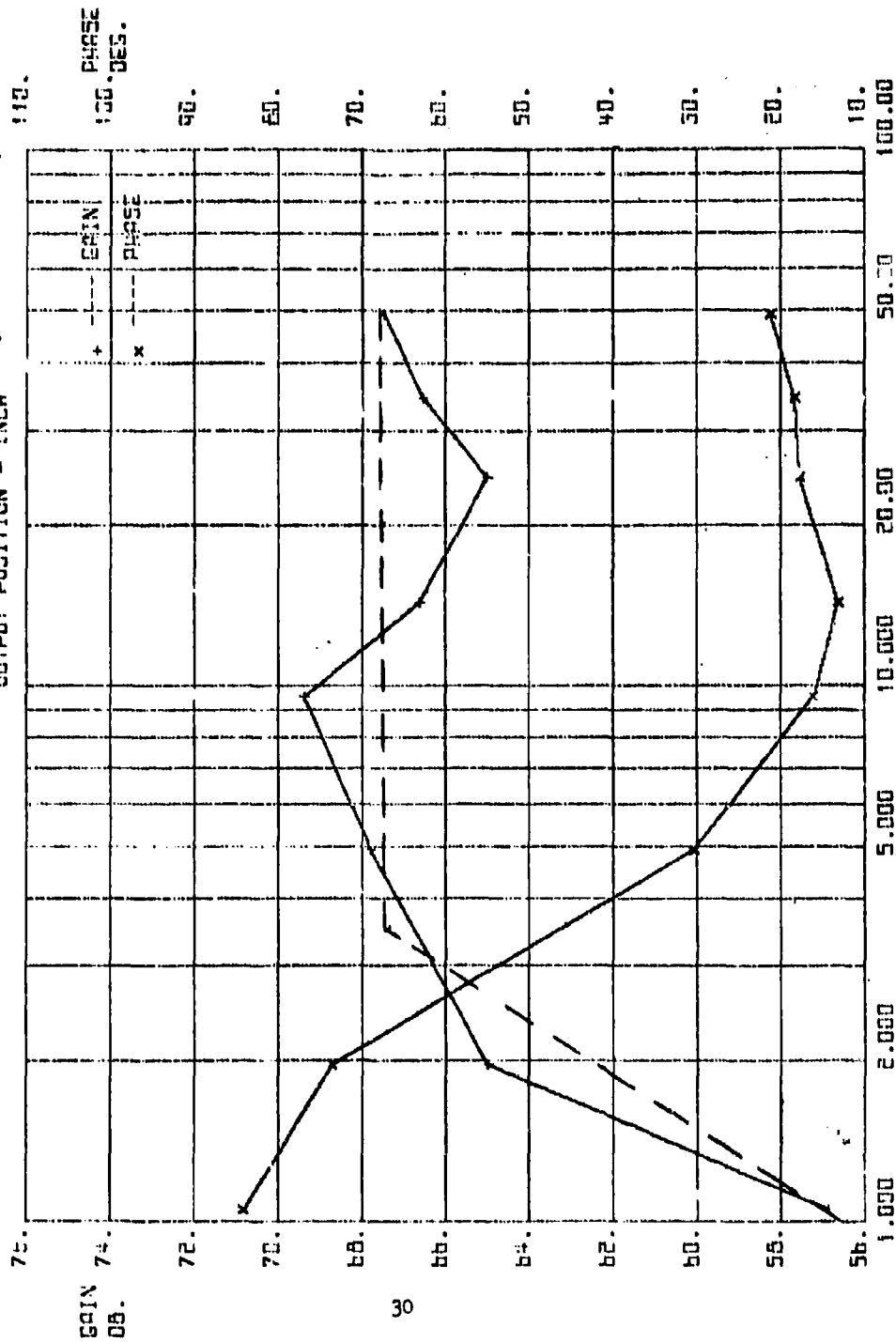SECONDS
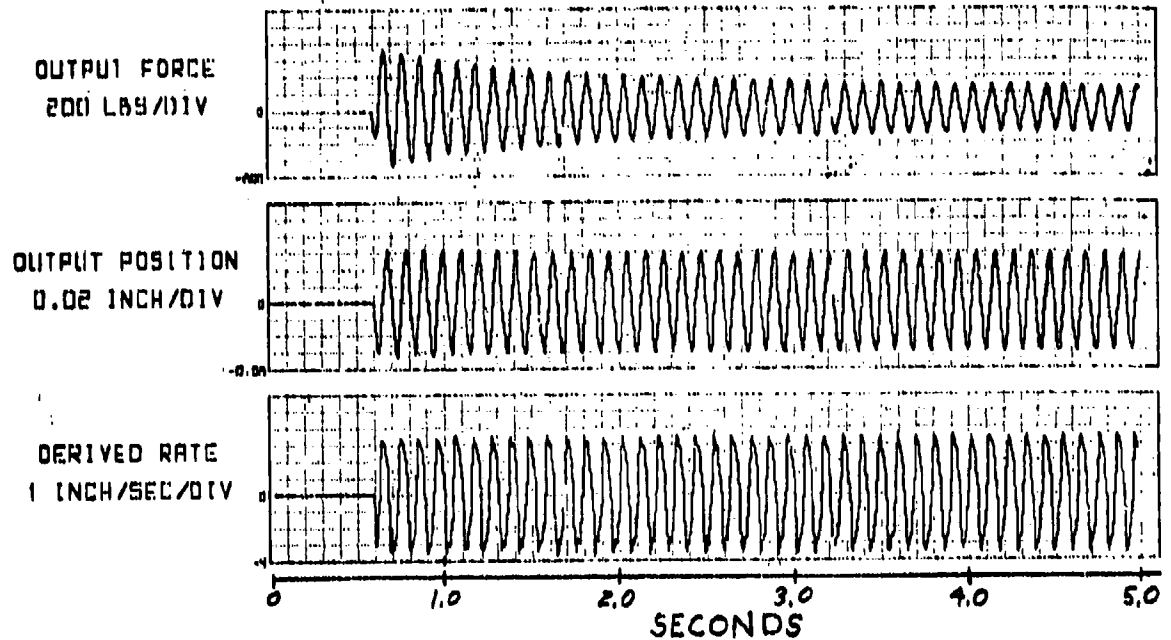
FIGURE 17 - STEERING VALVE TRANSIENT RESPONSE, SPOOL VALVE IN NEUTRAL POSITION

RUN 4

OUTPUT FORCE
200 LBS/DIV

OUTPUT POSITION
0.02 INCH/DIV

DERIVED RATE
1 INCH/SEC/DIV

SECONDS
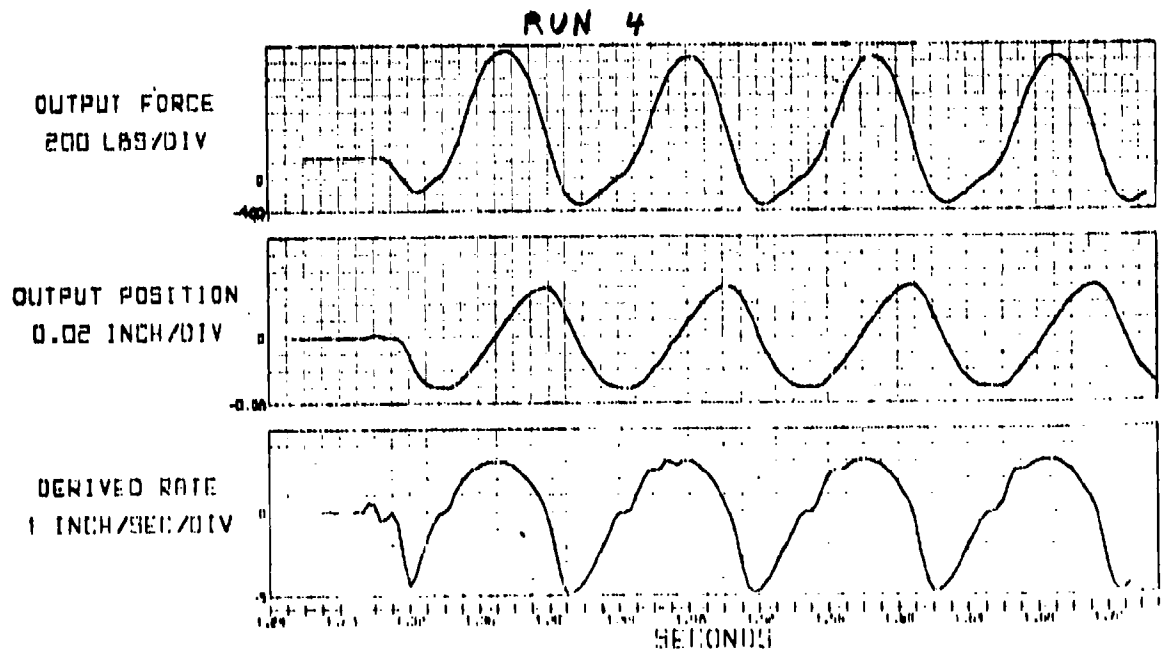
FIGURE 18- STEERING VALVE TRANSIENT RESPONSE, BIASED SPOOL VALVE

33

ACTIVE SHIMMY CONTROL ACTUATOR RESPONSE

TEST 24506   RUN 1

INPUT POSITION
0.005 INCH/DIV

OUTPUT POSITION
0.05 INCH/DIV

DERIVED RATE
.2 INCH/SEC/DIV

0   0.5   1.0   1.5   2.0

RUN 4

INPUT POSITION
0.05 INCH/DIV

OUTPUT POSITION
0.02 INCH/DIV

DERIVED RATE
5 INCH/SEC/DIV

SECONDS
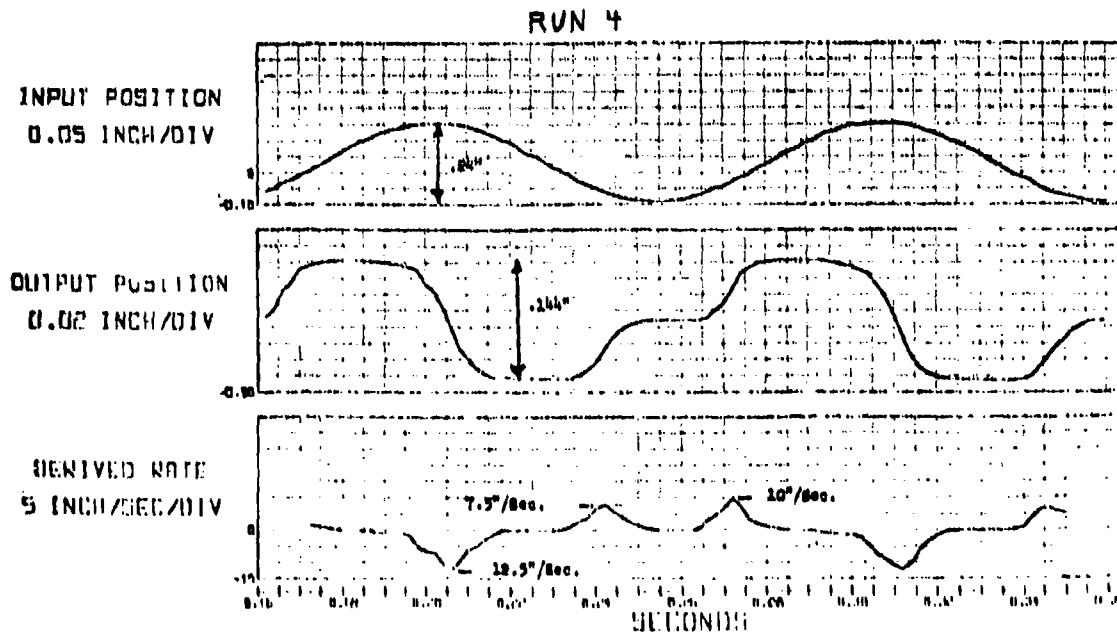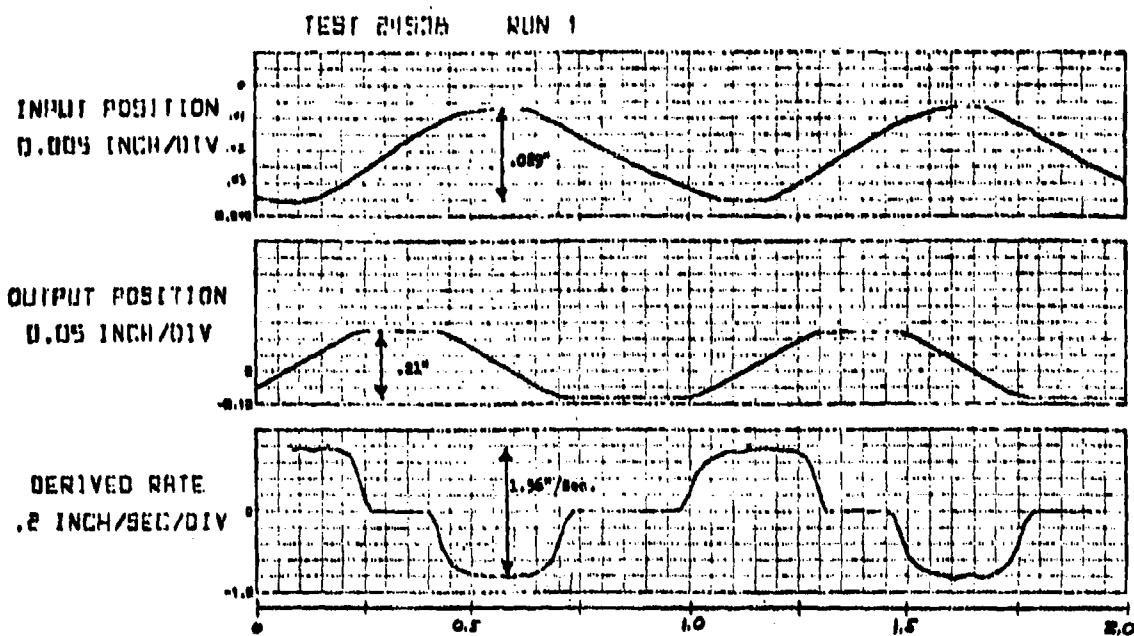
FIGURE 19 -   INPUT RESPONSE TESTS, SMALL AND LARGE INPUTS

34

FIGURE 20- INPUT RESPONSE TESTS, INTERMEDIATE INPUTS

35

piston rate. Note the gross non-linear gain characteristics of the piston rate response. Run 2 shows the response at a slightly reduced spool valve travel of 0.17 in. peak-to-peak which produces only 4.6 in./sec. peak-to-peak piston rate. This was the maximum spool valve amplitude at which a reasonably linear response could be obtained.

Figure 21 shows a Bode plot of output piston rate with respect to input valve position in the linear region of operation (0.16 in. peak-to-peak spool valve travel). The response is well behaved with approximately 5 DB attenuation and 45 degrees phase lag at 46 Hz.
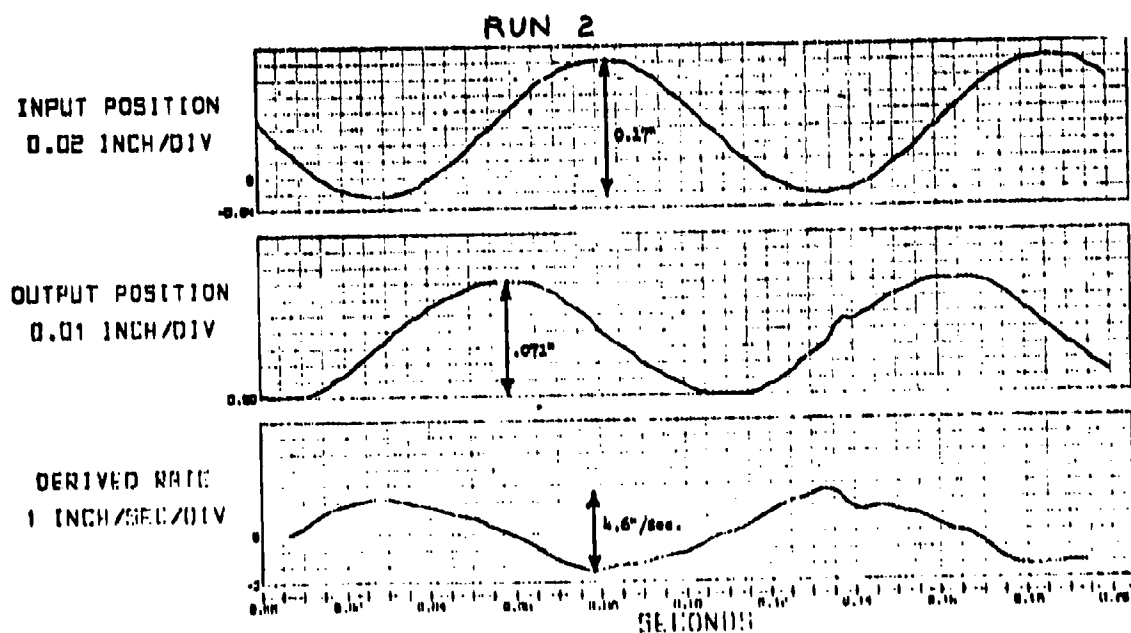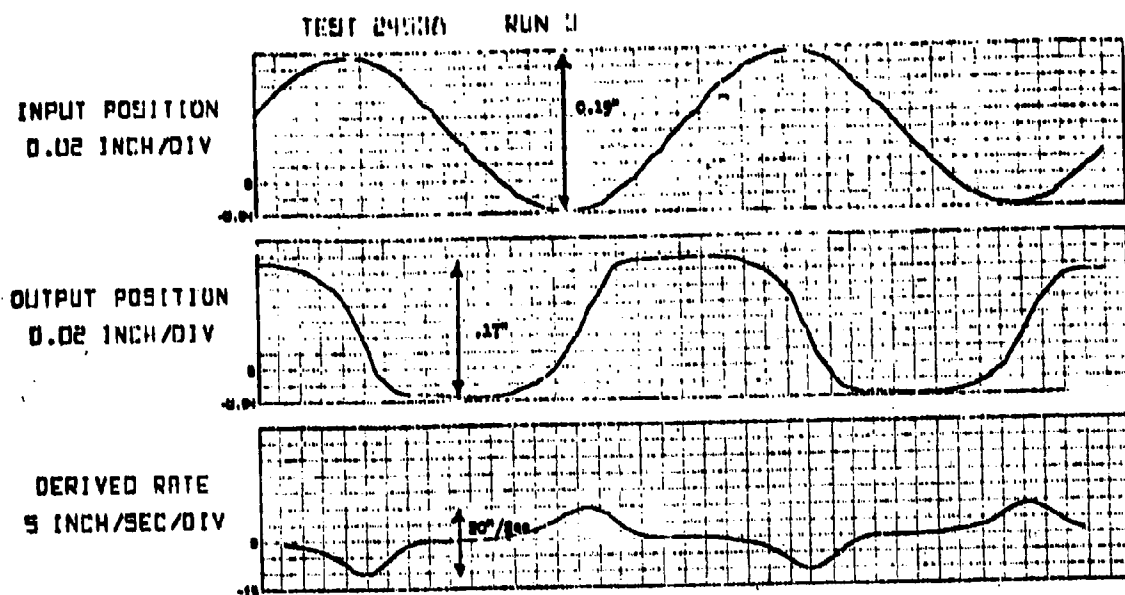
The above test data indicates an extremely non-linear gain characteristic at output rates above $\pm$ 2.3 in/sec and a significant threshold characteristic. Both effects are undoubtedly caused by the shaping of the spool valve flow characteristic. The linear region of response corresponds to approximately $\pm$ 87 deg./sec. of gear rotational rate or $\pm$ 0.56 deg. (.01 radians) at 25 Hz. Since the active shimmy controller must operate at larger rates to be effective, and since closing the shimmy controller loop around an extremely non-linear rate characteristics is not practical, it is concluded that the active shimmy controller cannot be implemented using a modulating piston stage for driving the present actuator spool valve.

The best alternative approach, without modifying the actuator spool valve, appears to be a configuration in which an electro-hydraulic valve is used to directly port flow to the steering actuator piston in parallel with the spool valve. Such an approach presents certain problems in synchronization, hydraulic interaction with the spool valve, valve null offsets, and failure modes, but is felt to be satisfactory for investigating the potential for active shimmy control in this experimental program.

ACTIVE ELBOW CONTROL SENSOR RESPONSE

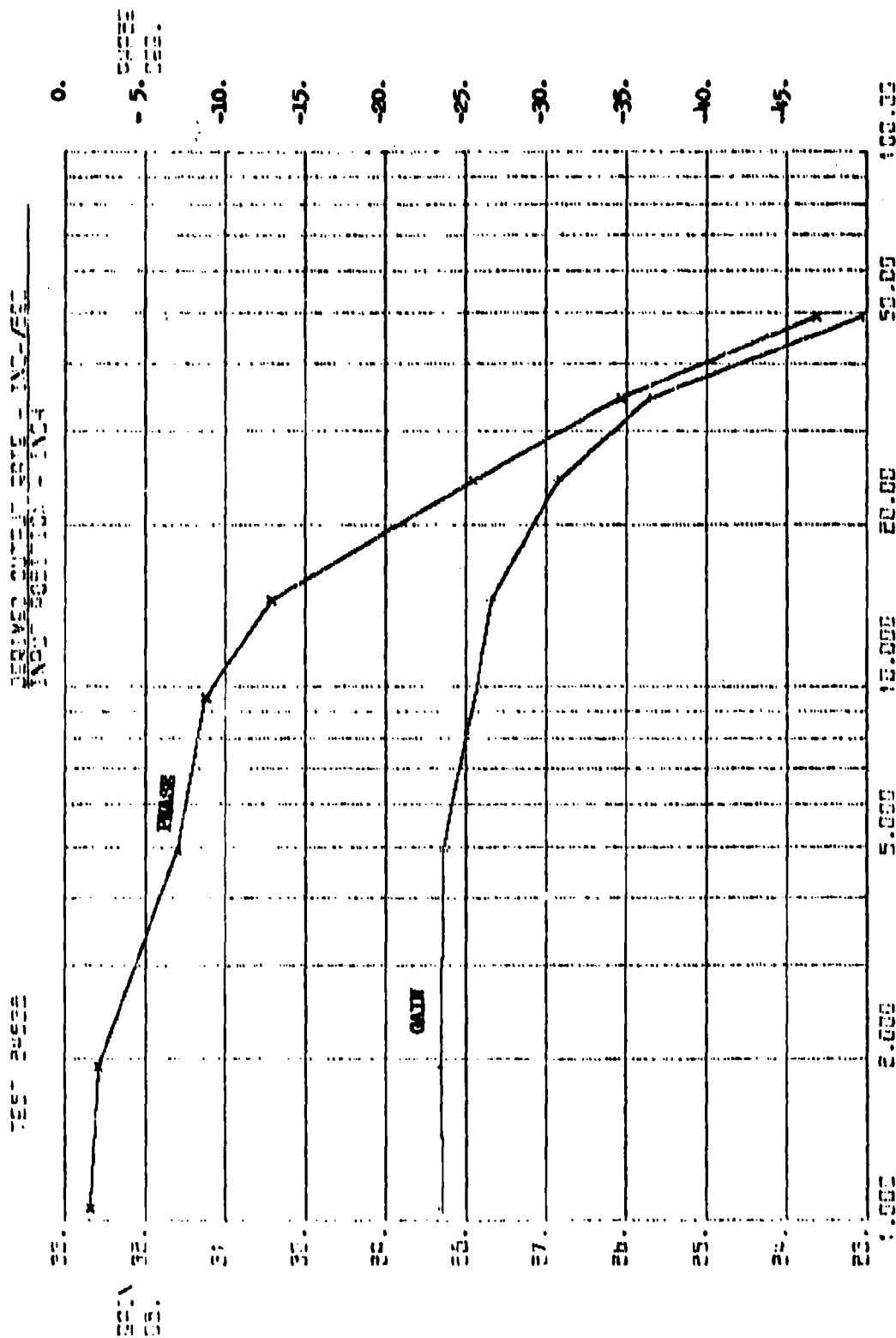FREQUENCY - HZ.

FIGURE 21.— BODE PLOT, INPUT RESPONSE TESTS

PHASE

GAIN

ANALYTICAL RESULTS

General

The types of feedback investigated for the control signal ALT2C all involve using some form of THD (axle torsional velocity). The objective is to control the actuator displacement ALT2 in phase with the axle velocity THD, resulting in actuator forces acting on the axle (via the outer cylinder and torque arms) which oppose THD motion. Of the systems investigated, the simplest was selected. It uses the overall actuator loop as a pseudo-integrator of a control signal ALT2C that is just the direct output THDD (times a gain G1) from the accelerometer. This results in the actuator displacement ALT2 being in phase with axle velocity THD at frequencies well above the cutoff frequency for the actuator loop. To achieve the desired phase for ALT2 (in phase with THD, or lagging THDD by 90 deg.) at a shimmy frequency of around 16 Hz, the actuator loop cutoff frequency is adjusted (via K7 in Figure 6) to about 5 Hz. With the loop set to 5 Hz and the system operating at 16 Hz, the loop contributes 73 deg. of phase lag, and the accelerometer and servovalve together add about 17 deg., giving the desired 90 deg. lag of ALT2 relative to THDD. Therefore, at the shimmy frequency of 16 Hz the active system forces the actuator displacement ALT2 to be in phase with the axle velocity THD.

At lower operating frequencies the actuator displacement lags THDD by less than 90 deg., and at higher frequencies by more than 90 deg. The system will only be operating at frequencies other than the shimmy frequency when it is driven by a cyclic disturbance such as wheel imbalance. For the T-37 nose wheel and tire in the static position, the relationship between airplane velocity and the resulting driving frequency from wheel imbalance is

$$f = 0.46 \ V \tag{13}$$

where f is the driving frequency in Hz and V is the airplane ground speed in knots. From the above equation it can be seen that an airplane ground speed range of 10 to 100 knots results in wheel imbalance driving frequencies from 4.6 to 46 Hz, or roughly 5 to 50 Hz. Since the amplitude of the

38

moment, due to wheel imbalance, is proportional to the velocity squared, velocity inputs below 5 knots are no problem with any reasonable wheel imbalance (less than 10 times the normal imbalance).

Figure 22 shows a phase diagram for an active system tuned to 5 Hz. The vectors shown in the diagram are rotating clockwise at the system operating frequency. The phase relationship between actuator displacements (ALT2) and axle velocity THD are shown at system response frequencies of 5, 16 and 50 Hz.

At 5 Hz the actuator displacement leads THD by 40 deg., and at 50 Hz it lags by 46 deg., while ALT2 is in phase with THD at 16 Hz. Therefore, tuning the system for optimum performance at the shimmy frequency of 16 Hz (the system will oscillate at this frequency if given an impulsive disturbance) results in acceptable performance over a broad spectrum of cyclical disturbance frequencies. The phase lags from the servovalve and accelerometer prevent reducing the phase angle differences resulting from an operating frequency range of 5 to 50 Hz.

This active system without any lead-lag signal shaping and with nonlinear gain control constitutes the baseline active shimmy control system. The results obtained with the lead-lag network are very similar to those with the baseline system. The purpose of the lead-lag system is to provide feedback signal amplitude attenuation at high frequencies (> 50 Hz), while retaining the desired gain at lower frequencies (10-20 Hz) corresponding to the shimmy response frequency. Although there appear to be only slight benefits in system stability to be obtained from the lead-lag network, it is included in the breadboard model to provide greater signal shaping flexibility during shimmy testing of the system.
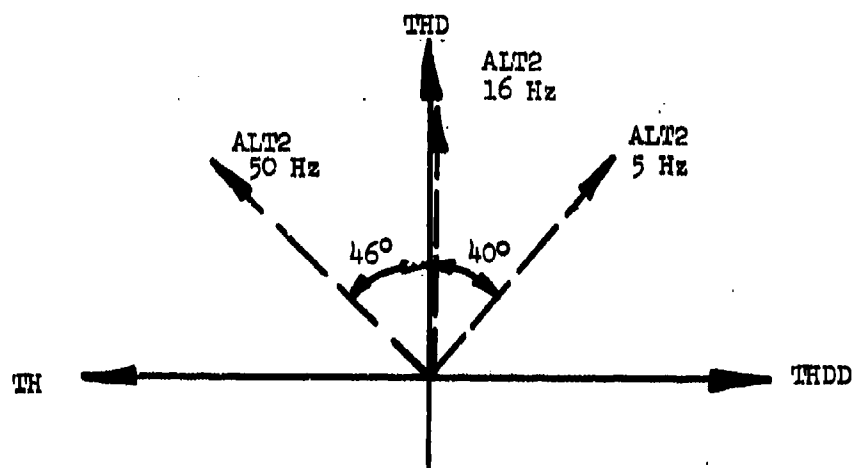
FIGURE 22 — ACTIVE SYSTEM PHASE DIAGRAM

Baseline Active-Passive System Comparisons

Utilizing the passive/active system model and parameters delineated in the previous section, the performance of the baseline active system is compared with that of the basic passive gear. Two types of input disturbing functions are used to excite the gear. One is an initial torsional angular velocity (THD)at the axle at time zero. No driving force is involved; the system dynamic equations are solved with an imposed initial condition on axle angular velocity. This type of excitation simulates the impulsive type of driving force that is used in most shimmy tests, where the force usually comes from an air blast applied to the wheel rim. An initial condition of THD = 5 rad/sec is used.

The other type of excitation used is wheel imbalance. With a single wheel gear this would not tend to excite shimmy motions if the imbalance were symmetric about the wheel center plane. However, if the imbalance corresponds to a weight located at the wheel rim on one side only, the result is a sinusoidal driving moment both in torsion (TH) and lateral bending (PH), the two being 90 deg. out of phase. The magnitude of the driving force is proportional to the imbalance and varies with the square of airplane forward velocity (or wheel angular velocity). A wheel imbalance about the axis of wheel rotation of 10 in-oz is used, assuming all this imbalance is due to one weight located at the wheel rim on one side only. This magnitude of imbalance is slightly greater than that normally allowed in service for this size of wheel and tire.

Figure 23 shows the comparison of the active and passive systems for an impulsive type of input, with the landing gear at mid extension. The limit cycle amplitude of oscillation of TH (axle torsional motion) obtained is shown plotted against airplane forward velocity. The passive gear is well behaved below 40 knots; between 40 and 80 knots the limit cycle amplitude rises rapidly, and above 80 knots the passive gear is unstable.
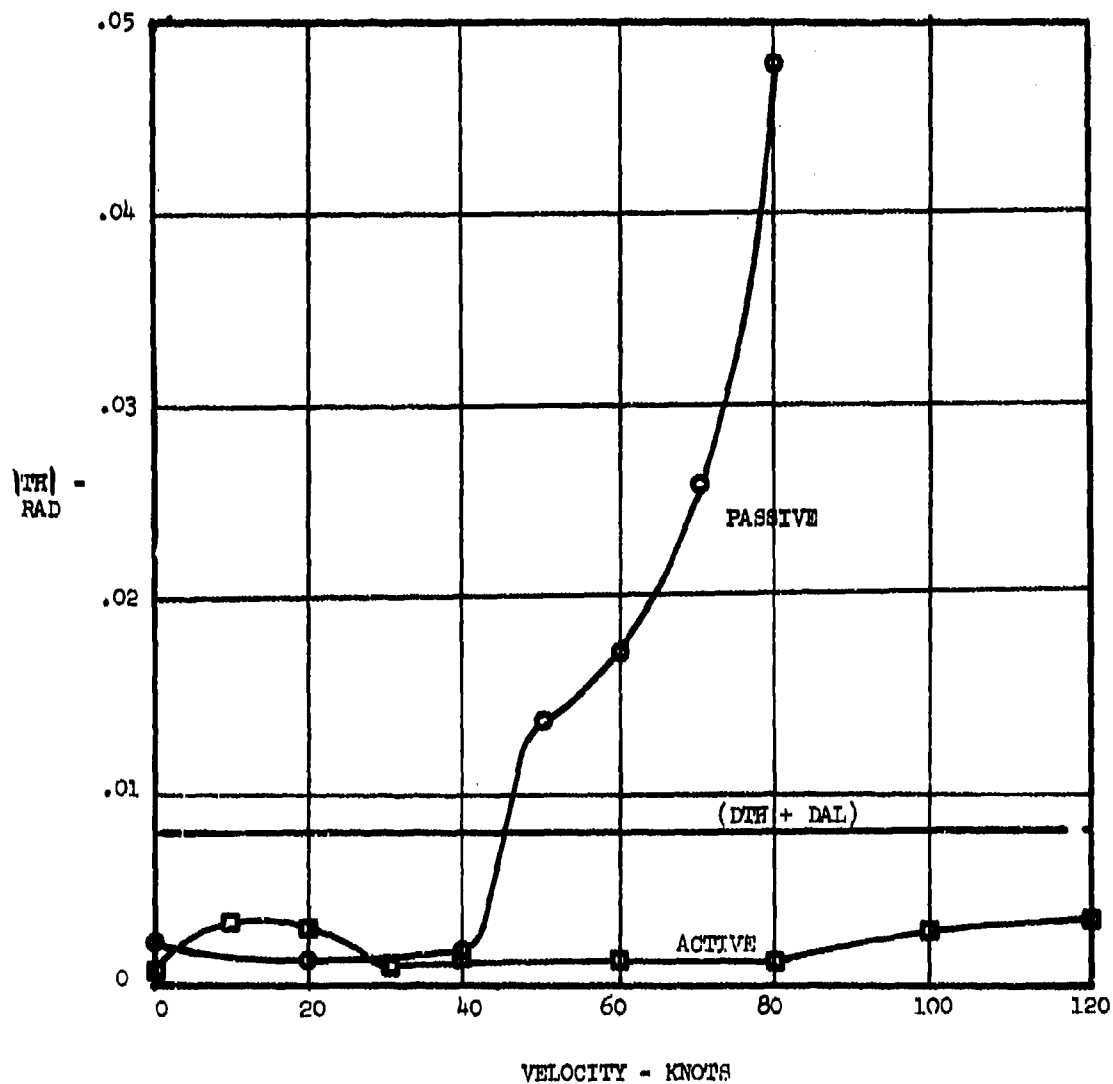
41

FIGURE 23 - ACTIVE/PASSIVE SYSTEM COMPARISON, IMPULSIVE INPUT, MID POSITION

42

In comparison, the active gear shows a dramatic reduction in response amplitude at velocities above 40 knots to well beyond the ground operating velocities of the T-37 airplane. The slightly higher active system response at velocities.between 5 and 30 knots is considered of no consequence because the amplitudes are still well below the total torsional backlash (DTH +DAL), shown as a horizontal line in Figure 23. This mild hump in the low velocity region response of the active system can be eliminated by either reverting to a passive system at low velocities or by reducing the feedback gain to zero.

Figure 24 shows the same comparison for the gear in the extended position. Below 80 knots, the passive gear is slightly more stable in the extended position than in the mid position. This is due to the tire input moments being much less with the gear fully extended. As shown in Table II, the tire torsional stiffness parameter KM in the extended position (tire vertical load = 200lb.) is only 251 compared to 845 with the gear in the mid position (vertical load = 650lb.).Although the susceptibility of the gear to shimmy is greater in the fully extended position because of its lower torsional stiffness and greater backlash, the greatly reduced tire torsional stiffness more than compensates for these effects. Again the active system shows clearly superior performance at all velocities above 40 knots, stabilizing what would be an unstable passive gear.

The comparison between the active and passive gears subjected to wheel imbalance is shown in Figures 25 and 26 for the gear in the mid and extended positions, respectively. As with the impulsive disturbance, the passive gear is unstable above 80 knots, whereas the actively controlled gear has very low response amplitudes at all velocities. The hump in the low velocity region for the active gear, extended gear position, shown in Figure 26, can be eliminated by reducing the feedback gain or reverting to a passive system below 30 knots.

The peak instantaneous power requirement for the active system is only .49 horsepower at V=100 knots with 10 in-oz of wheel imbalance. At 60 knots
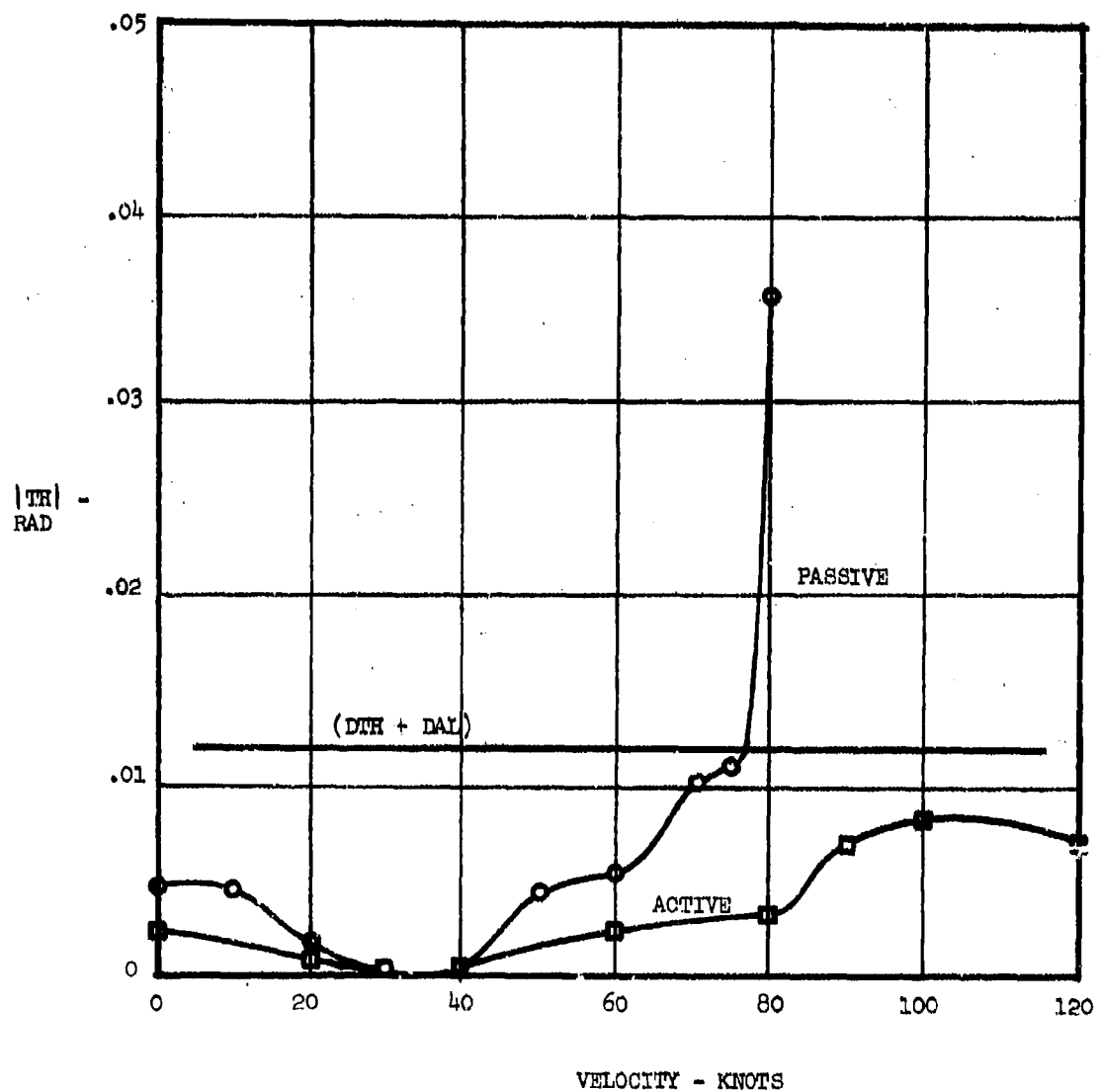
43

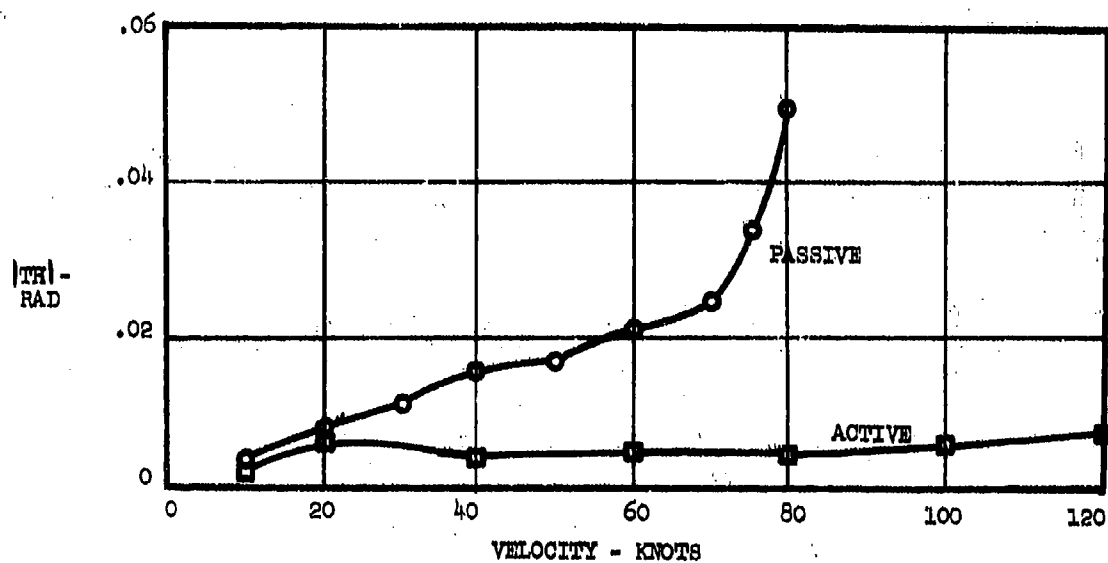FIGURE 24 - ACTIVE/PASSIVE SYSTEM COMPARISON, IMPULSIVE INPUT, EXTENDED POSITION

44

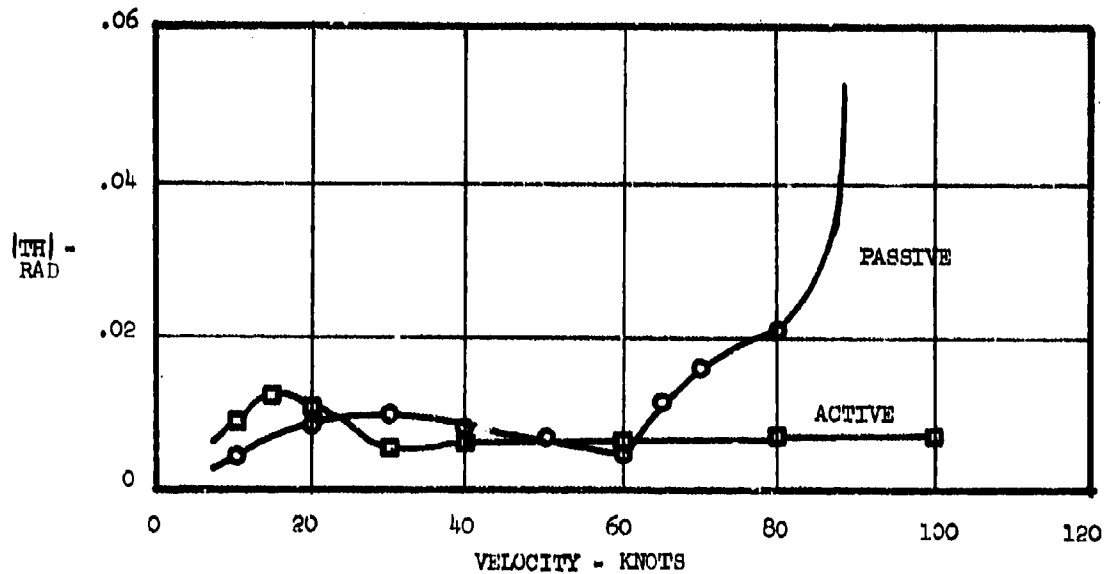FIGURE 25 - ACTIVE/PASSIVE SYSTEM COMPARISON, WHEEL IMBALANCE, MID POSITION

FIGURE 26 - ACTIVE/PASSIVE SYSTEM COMPARISON, WHEEL IMBALANCE, EXTENDED POSITION

45

this drops to .05 HP, and is only .02 HP at 20 knots. For an impulsive type of excitation the peak power requirement is .27 HP at all velocities from 60 to 100 knots. The maximum actuator force requirement is 685 lbs. at 100 knots with wheel imbalance. With an actuator area of 1.08 in^2, this requires a pressure differential of only 634 psi, compared to a system pressure of 1500 psi. The highest instantaneous valve flow rate requirement is 3.25 gallons per minute (GPM) with wheel imbalance at 100 knots. The rated no-load flow capability of the valve used for the system is 4.9 GPM. Even assuming the peak actuator pressure (634 psi) occurs simultaneously with the peak flow rate requirement, which is conservative, application of equation (12) shows that the flow capability of the valve under load decreases to

$$\sqrt{\frac{1500 - 634}{1500}} \quad (4.9) \quad = \quad 3.72 \quad \text{GPM}$$

which is still 15% above the maximum flow rate requirement (3.25 GPM). In order to provide a 6 dB gain margin the feedback gain for the baseline active system is one-half the value that results in marginally unstable behavior of the active system. No indications of unstable behavior are evident for any of the operating conditions analyzed. The 6 dB gain margin is based on G1SMAL, since G1BIG is only effective when the system is in the backlash region and can tolerate much larger gains without going unstable.

Parameter Variations

The sensitivity of the foregoing analytical results to variations in certain system parameters is described in this section. The parameters investigated include the following:

1. KALP and K3   Hydraulic fluid stiffness in the actuator
2. KTH   Torque arm stiffness
3. KPH   Gear lateral stiffness
4. DTH   Torque arm backlash
5. CP   Piston-cylinder friction
6. BF and BPH   Fuselage and lateral gear damping
7. ITH2   Fuselage inertia

46

Both active and passive systems were analyzed using the impulsive disturbance (THD = 5 rad/sec) at V = 60 knots with the gear in the mid position as a reference condition.

1. <u>KALP and K3</u> - Figures 27 and 28 show the effect of variations in the hydraulic stiffness parameters KALP and K3 on limit cycle amplitudes for the passive and active systems, respectively. The nominal values for these parameters are 18000 and 2.62E6. The passive system value corresponds to a very low effective bulk modulus of 4500 lbs/in^2. This value was obtained from the dynamic impedance tests performed on the steering actuator. Flow cavitation across the passive damping orifices is believed to be the cause of the very low observed actuator hydraulic stiffness. The active system has these orifices blocked, and the passages are sized to preclude any cavitation problems. An effective bulk modulus of 75200 lbs/in^2 is assumed for the nominal active system. This corresponds to approximately 3% entrapped air volume (Bulk Modulus(B)= 265000 lbs/in^2 for no air entrapment), which can be maintained with normal design and servicing.

Figure 27 indicates that the passive system cannot tolerate much lower hydraulic stiffness than the nominal case (below KALP = 15000, the system is unstable). This is to be expected in light of the very low hydraulic stiffness for the nominal condition. However, even much larger hydraulic stiffness values (> 3 times nominal) only reduce the torsional response to 0.011 rad., which is still an order or magnitude greater than the active system response. Furthermore, the passive system is still unstable at 100 knots, even with KALP = 50000. Allowing for cavitation relief from the additional flow that is available if the spool valve opens during shimmy, the highest value of KALP observed during the program tests (with open spool valve) is about 45000. It is not known whether spool valve opening is a common occurrence during shimmy; however, even allowing for this, the passive system limit cycle response to an impulsive disturbance at 60 knots is greater than 0.01 rad.
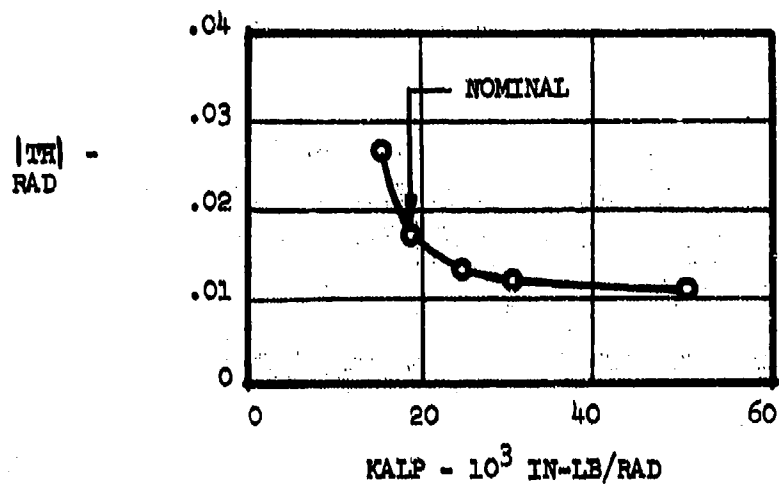
FIGURE 27 - VARIATION OF HYDRAULIC FLUID STIFFNESS,
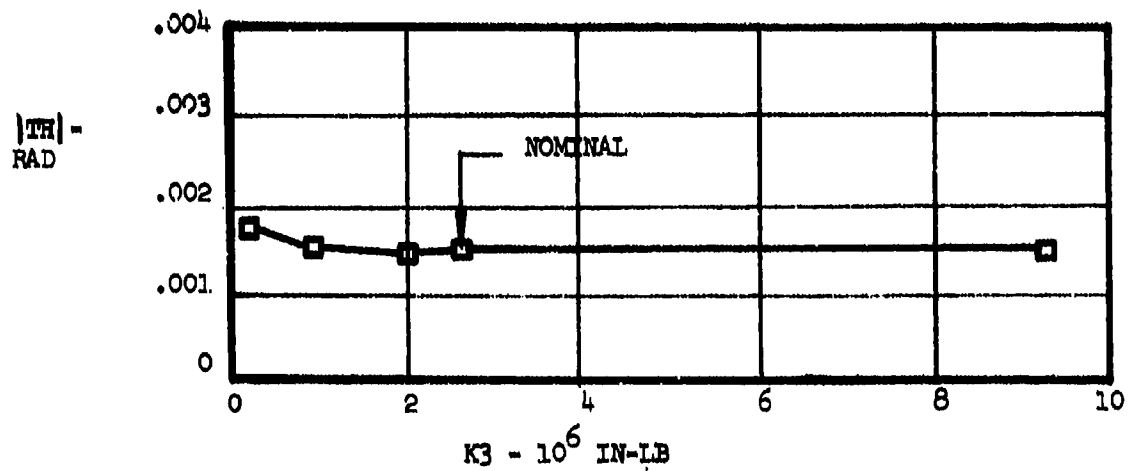PASSIVE SYSTEM

FIGURE 28 - VARIATION OF HYDRAULIC FLUID STIFFNESS,
ACTIVE SYSTEM

By way of contrast, the active system is relatively unaffected by wide variations in the hydraulic stiffness parameter K3, as shown in Figure 28. Only when K3 drops below 60000 (equivalent to B = 1700 lbs/in^2) does the active system performance start to degenerate. For any hydraulic stiffness greater than this, the active system exhibits response reductions of an order of magnitude relative to the passive system. Based on these results it would appear that the active system can be expected to perform very well at any value of effective hydraulic fluid bulk modulus that can be reasonably expected.

2. KTH - The sensitivity of the analytical results to variations in torque arm stiffness KTH is shown in Figure 29. Whereas the passive system performance starts to deteriorate at about 1/2 the nominal value (112000), the active system behaves properly down to less than 10000 for KTH which is less than 1/10 the nominal value. At values greater than nominal, both the active and passive results are the same as with the nominal KTH.

3. KPH - Figure 30 shows the active and passive system performance with variations in KPH, the lateral gear stiffness. Again the active system behaves well in the range from below 1/4 of the nominal stiffness to above 2 times the nominal. The passive system is quite sensitive to KPH, with an optimum value at about 60% of the nominal value. At this KPH, the passive response is about 6 times greater than the active system (0.009 rad. vs. 0.0015 rad.).

4. DTH - The results of varying torque arm backlash are shown in Figure 31. The solid curves represent nominal values for CP1 and CP2, the piston-cylinder friction. The dashed curves represent zero friction. The nominal value of DTH, as measured in program tests, corresponds approximately to the value for the T-37 gear that was tested at AFFDL, as reported in Reference 3. It can be seen that the passive gear is quite sensitive to increased backlash, whereas the active system with nominal
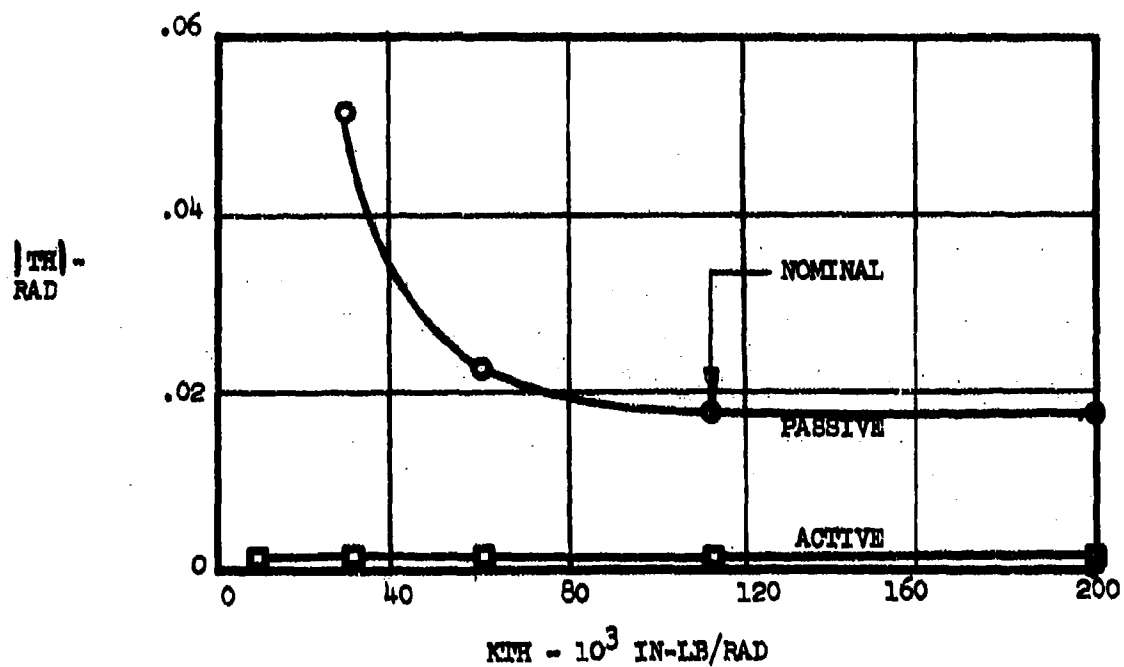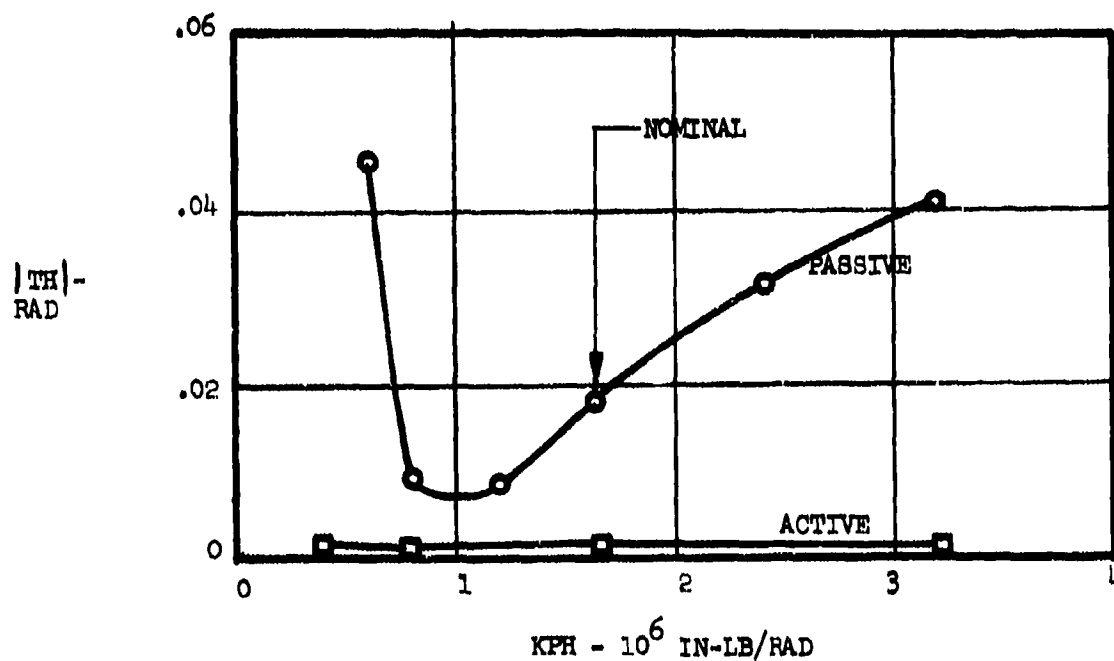
FIGURE 29 - VARIATION OF TORQUE ARM STIFFNESS, KTH

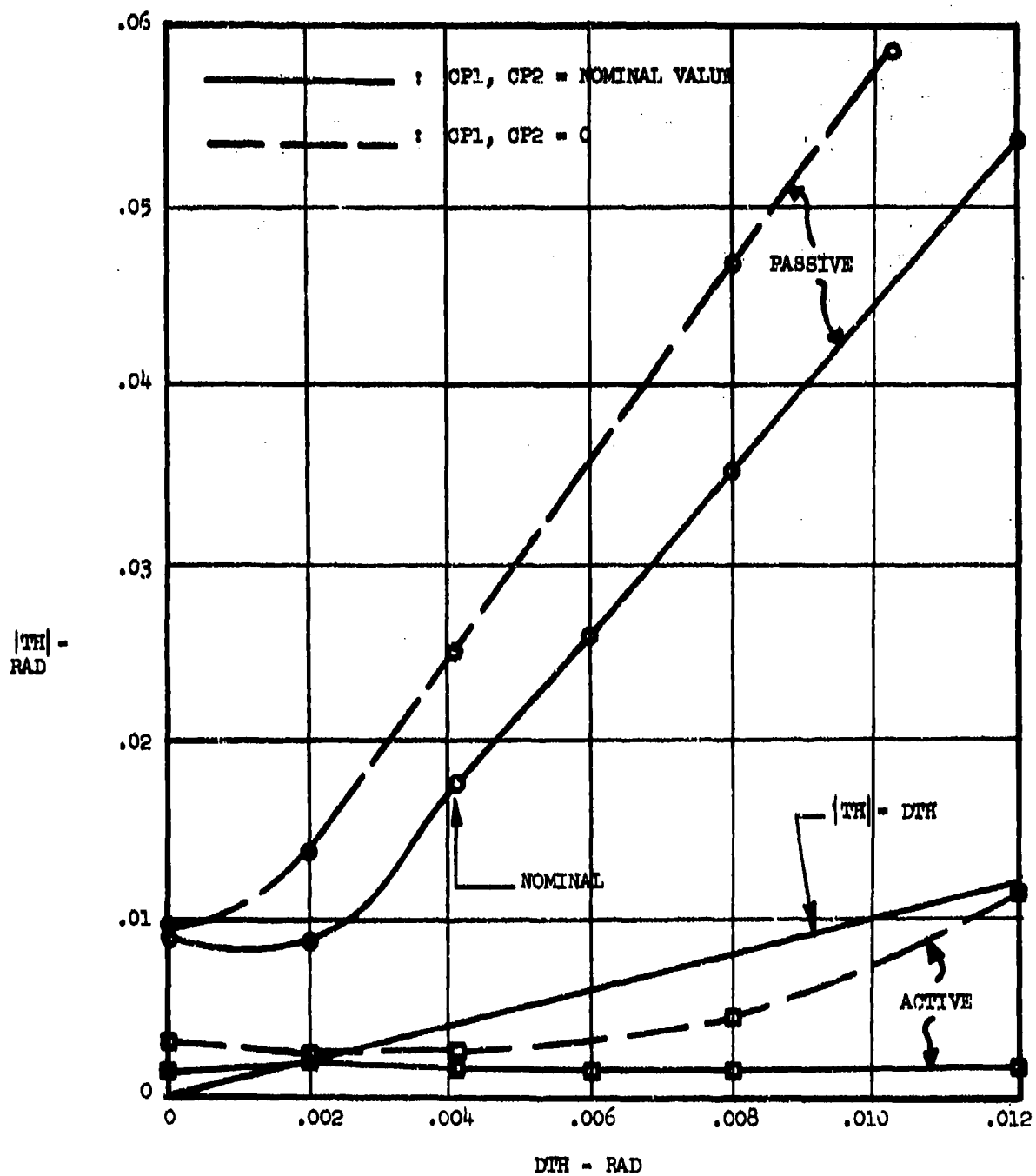FIGURE 30 - VARIATION OF LATERAL GEAR STIFFNESS, KPH

50

FIGURE 31 - VARIATION OF TORQUE ARM BACKLASH, DTH

51

friction is completely unaffected by the backlash up to 3 times the nominal value. Only with zero piston-cylinder friction is the active system somewhat sensitive to large backlash. This is because the active system utilizes the friction force to transmit forces from the actuator to the axle within the backlash region. When this friction is zero, actuator forces are transmitted to the axle only when the deadband region is traversed. Thus, the outer cylinder "bounces" back and forth across the deadband region to stabilize |TH| to a value less than DTH. However, even at three times the nominal backlash and zero friction, the active system stabilizes |TH| to within the magnitude of the backlash DTH (straight line curve through origin in Figure 17). From Figure 31 it is clear that the active system, even with zero friction, has a high degree of tolerance for increased torque arm backlash.

5. **CP** - The sensitivity of the results to piston-cylinder friction CP is indicated in Figure 32. The backlash DTH is fixed at the nominal value for these results. CP1, the constant on Coulomb type friction is varied while CP2, the friction proportional to gear side load, is held constant at either zero or the nominal value. The active system appears to have a slightly improved performance at zero CP2, while the opposite is true for the passive gear. The passive gear becomes significantly more stable at values of CP1 greater than 40-50 in-lbs. Even at these friction levels, however, the active system reduces |TH| response to less than 1/4 the passive value. Furthermore, the performance of the active system is quite insensitive to the magnitude of the piston-cylinder Coulomb friction CP1. However, it should be recalled from Figure 31 that the performance of the active system starts to deteriorate slightly at zero friction with 3 times the nominal backlash.

6. **BF and BPH** - Figure 33 shows the results of varying the structural damping coefficients BF (fuselage torsional damping) and BPH (gear/ fuselage lateral damping). Both values are nominally set at 4% of critical. In Figure 33, both constants are varied together, keeping a constant percent of critical damping for each. The response of both the
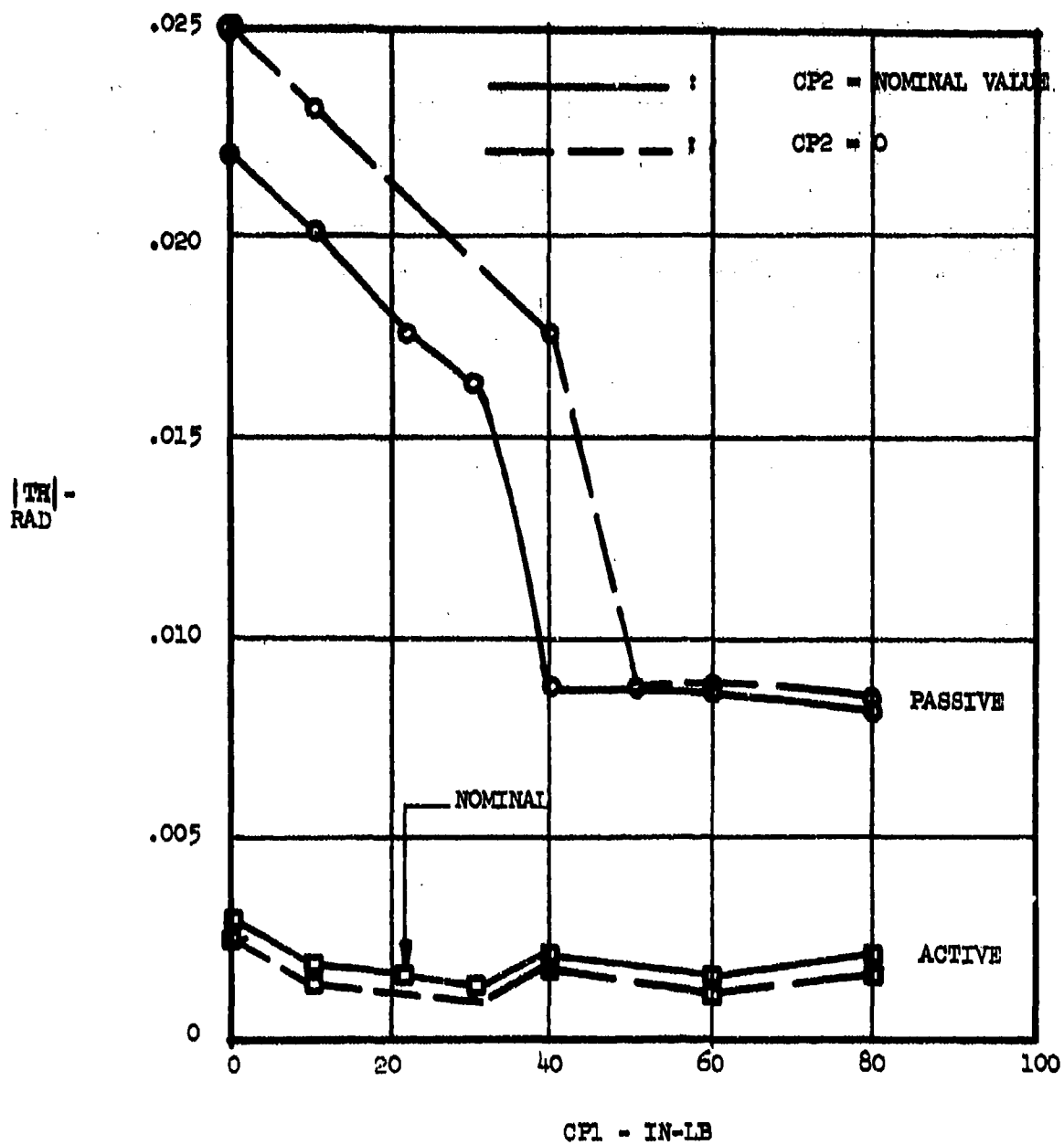
FIGURE 32 - VARIATION OF PISTON-CYLINDER FRICTION, CP1
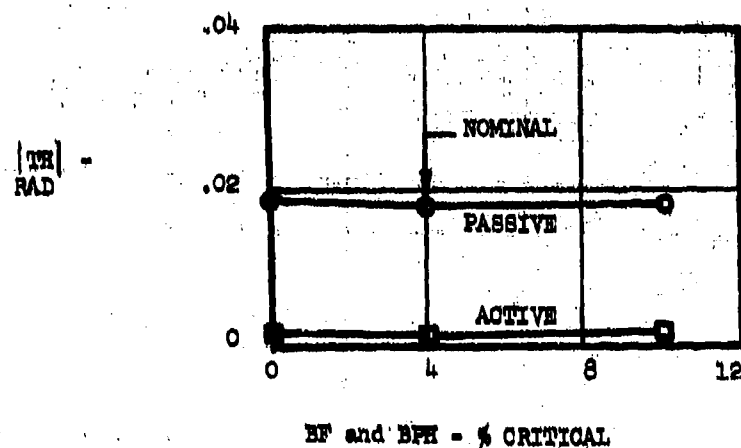
53

FIGURE 33 - VARIATION OF FUSELAGE AND LATERAL GEAR
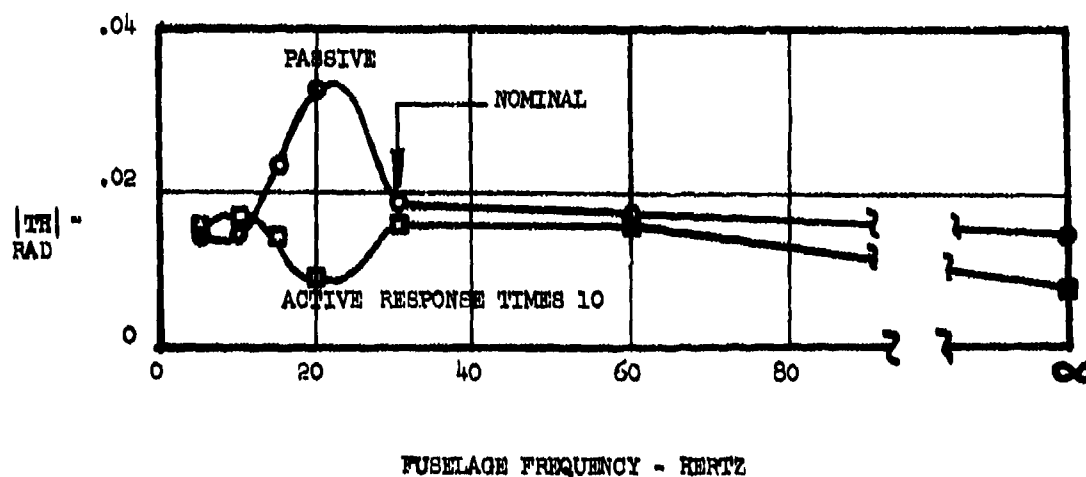DAMPING, BF AND BPH

FIGURE 34 - VARIATION OF FUSELAGE NATURAL FREQUENCY

active and passive systems is virtually unchanged in the range from 0 to 8% of critical. This indicates that the structural damping energy absorbed is insignificant in comparison to the energies from torsional friction and actuator damping (either passive or active).

7. ITH2 - Figure 34 indicates the degree to which the passive and active system results depend on the natural frequency of the local fuselage structure. This frequency was varied by changing the local fuselage inertia ITH2, since a reasonable estimate of the correct fuselage stiffness KF is available from Reference (3). The nominal value of ITH2 used corresponds to a fuselage natural frequency of 30 Hz. The right hand data point in Figure 34 corresponds to a completely rigid fuselage. From the figure it can be seen that the results are insensitive to this parameter except in the range from 10-30 Hz. In this region the passive system performance deteriorates appreciably and the active system improves somewhat. Since the shimmy frequency is in the neighborhood of 12 to 20 Hz, it is to be expected that fuselage natural frequencies in this same region would significantly couple with the gear modes and alter the shimmy response amplitudes. However, it is not clear why the passive system becomes less stable and the active system more stable. (Note that in Figure 34 the curve plotted for the active system is 10 times the response, so that its variation can be more clearly seen.)

ACTIVE SHIMMY CONTROL SYSTEM DESCRIPTION

A breadboard version of the Active Shimmy Control System described in the previous sections was assembled using for the most part off-the-shelf hardware. The system consists of the following major elements:

o An electro-hydraulic servovalve attached to the existing steering cylinder.

o System feedback sensors:
   (a) Angular accelerometer mounted on the top of the wheel fork.

   (b) Position transducer on the actuator body/piston rod (LVDT).

   (c) Differential pressure transducer on the steering actuator to sense actuator load.

o An electronic signal shaping and gain control network to convert the angular accelerometer and actuator pressure and position LVDT outputs into the desired feedback signal for the servovalve.

Figure 35 shows a schematic diagram of the T-37 steering actuator with the active control system installed. The system utilizes the existing damping orifice ports to attach an adaptor manifold. The manifold mounts the electro-hydraulic servovalve, differential pressure transducer, and actuator position transducer. The aircraft damping orifices are removed, plugs are installed in their place and the pressure and return lines are moved from their connection on the steering actuator body to new ports on the manifold to form the active damper configuration. Thus, the aircraft steering actuator control valve and related passive damping orifices are not used. For comparative system test purposes, the standard aircraft configuration can easily be tested with the added actuator position and load differential pressure instrumentation retained as shown in Figure 36. Detailed instructions for converting between the active and passive systems are contained in Appendix A.
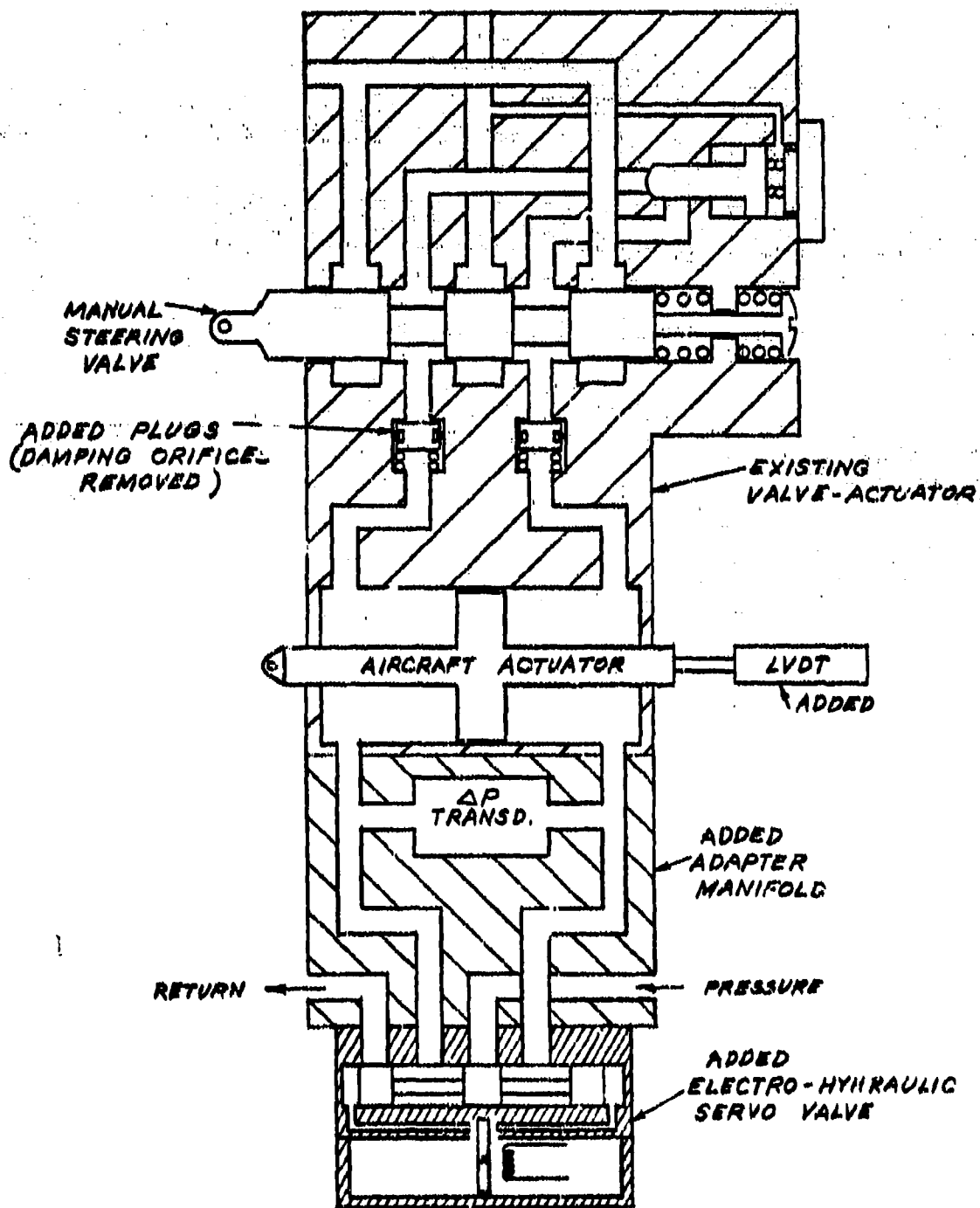
56

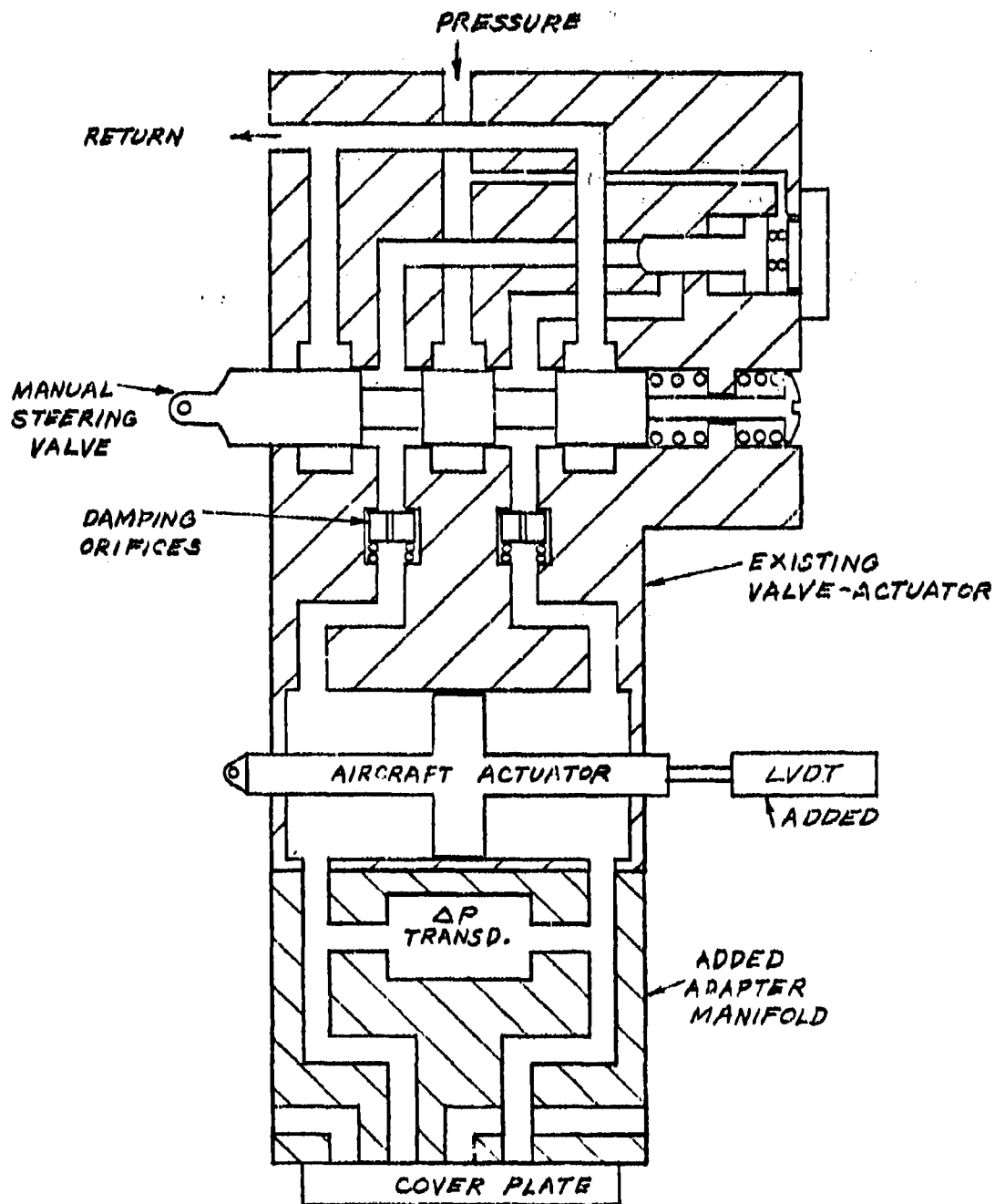FIGURE 35 - T-37 NOSE STEERING ACTUATOR IN ACTIVE CONFIGURATION

FIGURE 36 — T-37 NOSE STEERING ACTUATOR IN PASSIVE CONFIGURATION

58

The complete active control system is shown in Figure 37. The angular accelerometer mounts to the top of the wheel fork to feed back rotational acceleration of the fork about the strut steering axis. The output signals from the differential pressure transducer and LVDT mounted on the actuator also feed back to the controller. Nose gear steering for the shimmy tests is accomplished through electrical commands to the active system.

The specific system hardware consists of the following:

o Angular accelerometer: Systron-Donner model 4575-CG servo accelerometer; range, $\pm$ 500 rad. per sec^2.

o Actuator displacement sensor: Schaevitz model 2002XS-D linear variable differential transducer; range, $\pm$ 2 in.

o Differential pressure sensor: Standard Controls Model 210-60-010-06 strain gage differential pressure transducers; range, $\pm$ 3000 psig.

o Linear accelerometers:

(a) Yoke angular acceleration (2 units): Statham Model A400TC-15 linear strain gage accelerometer; range, $\pm$ 15g

(b) Lateral acceleration: CEC Model 4-202-0001 linear strain gage accelerometer; range, $\pm$ 25g

A block diagram of the complete breadboard electronics system is shown in Figure 38. Control and instrumentation electronics are housed in a pair of 7" x 19" rack-mount card cages. All necessary d.c. power supplies are included so that only 115 vac. 60 Hz external power is required. System electronics are packaged in modular functional-unit cards. A fully detailed circuit diagram is shown in Appendix B.
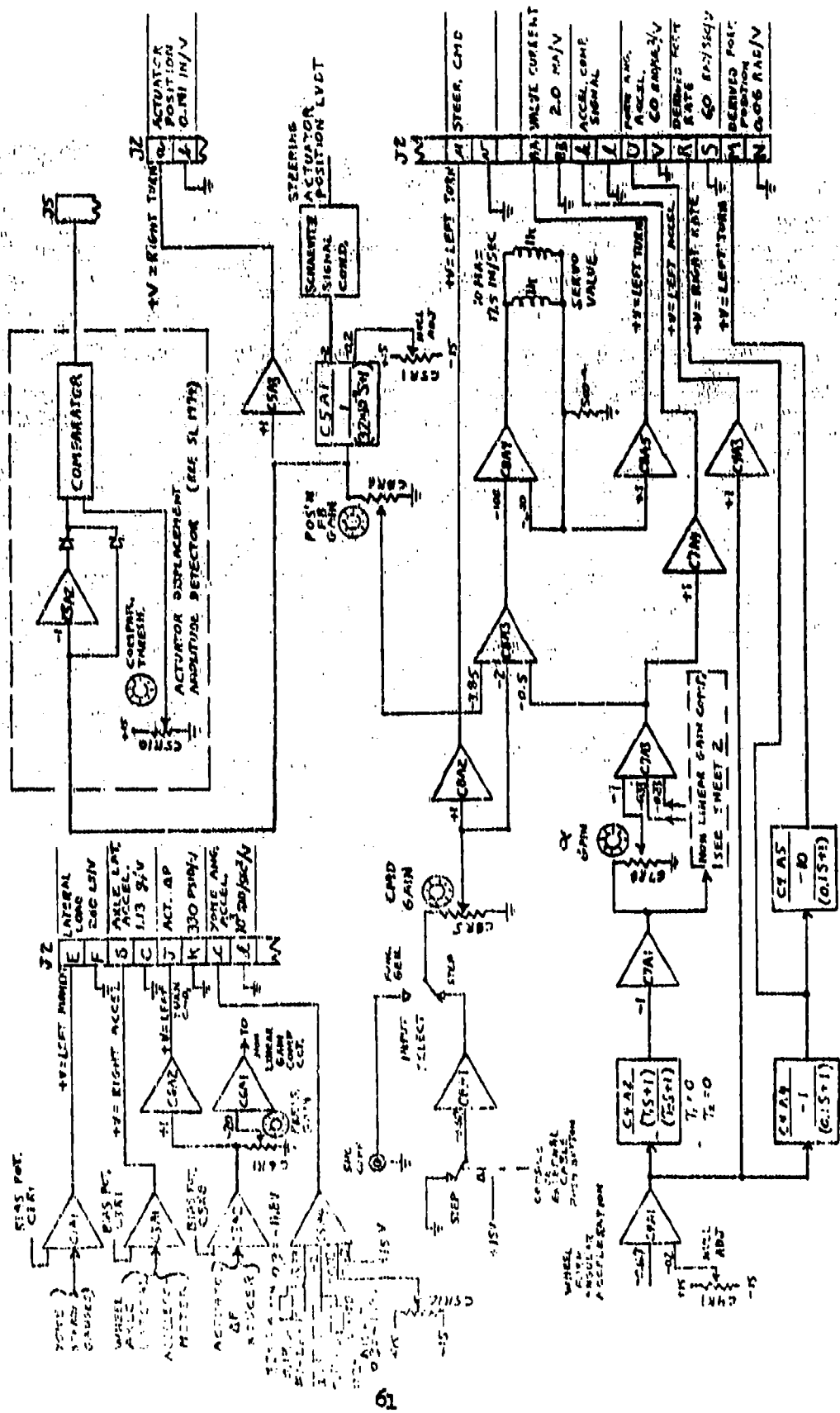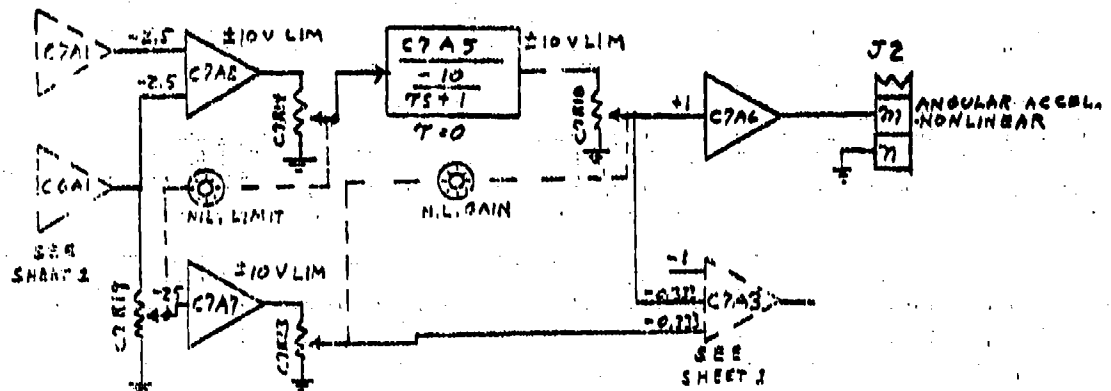
59

FIGURE 37 - SCHEMATIC OF ACTIVE CONTROL SYSTEM

60

FIGURE 38 - BLOCK DIAGRAM, ACTIVE SHIMMY CONTROL SYSTEM

61

NONLINEAR GAIN COMPENSATION

I. COMPONENT DESIGNATION EXAMPLE

CARD 8
AMPLIFIER 4

FIGURE 38 - BLOCK DIAGRAM, ACTIVE SHIMMY CONTROL SYSTEM (Cont'd)

62

Card 8 is the central focus of the active control function. Summing amplifier A3 and driver A4 comprise the forward path of the controller. A3 receives a command input from the steering circuit on the same card and two feedback signals (wheel fork angular acceleration and actuator position). Actuator position is buffered on Card 5 before entering the loop on Card 8. Wheel fork angular acceleration receives linear shaping on Card 4 and non-linear gain adjustment on Card 7, before entering the loop. Actuator pressure, after shaping on Card 6, enters the non-linear gain circuit, acting primarily as a bias signal to remove the non-linear gain path on angular acceleration during steering and assymetric loading conditions. Signals used both for instrumentation and control functions are line driver isolated to prevent damage to test hardware from inadvertent recording system shorts.

Twelve signals are shown wired to a connector for interface to the test facility instrumentation tape-recorder. The lateral load strain gage bridge is amplified on Card 1, the lateral accelerometer on Card 3. The actuator pressure signal is amplified on Card 3 and isolated on Card 6. Angular acceleration is buffered, shaped for control use, and isolated for instrumentation on Card 4. It is also integrated twice in the frequency band of interest to provide fork rate and displacement for recording. The actuator position signal, as mentioned above, is buffered and isolated on Card 5. Conditioned by an absolute value circuit and a comparator, it is also available as an overrange warning or automatic shutdown signal. The two sensors arranged to measure yoke angular acceleration are summed and buffered for recording on Card 5.

Figures 39 and 40 show two views of the hardware connected to the steering actuator. In Figure 39 the servovalve can be seen mounted to the manifold block. Below the manifold block are visible the LVDT and the brackets attaching the LVDT rod to the steering actuator piston at both ends. The body of the LVDT is attached to the bottom of the manifold block, which in turn mounts on the steering actuator cylinder. Figure 40 shows the
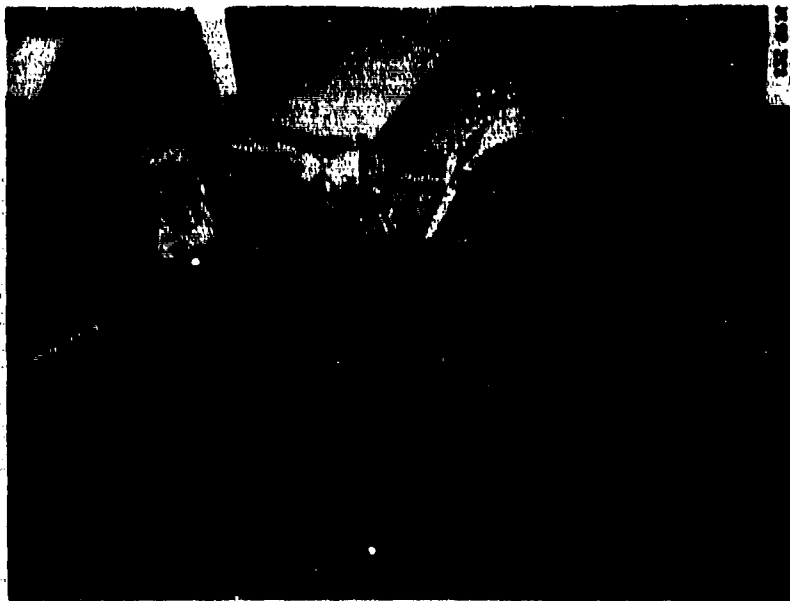
63

FIGURE 40 - SERVOVALVE INSTALLATION
LEFT SIDE

FIGURE 39 - SERVOVALVE INSTALLATION,
RIGHT SIDE

64

mounting of the manifold block to the steering actuator; the pressure and return line ports on the manifold block can also be seen.

Figures 41 and 42 show two views of the landing gear with all the active system hardware and test instrumentation installed. In Figure 41 the torsional accelerometer can be seen mounted on a bracket attached to the top rear of the wheel fork. The lateral accelerometer mounted on the left end of the axle is also visible. On the right web of the trunnion yoke assembly an accelerometer can be seen; this is used in conjunction with one on the other side phased so that yoke angular acceleration can be measured.

Figure 42 is a left side view in which the hydraulic system accumulators can be seen at the top of the photograph. The rectangular box mounted to the gear test fixture just above the gear is the LVDT signal conditioning module. The hydraulic lines are shown attached to the manifold block, which in turn, is mounted to the steering actuator.

Figures 43 and 44 are photographs showing front and rear views of the electronics module. This module contains all the feedback gain control and signal shaping circuitry, as well as all the instrumentation signal processing electronics and necessary D.C. power supplies. The front panel of the electronics module contains 5 potentiometers for adjusting the following active system control parameters:

  o Feedback linear gain, GISMAL

  o Feedback nonlinear gain, GIBIG

  o Nonlinear gain limit, THDDLM

  o Control loop position negative feedback
   gain constant, K7

  o Pressure feedback nonlinear gain biasing constant, K9
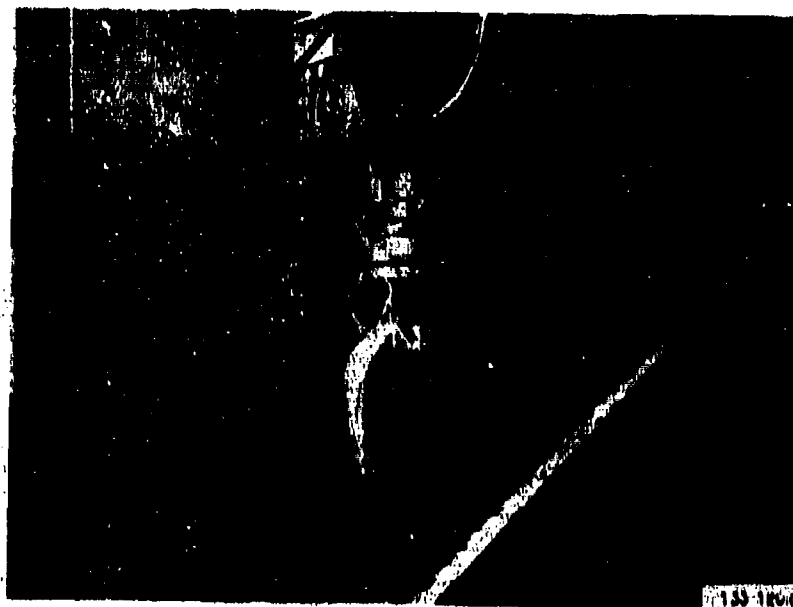
FIGURE 41 - LANDING GEAR, REAR VIEW

FIGURE 42 - LANDING GEAR, LEFT SIDE VIEW

66

The other two potentiometers shown in Figure 43 control the following test parameters:

o Steering angle to trigger automatic gear lift signal, if desired

o Amplitude of electrical steering angle command for active system steering

Lead-lag feedback signal shaping can be accomplished by means of plug-in capacitors on the front panel. In addition, the front panel contains provisions for patching any of the basic instrumentation signals into the rear panel outputs for the 8-track Brush recorder. One such connection is shown from card 3 to card 13 in Figure 43. Both a step input and sinousoidal electrical steering command inputs can be selected at the electronics module. The step command is used in the active system tests to steer the gear electrically.

Figure 44 shows the 8 pairs of connections to the 8-track Brush recorder. The two rectangular connectors on the top rear panel in Figure 44 are for the wire bundles leading to the gear and to the FM tape-recorder. The three smaller circular connectors on the top rear panel are for the following:

o Function generator input (for sinusoidal steering command)

o Output for automatic carriage lift triggered by preset gear responsible amplitude

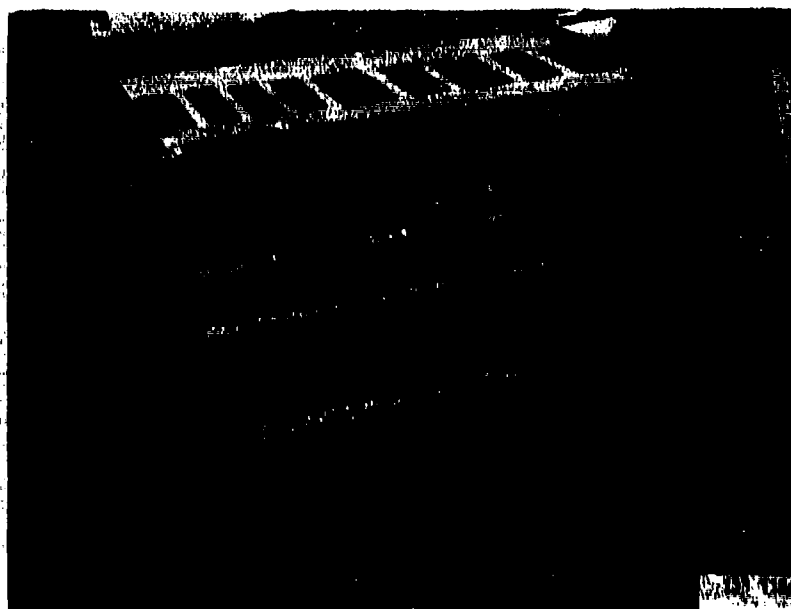o Hand-held push-button for initiating step input steering commands
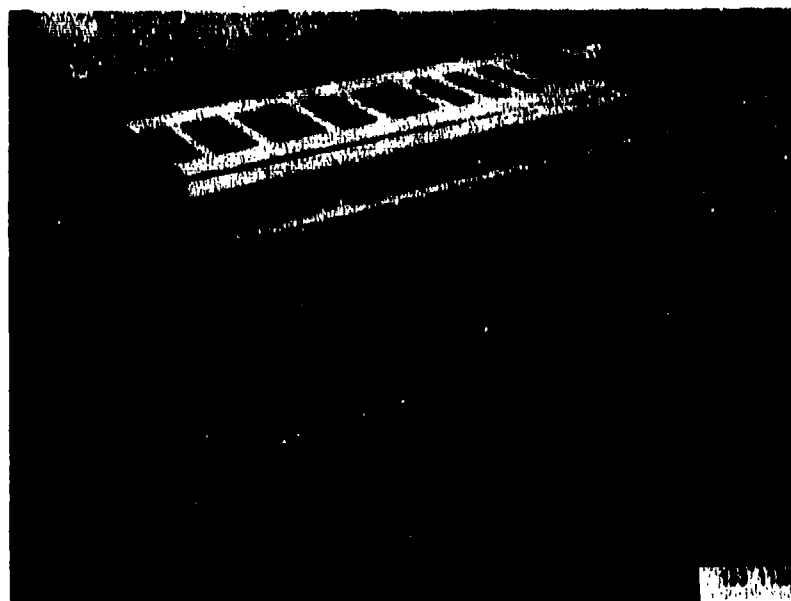
FIGURE 43 - ELECTRONICS MODULE, FRONT VIEW

FIGURE 44 - ELECTRONICS MODULE, REAR VIEW

68

Test Objectives

The objectives of the test program are to:

o Determine the shimmy characteristics of the passive gear.

o Demonstrate the anti-shimmy capabilities of the active system including its performance during nose gear steering.

o Provide data for evaluating the capability of the analytical model.

o Provide data by which limitations associated with the system and/or significant phenomena, not included in the analyses, can be defined.

Description of Test Set-Up

All tests were performed in the USAF Flight Dynamics Laboratory in Dayton, Ohio. The T-37 gear assembly, modified to allow both passive and active system operation, was installed in a forward fuselage section of a T-37 airplane. The fuselage section, in turn, was installed in the carriage of the 192 inch dynamometer such that the gear and tire had the proper geometric trail for the strut extention values to be tested.

A 1500 psi hydraulic source, to simulate a T-37 ships system, was used to power the steering actuator using MIL Standard 5606 hydraulic fluid. A 115 volt, 60 Hz alternating current electrical source was used to power the breadboard active shimmy control system and associated instrumentation. Torsional gear excitation was provided by a cable pull system for the passive gear and by electrical steering step inputs for the active gear. In addition, wheel imbalance displaced laterally from the wheel centerline was used to provide steady state cyclic inputs.

The breadboard electronics module was rack mounted and powered by a 110V, 60 Hz, electrical source. The electronics module was connected via cables

to the landing gear and to the F.M. tape-recorder interface. The tape-recorder is remotely located in the data room and is a standard 14 channel unit with standard speeds, single-ended input with a 100K ohm input impedance. The contractor supplied the Time Code Generator. Wright Field furnished an 8-Channel Brush Recorder and an oscilloscope local to the electronics for monitoring and direct-write recording. Banana jacks are provided on the rear of the breadboard electronics module for the Brush Recorder interface. The electronics module provides a non-latching, low power relay closure as a function of a selectable absolute steering angle for interface with Wright Field's gear-lift circuitry for use as an automatic safety feature when necessary.

Instrumentation

Table 3 shows a list of instrumentation utilized including types, location, purpose and specifications. Table 4 delineates the actual signals recorded on magnetic tape, including scale factors and tape attenuation factors. Also shown are the 8 responses recorded on the Brush Recorder for quick-look analysis.

Test Procedure

The following sequence of operations was followed for each shimmy test

1. Adjust the carriage for the desired strut extension.

2. Spin the drum up to a ground speed of 40 mph.

3. Activate the recording system.

4. Verbally record the run number and identifying information, on the tape-recorder.

5. Start the Brush Recorder (High Speed, 200 mm/sec.).

6. Lower the gear support carriage onto adjustable stops, bringing the tire into contact with the driver with the desired vertical load.

TABLE 3   INSTRUMENTATION TYPES, LOCATION, PURPOSE AND SPECIFICATIONS

TYPE	LOCATION	PURPOSE	SPECIFICATION
Active Control System			
1. Angular accelerometer	Top of wheel fork	Feedback rotational acceleration of the fork about strut steering axis. Integrated to obtain rate and position.	Systron-Donner Model 4575-CG Servo-Accelerometer; range ± 500 rad/sec²
2. Differential Pressure Transducer	Steering Actuator	Feedback to the controller. Measure actuator load.	Standard Controls Model 210-60-010-06 strain gage differential pressure transducer. Range ± 3000 psig.
3. Linear Variable Differential Transducer (LVDT)	Steering Actuator	Feedback to the controller. Determine steering unit position.	Schaevitz Model 2002XS-D LVDT range ± 2 inches.
Strut Mounted			
4. Linear Accelerometer	Trunnion yoke	Accelerometers mounted on opposite sides such that their output signals can be summed to sense rotational acceleration of yoke.	Statham Model A400TC-15 linear strain gage accelerometer; range, ± 15G, 700 Hz.
5. Linear Accelerometer	Trunnion yoke		
6. Strain Gage	Trunnion yoke	Determine lateral load	BLH EA-13-250BG-120 120 Ω Strain Gage Gage factor = 2.9
7. Linear Accelerometer	Side of wheel fork	Determine lateral acceleration	CEC Model 4-202-0001 Linear-strain gage accelerometer; range ± 25G, 650 Hz

71

TABLE 4 - TAPE RECORDING SET-UP

Tape Channel	Brush Channel	Signal	Source	Tape Attenuation	Scale Factor
1	2	CMD	C8A2	.1	.0735 In/V
2	1	ΔX	C5A3	.3	.141 In/V
3	3	$\ddot{\Theta}$	C4A3	.1	60 rad/sec^2/V
4	4	$\dot{\Theta}$	C4A4	.6	6 rad/sec/V
5	5	Θ	C4A5	.25	.06 rad/V
6	6	ΔP	C6A2	.25	330 psid/V
7		Ay		.1	1.13 g/V
8	8	Yoke Ang. Accel.	C5A4	1	10^3/rad/sec^2/V
9		Yoke Lat. Load		.25	260 lb/V
10	7	Δi	C8A5	.2	2 ma/V
11		Strut Pressure		1	250 psi/V
12		Nonlin.Accel.Fdback*	C7A6	.1	
13		Drum Speed		(1)	100 mph/V
14		Time Code			
Edge		Voice			

* Filtered acceleration feedback signal beginning with Run 119

72

7. After 2-3 seconds of free rolling on the drum, input a step electrical steering command using the hand held push button control. (For passive system testing, a cable-pull system is used to directly disturb the wheel fork in torsion). With the active system, a step command of 3° is used for cases with wheel imbalance, and 6° for cases without imbalance. Two types of input are used: (a) as brief an input as possible (≈.2 sec.), (b) Sustained input (≈ 2 sec).

8. Raise the gear support carriage.

9. Stop the Brush-Recorder.

10. Stop the Tape-Recorder.

11. Accelerate the drum to 60 mph.

12. Repeat steps 3 through 10.

13. Continue above steps up to 120 mph in 20 mph increments.

For each run, the tire is on the drum for around 10 seconds. About 5 minutes are required to accelerate the drum each 20 mph increment. Tire heating and wear presented no problems.

Test Sequence

The passive shimmy tests were performed from 16 June 1975 to 20 June 1975. The active system testing occurred from 23 June 1975 to 27 June 1975. Table 5 shows the run log for the passive system tests. Runs 1-12 were performed with the gear in the mid position and nominal torsional backlash. No indications of free shimmy were present. The next series of runs (13-18) were made with the strut in the 3/4 extended position. A slight amount of shimmy is evident at lift-off at 120 mph. Runs 19-23 were made with the strut fully extended. Free shimmy is evident at 100 and 120 mph.

73

TABLE 5 - PASSIVE SHIMMY TESTS

RUN	SPEED MPH	STRUT PRESS. PSI	STRUT* EXT SHOWING INCH	TIRE PRESS. PSI	TIRE IMBAL. IN-OZ.	BACK-LASH RAD.	NOTES
1	40	105	3.9	35	0	NOM	
2	60						
3	80						
4	80						NO
5	100						DATA
6	100						
7	120	↓	↓	↓	↓	↓	
8	40	105	3.9	35	10	NOM	
9	60						
10	80						
11	100						
12	120	↓	↓	↓	↓		
13	40	72	5.67	35	10	NOM	
14	40						
15	60						
16	80						
17	100						
18	120	↓	↓	↓	↓	↓	

* "Strut Ext. Showing" fully extended = 7.5 inch
" compressed = 0.25 inch

74

TABLE 5 — PASSIVE SHIMMY TESTS (Cont'd)

RUN	SPEED MPH	STRUT PRESS PSI	STRUT* EXT. SHOWING INCH	TIRE PRESS. PSI	TIRE IMBAL. IN-OZ.	BACK-LASH RAD	NOTES
19	40	53	7.25	35	10	NOM	
20	60	↓	↓	↓	↓	↓	
21	80						
22	100						Shimmy
23	120						Shimmy
24	40	53	7.0	50	10	NOM	
25	60	↓	↓	↓	↓	↓	
26	80						
27	100						Shimmy
28	120						Shimmy
29	40	50-53	7.3	50	10	NOM	
30	60	↓	↓	↓	↓	↓	
31	80						Shimmy
32	100						Shimmy
33	80	50-53	7.3	50	0	NOM	
34	100	↓	↓	↓	↓	↓	
35	120						Shimmy
36	110						
37	40	51	7.3	50	0	$\pm$0.028	
38	60	↓	↓	↓	↓	↓	
39	80						Shimmy
40	100						Shimmy
41	120						Shimmy
42	LAND AT 70 MPH DEC. SPD. TAKE OFF AT 50 MPH						

TABLE 5 - PASSIVE SHIMMY TESTS (Cont'd)

RUN	SPEED MPH	STRUT PRESS. PSI	STRUT* EXT. SHOWING INCH	TIRE PRESS. PSI	TIRE IMBAL. IN-OZ.	BACK-LASH RAD	NOTES
43	40	108	3.9	50	0	±.024	
44	60	↓	↓	↓	↓	↓	
45	80						
46	100						Shimmy
47	120	↓	↓	↓	↓	↓	Shimmy
48	40	108	3.9	50	10	±.024	
49	60	↓	↓	↓	↓	↓	
50	80						Shimmy
51	100						Shimmy
52	120	↓	↓	↓	↓	↓	Shimmy
53	40	108	3.9	50	10	±.016	
54	60	↓	↓	↓	↓	↓	
55	80						
56	100						Shimmy
57	120	↓	↓	↓	↓	↓	Shimmy

76

Runs 24-32 repeat the previous series with the tire pressure increased to 50 psi (from 35 psi). Again shimmy is evident at 100 and 120 mph. The above runs were made with 10 in.-oz. wheel imbalance. Runs 33-36 were done with zero wheel imbalance; some shimmy was evident at 120 mph. At this point, the torsional backlash was increased from ± 0.012 rad. to ± 0.028 rad for Runs 37-42. Free shimmy at 100 and 120 mph is evident with some tendency to shimmy at 80 mph.

The remaining passive runs were done with the gear in the mid position. Runs 43-47 had zero tire imbalance, Runs 48-52 had 10 in-oz tire imbalance, and Runs 53-57 had an intermediate level of backlash. In all these cases the gear shimmies at 100 and 120 mph, and in some cases at 80 mph.

Table 6 shows the run log for the active system tests. Runs 101 through 118 wer· performed with the basic active system without nonlinear gain control. The K_a parameter shown in Table 6 is related to the linear feedback constant G1SMAL as follows:

$$G1SMAL = 0.0063 \times K_a$$

Since the fully extended gear position was the most critical for the passive system, this position was used for the active system tests until the feedback signal shaping was finalized. While the performance of the basic system was acceptable in that no shimmy oscillations were evident, the system had a 180 Hz structural mode that was being driven to unacceptable levels at feedback gains that were lower than desired for good damping of the shimmy mode.

In an effort to eliminate the deleterious effects of the 180 Hz mode, a Twin-T notch filter was designed, fabricated and installed. Runs 119-124 were performed with this filter in the feedback loop. This approach was successful in attenuating the 180 Hz responses, but the additional phase lags, introduced by the notch filter at lower frequencies, resulted in a 40 Hz mode of unacceptable amplitude.

TABLE 6 - ACTIVE SHIMMY TESTS

RUN	SPEED MPH	STRUT PRESS. PSI	STRUT EXT. SHOWING INCH	TIRE PRESS. PSI	TIRE IMBAL. IN-OZ.	BACK-LASH RAD.	K_a	NOTES
101	40	53	7.3	50	10	Nom.	0.3	NOTHING ON TAPE
102	60	↓	↓	↓	↓	↓	↓	
103	80							
104	40	53	7.3	50	10	Nom.	0.5	
105	60	↓	↓	↓			↓	
106	80							
107	100							
108	120							
109	40	53	7.3	50	10	Nom.	0.3	
110	60	↓	↓	↓			↓	
111	80							
112	100							
113	120							
114	40	53	7.3	50	0	Nom.	0.3	Oil hot, 178° F @ end of run
115	60	↓	↓	↓	↓	↓	↓	
116	80							
117	100							
118	120							
119	40	53	7.3	50	0	Nom.	0.7	Added notch filter, doubled K_a gain range
120	40	↓	↓	↓	↓	↓	0.5	
121	60						↓	
122	80							
123	100							
124	120							

78

TABLE 6 - ACTIVE SHIMMY TESTS (Cont'd)

RUN	SPEED MPH	STRUT PRESS. PSI	STRUT EXT. SHOWING INCH	TIRE PRESS. PSI	TIRE IMBAL. IN-OZ.	BACK-LASH RAD.	K_a	NOTES
125	40	53	7.3	50	0	Nom.	0.3	Removed notch filter. Added lag (48), lead (96) filter
126	60	↓	↓	↓	↓	↓	↓	
127	80							
128	100							
129	120							
130	40	53	7.3	50	10	Nom.	0.3	
131	60	↓	↓	↓	↓	↓	↓	
132	80							
133	100							
134	120							
135	80	53	7.3	50	10	Nom.	0.3	Replaced servo valve
136	100	↓	↓	↓	↓	↓	0.3	
137	100						0.5	No mag. tape
138	120						0.3	
139	120						0.5	
140	80						0.5	
141	40	53	7.3	50	10	Nom.	0.5	Doubled i'oa'n loop gain (to 16 Hz)
142	60	↓	↓	↓	↓	↓	↓	
143	80							
144	100							
145	120							

TABLE 6 - ACTIVE SHIMMY TESTS (Cont'd)

RUN	SPEED MPH	STRUT PRESS. PSI	STRUT EXT. SHOWING INCH	TIRE PRESS. PSI	TIRE IMBAL. IN-OZ.	BACK-LASH RAD.	K_α	NOTES
146	40	53	7.3	50	0	Nom.	0.3	Removed lag-lead filter; installed bridged-T, tuned to - 180 Hz
147	40						0.3	
148	40						0.5	
149	60						0.3	
150	60						0.5	
151	80						0.3	
152	80						0.5	
153	80						0.7	
154	100						0.3	
155	100						0.5	
156	100						0.7	
157	120						0.3	
158	120						0.5	
159	120						0.7	
160	40	53	7.3	50	10	Nom.	0.7	
161	60							
162	80							
163	100							
164	120							
165	40	53	7.3	50	0	0.028	0.7	
166	60							
167	80							
168	100							
169	120							

TABLE 6 - ACTIVE SHIMMY TESTS (Cont'd)

RUN	SPEED MPH	STRUT PRESS. PSI	STRUT EXT. SHOWING INCH	TIRE PRESS. PSI	TIRE IMBAL. IN-OZ.	BACK-LASH RAD.	K_a	NOTES
170	40	53	7.3	50	10	0.028	0.7	
171	60	│	│	│	│	│	│	
172	80	│	│	│	│	│	│	
173	100	│	│	│	│	│	│	
174	120	↓	↓	↓	↓	↓	↓	
175	40	53	3.9	50	10	0.028	0.7	
176	60	│	│	│	│	│	│	
177	80	│	│	│	│	│	│	
178	100	│	│	│	│	│	│	
179	120	↓	↓	↓	│	│	│	
180	40	109.5	3.9	50	0	0.028	0.7	
181	60	│	│	│	│	│	│	
182	80	│	│	│	│	│	│	
183	100	│	│	│	│	│	│	
184	120	↓	↓	↓	↓	↓	↓	
185	40	53	7.3	50	0	Nom.	0.7	
186	60	│	│	│	│	│	0.7	
187	80	│	│	│	│	│	0.7	
188	80	│	│	│	│	│	1.0	
189	80	│	│	│	│	│	1.2	
190	80	│	│	│	│	│	1.4	
191	80	│	│	│	│	│	1.7	
192	80	│	│	│	│	│	0.5	
193	80	│	│	│	│	│	0.3	
194	80	↓	↓	↓	↓	↓	0.2	

TABLE 6 - ACTIVE SHIMMY TESTS (Cont'd)

RUN	SPEED MPH	STRUT PRESS. PSI	STRUT EXT SHOWING INCH	TIRE PRESS. PSI	TIRE IMBAL. IN-OZ.	BACK-LASH RAD.	K_a	NOTES
195	80	53	7.3	50	0	Nom.	0.1	
196	80	↓	↓	↓	↓	↓	0.05	
197	80						0	
198	80	53	7.3	50	0	Nom.	0.7	5 Hz Sine
199	80							10 Hz Sine
200	80							15 Hz Sine
201	80							20 Hz Sine
202	80							25 Hz Sine
203	80							30 Hz Sine
204	80							40 Hz Sine
205	80	↓	↓	↓	↓	↓	↓	50 Hz Sine
206	Servo Freq. Response							
207	Filter Freq. Response							

At this point in the testing the notch filter was removed from the system and a lag-lead network, tuned to 48 Hz and 96 Hz respectively, was installed. Runs 125-145 were made with this feedback configuration. At Run 135 th servo-valve was replaced with a spare unit, since the system was exhibiti... sporadic drifting away from neutral with the wheel off the drum and no feedback or steering commands applied to the valve. Apparently the valve had been contaminated at some point in the previous test series. The new valve eliminated the drifting problem, which never reappeared during the remainder of the active system tests.

In an effort to achieve tighter damping control at the higher driving frequencies, the actuator position loop feedback gain constant (K7 in the analytical model) was doubled, beginning at Run 141. This increased the cutoff frequency for the position loop to 16 Hz. The lag-lead network suppressed the 180 Hz mode adequately, but the damping performance with wheel imbalance was reduced from that of the basic system.

Finally, a more refined Bridged-T notch filter was employed in conjunction with the 16 Hz position loop. This system sharply attenuated the 180 Hz mode, allowing an increase in the nominal feedback gain from $K_a = 0.3$ to 0.7, and also damped the 40 Hz mode. This final configuration is used from Run 146 on. Runs 146-159 are variations in the K_a gain, resulting in the selection of $K_a = 0.7$ as the nominal value.

Runs 160-174 test the system with the gear fully extended, with nominal and increased torsional backlash, and with and without wheel imbalance. Runs 175-184 verify the performance of the system with the gear in the mid position. Runs 185-197 represent extreme variations in feedback gain constant K_a from 0 to 1.7, more than twice nominal. These runs were made with the gear fully extended.

Runs 198-205 consisted of steering the gear electrically with a sinusoidal steering command while the tire was running on the drum at 80 mph. Input

83

steering frequencies from 5 to 50 Hz were run. Finally, Runs 206 and 207 consist of frequency responses for the servovalve and the notch filter, respectively.

Table 7 shows a summary of the pertinent test run numbers for the passive and final active systems, for different combinations of torsional backlash and wheel imbalance. The passive system was never run in the extended position with both wheel imbalance and increased torsional backlash in order to prevent possible damage to the gear. The active system was never run in the mid position with nominal backlash, since this configuration was clearly not critical.

TABLE 7 - SUMMARY OF SHIMMY TEST RUN NUMBERS

STRUT POS.	BACKLASH	WHEEL IMBAL.	PASSIVE	ACTIVE (BRIDGED-T NOTCH ONLY K_α = 0.7)
Ext.	Nom.	0	33-36	153, 156, 159, 185, 186, 187
		10	24-32	160 - 164
	±0.028	0	37-42	165 - 169
		10	————	170 - 174
Mid	Nom.	0	1-7	————
		10	8-12	————
	±0.024	0	43-47	180 - 184
		10	48-52	175 - 179

Test Results

The most important result of the shimmy testing is that the passive system exhibits free shimmy for a number of parametric combinations, whereas none of the active systems tested ever allowed the gear to shimmy. The passive system appears more susceptible to shimmy with tire imbalance. It is felt that the cyclic stroking of the steering actuator caused by wheel imbalance tends to promote cavitation of the actuator, resulting in the very low effective stiffness observed in the output impedance tests performed initially. However, the passive system also shimmies without wheel imbalance.

A set of time history traces for the more pertinent passive and active system shimmy tests is included in Appendix C. Figure 45 illustrates a typical time history of a passive system test wherein free shimmy occurs. The results shown are from Run 32, 100 mph with fully extended gear, wheel imbalance and nominal backlash. The large oscillations evident in axle torsional acceleration are self-induced and occur at a frequency of 22 Hz, even though the frequency of the driving moment due to wheel imbalance is 36 Hz at this speed. This clearly represents a degeneration of the response into free shimmy, and it is alleviated only by steering inputs or by lifting the gear off the drum.

In contrast, Figure 46 shows the corresponding condition with the final active system (Run 163). In this case, not only are the oscillation amplitudes lower, they are also at the wheel imbalance driving frequency of 36 Hz. Note that the transient response following the sharp step input in steering angle is very well damped, lasting only one cycle or less. This is also illustrated in Figure 47, which is the same condition without wheel imbalance (Run 156).

The sharp step steering command used for the active system tests could not be duplicated with the cable pull system used to excite the passive gear. Had it been possible to sharply pulse the passive gear, it is felt that the resulting shimmy oscillations would have provided a graphic contrast to the active system damping evident in Figure 47. With the results available, Figure 48 shows the zero wheel imbalance, passive system response at 100 mph, from Run 34. A slight tendency to go into the shimmy mode is evident.

Another phenomenon of interest is observable in Figure 47. For the active system, the damping of the transient response immediately following the initiation of the step steering command is superior to the damping following the return of steering command to zero. This is probably the result of providing a steady lateral tire load and taking up system backlash when steering away from neutral, while the tire load comes off and the system

ACTIVE AND PASSIVE SHIMMY TESTS
FIELD RUN 32 PASSIVE

TEST 26617   RUN 9   18 SEP 75

FIGURE 45 - PASSIVE SYSTEM TIME HISTORIES, TIRE IMBALANCE

ACTIVE AND PASSIVE SHIMMY TESTS
FIELD RUN 163

TEST 265262   RUN 1   16 SEP 75

CMO
0.02 INCHES/DIV

\NX
0.02 INCHES/DIV

D² THETA/DT²
200 RAD/SEC² /DIV

D THETA/DT
.5 RAD/SEC/DIV

THETA
0.005 RADIANS/DIV
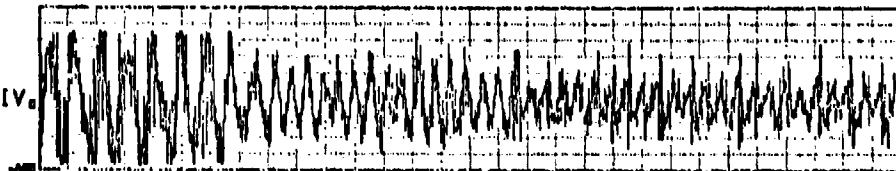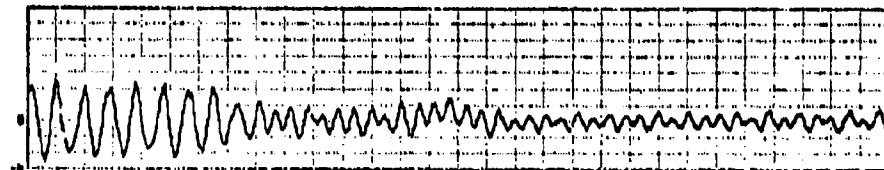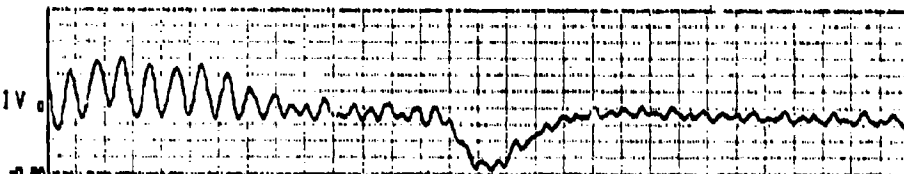
\NP
100 PSID/DIV

SECONDS
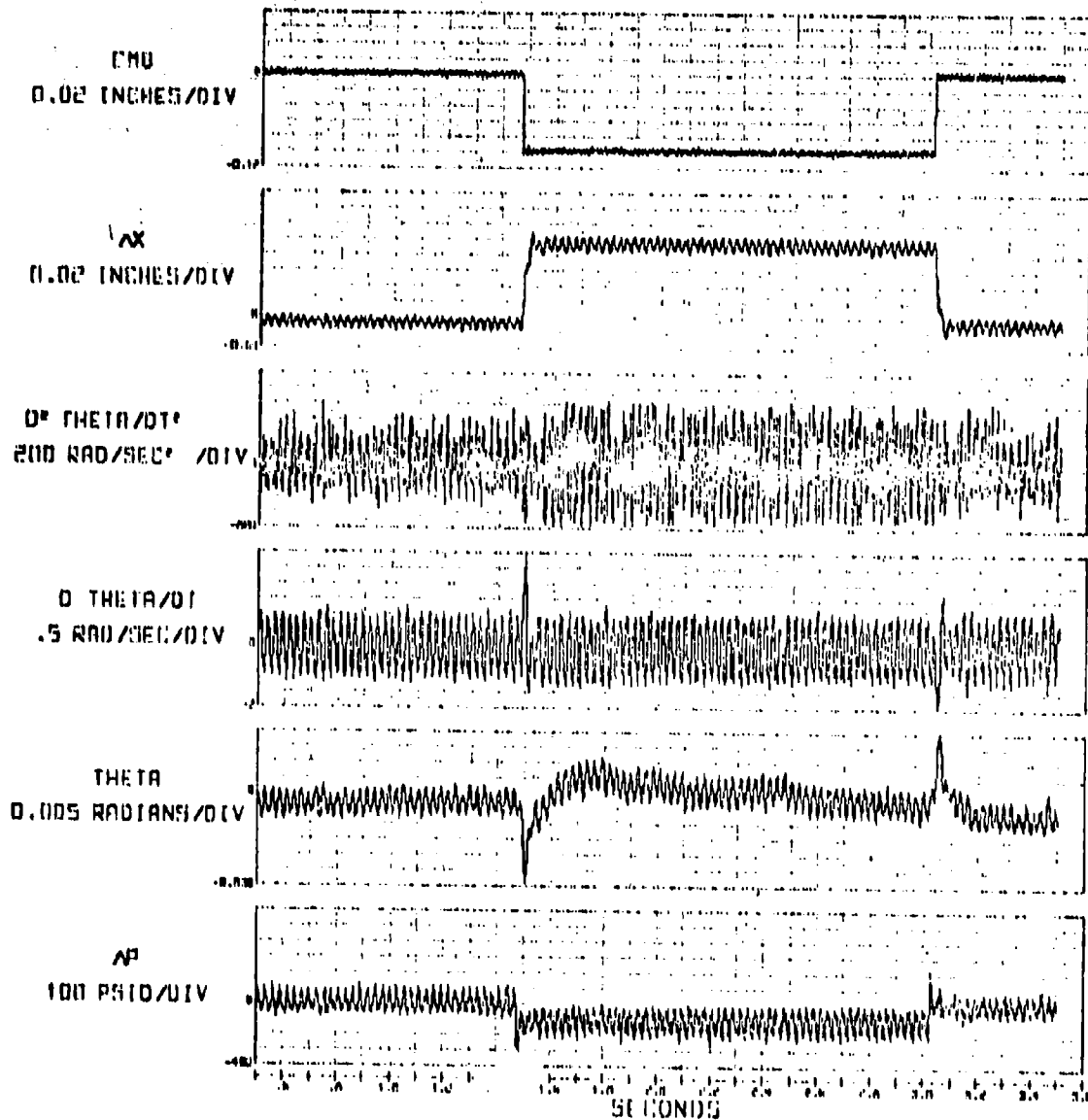
FIGURE 46 - ACTIVE SYSTEM TIME HISTORIES, TIRE IMBALANCE

87
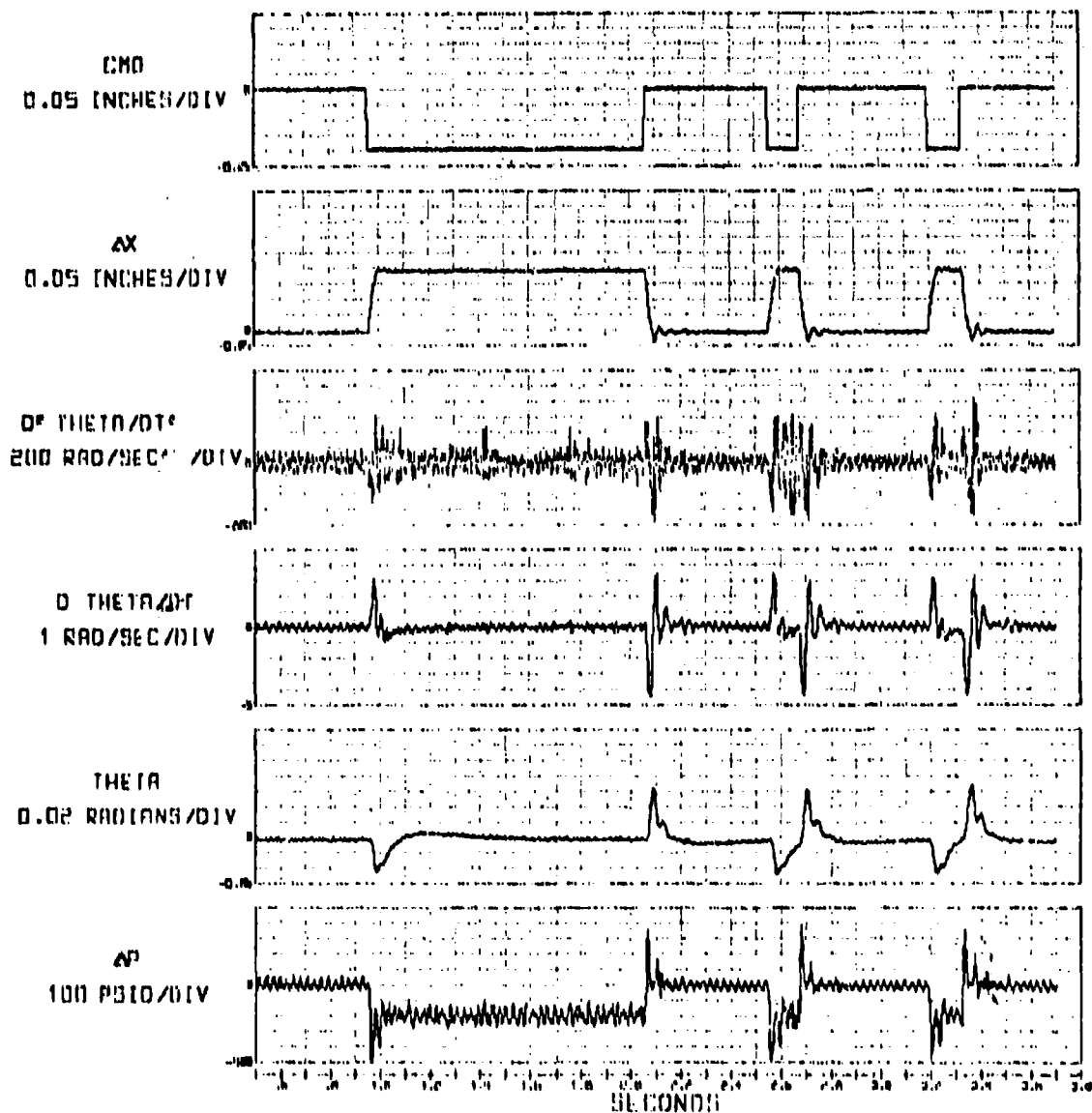
FIGURE 47 - ACTIVE SYSTEM TIME HISTORIES, ZERO TIRE IMBALANCE

88
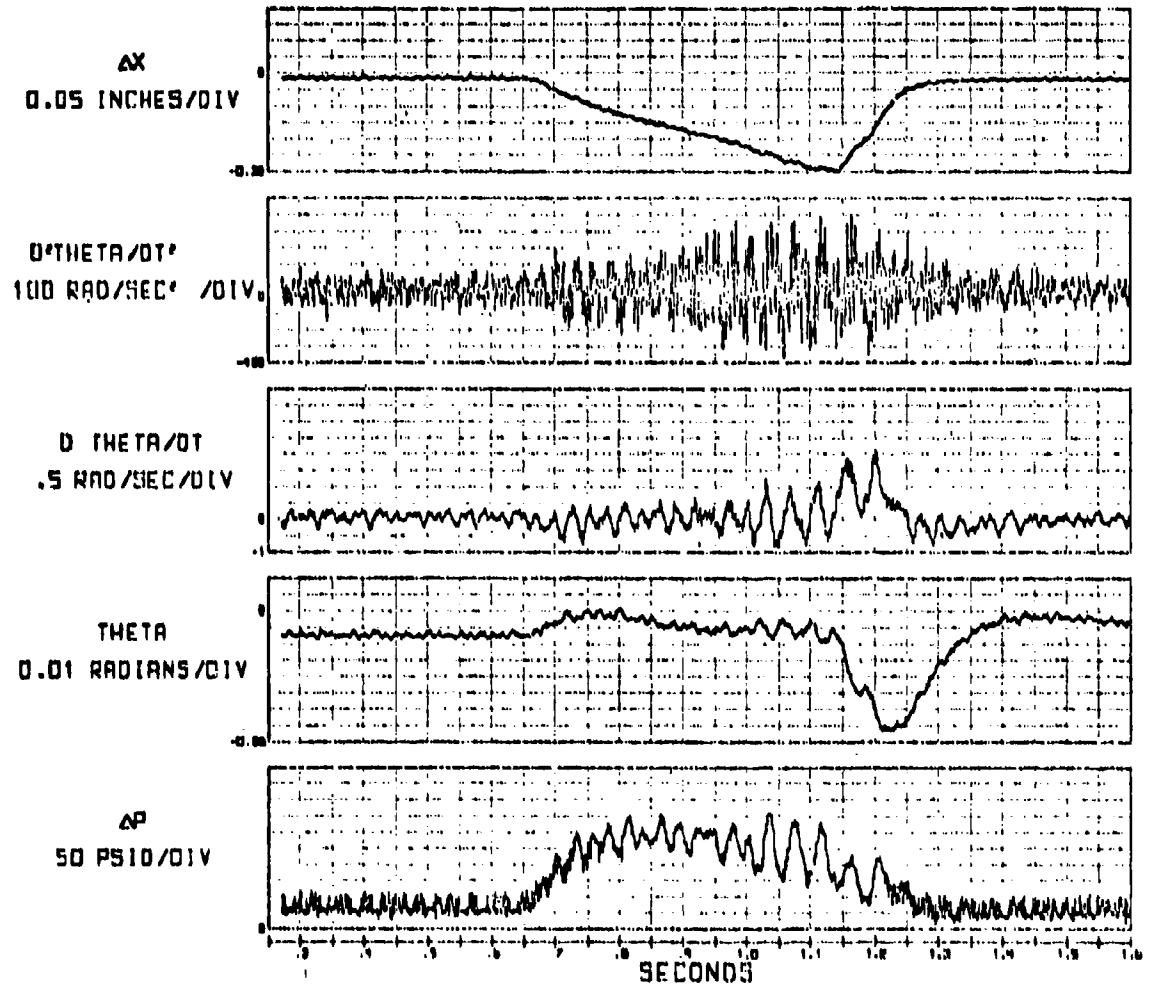
FIGURE 48 - PASSIVE SYSTEM TIME HISTORIES, ZERO TIRE IMBALANCE

89

reenters the backlash region as the steering returns to neutral, rather than any asymmetric characteristics of the servovalve and actuator.

A comparison of active and passive system performance with wheel imbalance is shown in Figure 49 for the fully extended gear with nominal backlash. The peak-to-peak axle angular acceleration is plotted versus airplane velocity. Since the angular acceleration traces are somewhat spiky and irregular, the data in Figure 49 is obtained from the cleaner angular velocity, $\dot{\theta}$, traces, using the relationship

$$|\ddot{\theta}| = \omega |\dot{\theta}|$$

where ω is the response frequency in rad/sec. Also shown in Figure 49 is the "input" angular acceleration due to the wheel imbalance, given by

$$|\ddot{\theta}|_{input} = \frac{|M_{imbal}|}{I_\theta}$$

M_{imbal} is the sinusoidal forcing moment about the steering axis due to wheel imbalance; I_θ is the mass moment of inertia of the wheel, tire and piston about the steering axis.

The passive results at 100 and 120 MPH are not at the wheel imbalance driving frequencies of 36 and 43 Hz, respectively, but at the shimmy frequency of 22 Hz. These results are sustained limit cycle shimmy oscillations. At all velocities, the measured response amplitudes of the passive system are greater than the input forcing function from wheel imbalance. For the active system, the responses are attenuated below the input at all velocities except for the resonance at 80 MPH, corresponding to a driving frequency of 29.5 Hz. The results of the steering sine sweep tests of the active system indicate a fundamental system resonance of 30 Hz. It is shown in Appendix E how the active system has raised the basic torsional mode natural frequency to 30 Hz or above.
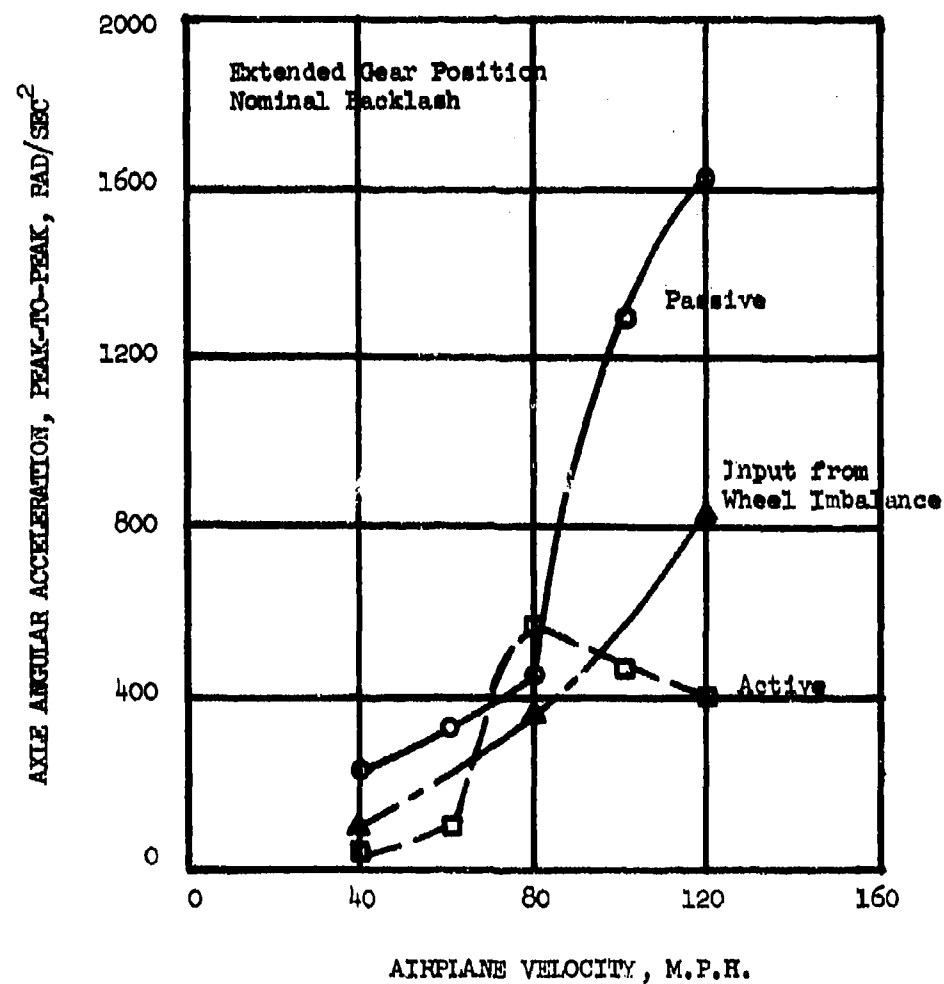
FIGURE 49 - COMPARISON OF ACTIVE AND PASSIVE SYSTEM RESPONSES
WITH WHEEL IMBALANCE, GEAR EXTENDED

The active system response peaks were driven at the system resonant frequency whereas the passive system response continues to increase at high velocities when the response breaks down into the shimmy frequency even though driven at higher frequencies. (The 22 Hz resonant frequency of the passive system corresponds to 60 m.p.h.). Thus, the passive system clearly exhibits sustained shimmy oscillations, while the active system only responds naturally at the driving frequency.

Figure 50 illustrates the same results as Figure 49, only with the gear in the mid position and with increased backlash (± 0.024 rad.). The active system results are similar in that a resonance at 80-100 mph occurs, while the responses are always lower than those of the passive system, which shimmies at 100 and 120 mph.

When the passive system is sufficiently stable (no shimmy), it also exhibits a resonance at around 80 mph in its response to wheel imbalance. Figure 51 shows the response of the passive system with the gear in the mid position and nominal backlash. This configuration does not shimmy at the high velocities (100 and 120 mph), and as a result the response peaks at 80 mph. It should be noted, however, that the dynamic amplification of the wheel imbalance input is greatest at 60 mph, which corresponds to a driving frequency of 22 Hz, the gear's observed shimmy frequency. Thus, the dynamic amplification of the gear peaks at the expected excitation frequency, while the absolute magnitude of the response peaks at a higher frequency (corresponding to 80 mph) because the magnitude of the input excitation increases with velocity.
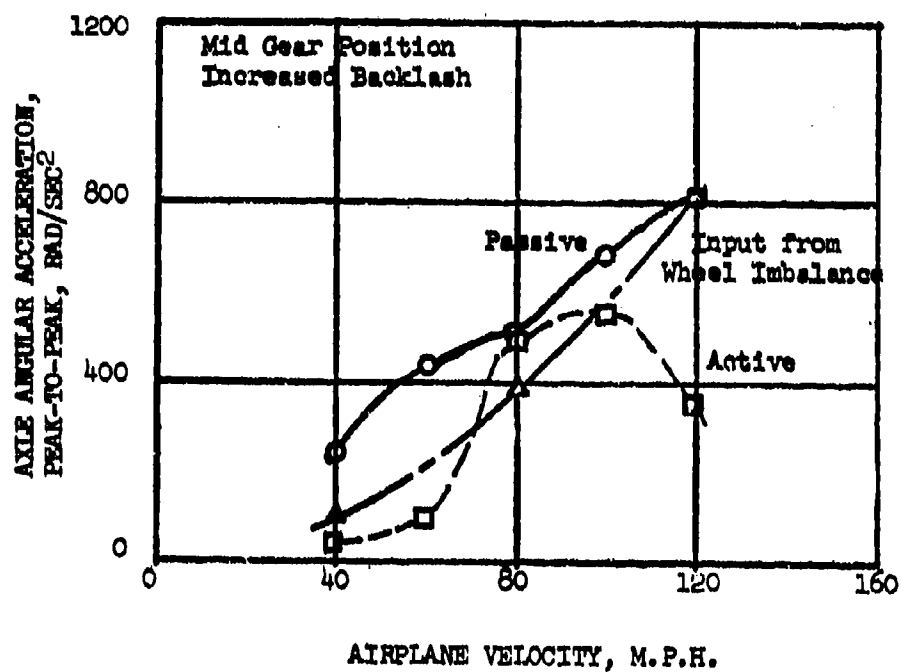
FIGURE 50 - COMPARISON OF ACTIVE AND PASSIVE SYSTEM RESPONSES
WITH WHEEL IMBALANCE, GEAR MID POINT

93
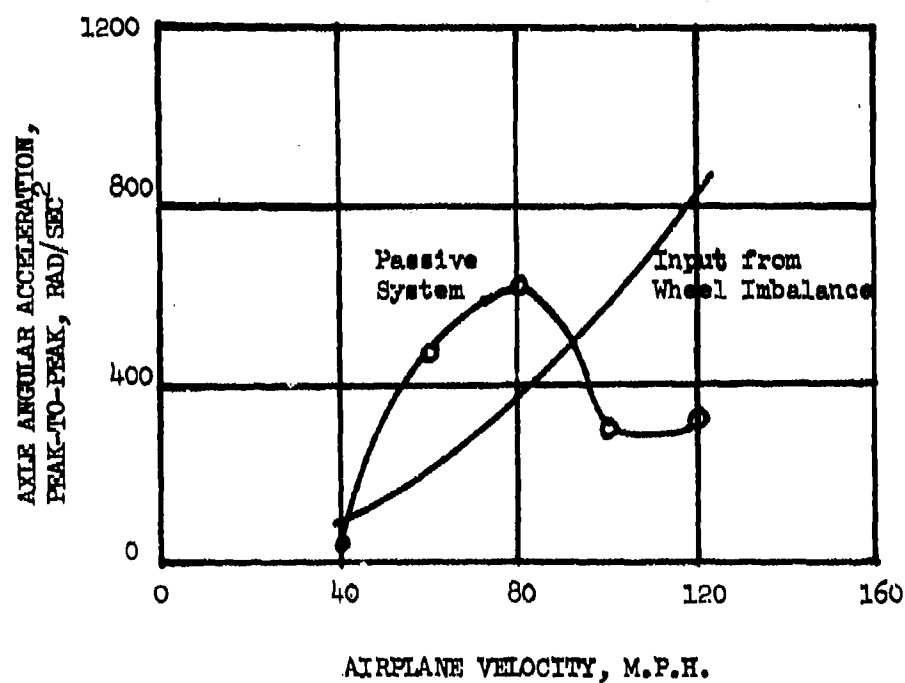
FIGURE 51 - PASSIVE SYSTEM RESPONSE TO WHEEL IMBALANCE, MID POSITION, NOMINAL BACKLASH

Analytical Model Parameters

Information gained from the preliminary laboratory tests performed in the program prior to the shimmy tests at Wright-Patterson, as well as changes made to the active system during shimmy testing, alter the values of some of the analytical model parameters previously summarized in Table 2. The revised values are shown in the following table. (Refer to Table 1 for parameter definitions).

TABLE 8.   REVISED ANALYTICAL MODEL PARAMETERS

PARAMETER	VALUE	NOTES
G1SMAL	0.0044	2
IAL(active)	0.068	1
K3	873000	1
K5	0.000309	1
K6	3.15E-6	1
K7	100.5	2
ZETAA	0.8	1
OMEGAA	1000	1
ZETAS	0.65	1
OMEGAS	750	1

Table 8 Notes

1. Revision based on preliminary laboratory active system test results.

2. Revision based on active system changes made during shimmy testing.

G1SMAL and K7 are the outer and inner loop feedback gains which were both revised during shimmy testing. The Bridged-T notch filter tuned to 180 Hz, which was employed in the shimmy tests, is not incorporated in the analytical model. In the analytical model, the 180 Hz structural mode is at 230 Hz and never gets driven. Since the purpose of the notch filter is solely to suppress this mode, the filter is not included in the analytical model because the mode is never excited.

Correlation-Results

The passive free shimmy tests were initiated by a cable pull system which resulted in a rather irregular, prolonged transient input to the gear that is difficult to duplicate analytically. For the purposes of correlation studies between analysis and test results, it is desirable to have a well defined input forcing function. A deliberately induced wheel imbalance provides an input excitation that is accurately known both in magnitude and frequency. It is for this reason that the correlation studies are based on the tests wherein wheel imbalance was used to drive the gear.

Analytical results for the passive system with 10 in-oz wheel imbalance are compared with the test results in Figure 52. The extended gear position with nominal backlash is used. Axle angular acceleration derived from angular velocity is plotted against airplane velocity. The agreement between analysis and test data is fairly good at all velocities. However, at 100 and 120 mph, the analytical responses are at the wheel imbalance driving frequencies (35 and 42 Hz, rather than at the shimmy frequency of 22 Hz, as observed in the test results. A steering actuator stiffness of 50,000 in-#/rad is used for these analyses, rather than the 18000 in-#/rad shown in Table 2. The lower stiffness value will result in a 22 Hz divergent instability at 120 mph, with good correlation at the lower velocities. Therefore, depending on what value of actuator stiffness is employed, the 120 mph analytical results will agree with the test results either in terms of response amplitude or response frequency, but not both. (If free shimmy is analyzed, the correct shimmy response frequency of 22 Hz results for a broad range of actuator stiffnesses).

96
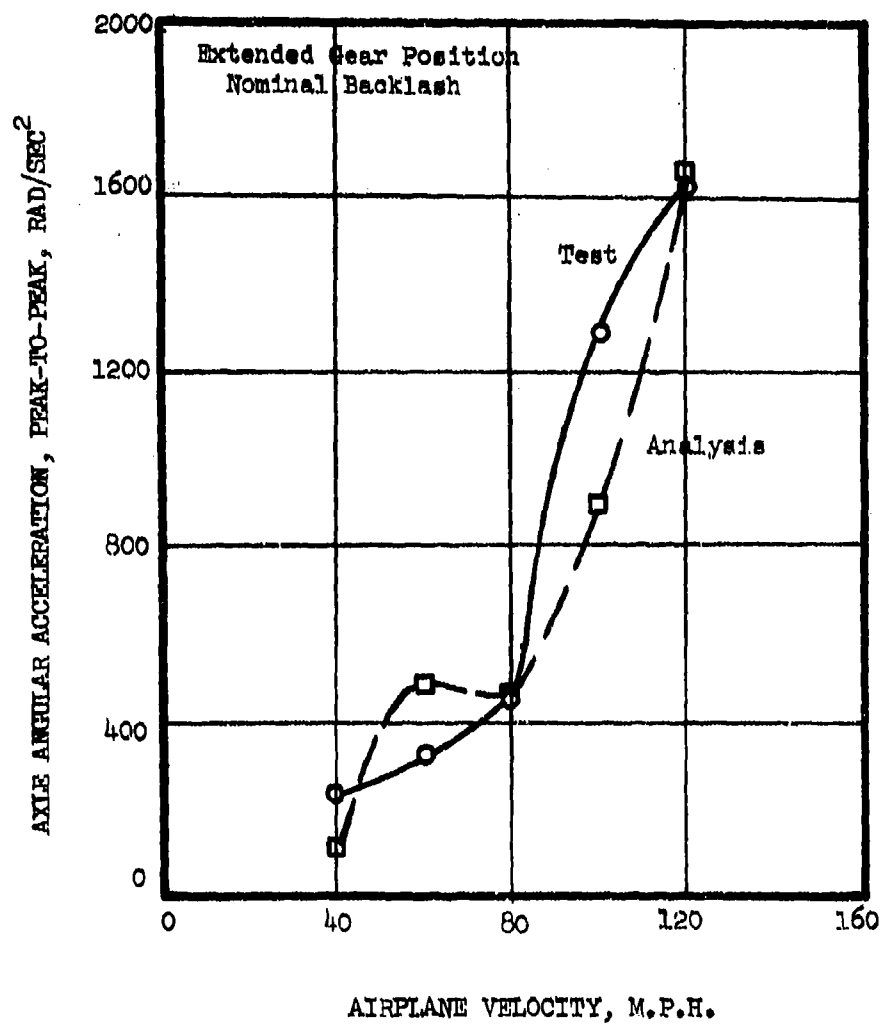
FIGURE 52 - COMPARISON OF TEST AND ANALYTICAL PASSIVE SYSTEM RESPONSES
WITH WHEEL IMBALANCE, EXTENDED GEAR POSITION

97

Figure 53 shows the same information for the active system, with the gear in the extended position and nominal backlash. In this case, the correlation is fair from 40 to 100 mph, but at 120 mph the analysis indicates a much larger response than that observed during testing.

Figures 54 and 55 show the correlation results for the passive and active systems for the mid gear position with increased torsional backlash (±0.024 rad.). The results are very similar to the extended gear findings; the passive system correlates rather well at all velocities while the active system analytical results are too high at the high velocities.

For these mid gear position analyses, the estimated tire parameters shown in Table 2 produce high negative tire energy inputs to the system. In particular, the passive system is divergently unstable at 80 mph and above. Since no tire parameter test data of the type needed for shimmy analysis was available for the tire used, estimates of the tire data were made using empirical equations from Reference 2. The analytical results, when compared with the test results, indicate that the magnitude of the tire stiffness as obtained from Reference 2 may be high. Because most of the test data which formed the basis of the empirical equations contained in Reference 2 exhibited considerable scatter, reduced values of the tire parameters obtained from the equations are justified and are used for the correlation studies.

The tire parameters may also contribute to the poor correlation encountered with the active system at 120 mph. In the analysis, the tire acts as a source of energy to the system at 120 mph. Since driven shimmy tests were not performed, it is unknown whether the real tire served as an energy source or sink. However, if the tire actually absorbed energy at 120 mph, that could explain the low magnitude of the test response (relative to the analysis) at 120 mph for the active system.

This would imply that a "correct" set of tire parameters would lower the analytical responses at 120 mph. However, this would also hold true for
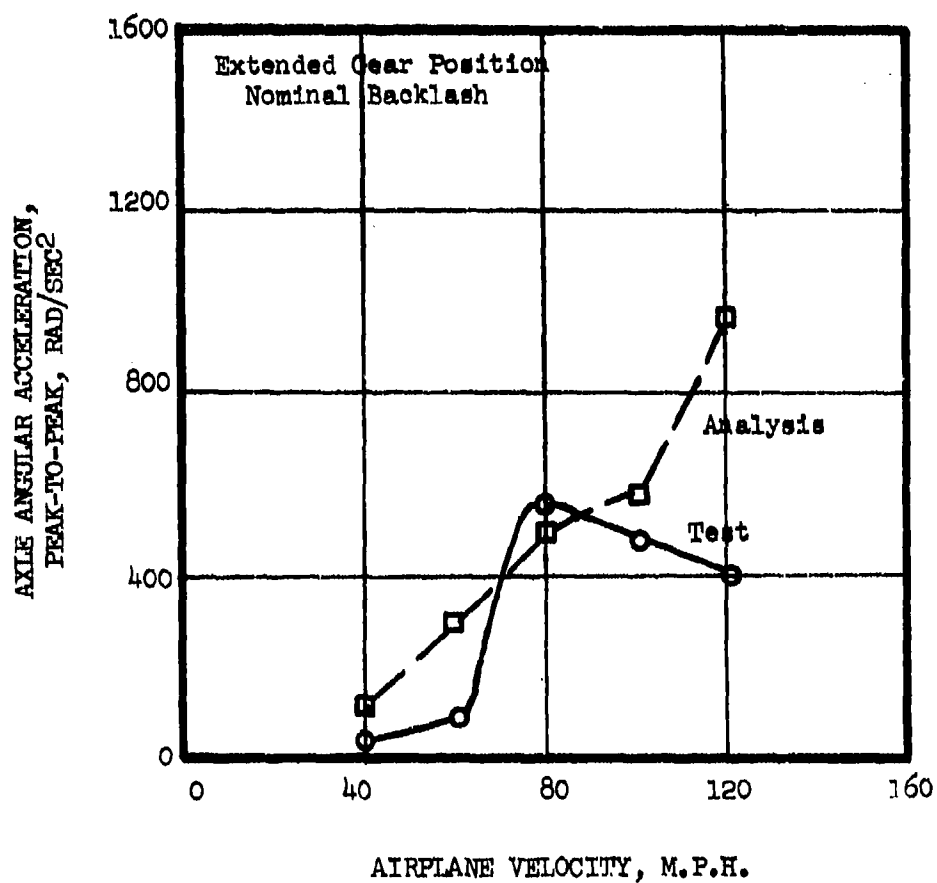
FIGURE 53 - COMPARISON OF TEST AND ANALYTICAL ACTIVE SYSTEM RESPONSES
WITH WHEEL IMBALANCE, EXTENDED GEAR POSITION

99
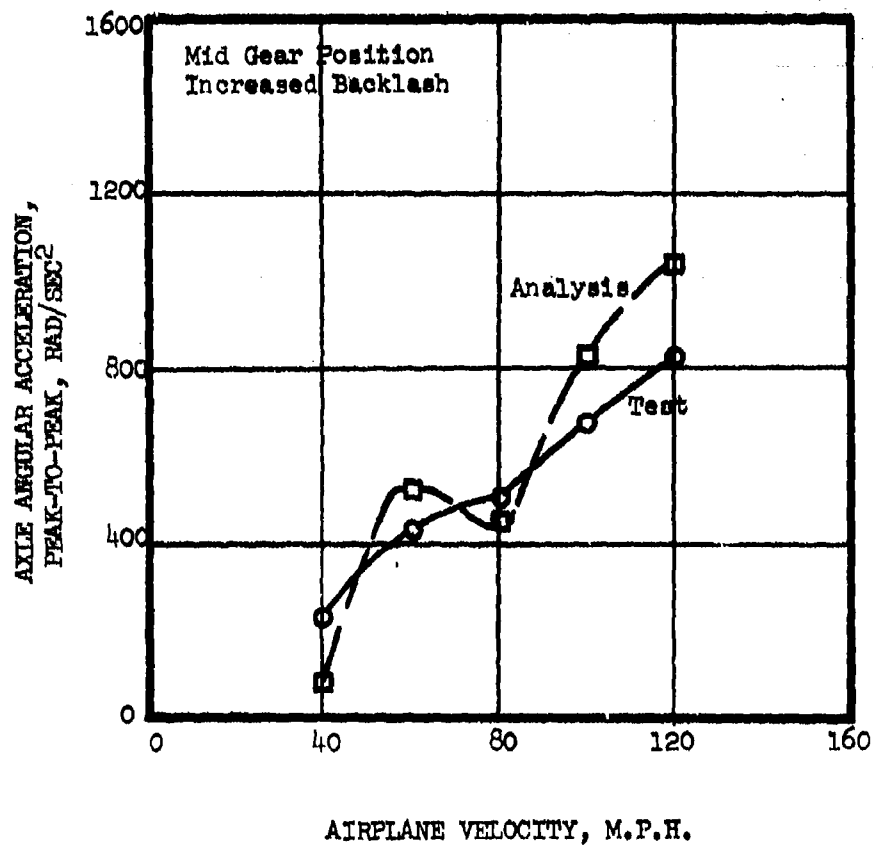
FIGURE 54 – COMPARISON OF TEST AND ANALYTICAL PASSIVE SYSTEM RESPONSES
WITH WHEEL IMBALANCE, MID GEAR POSITION
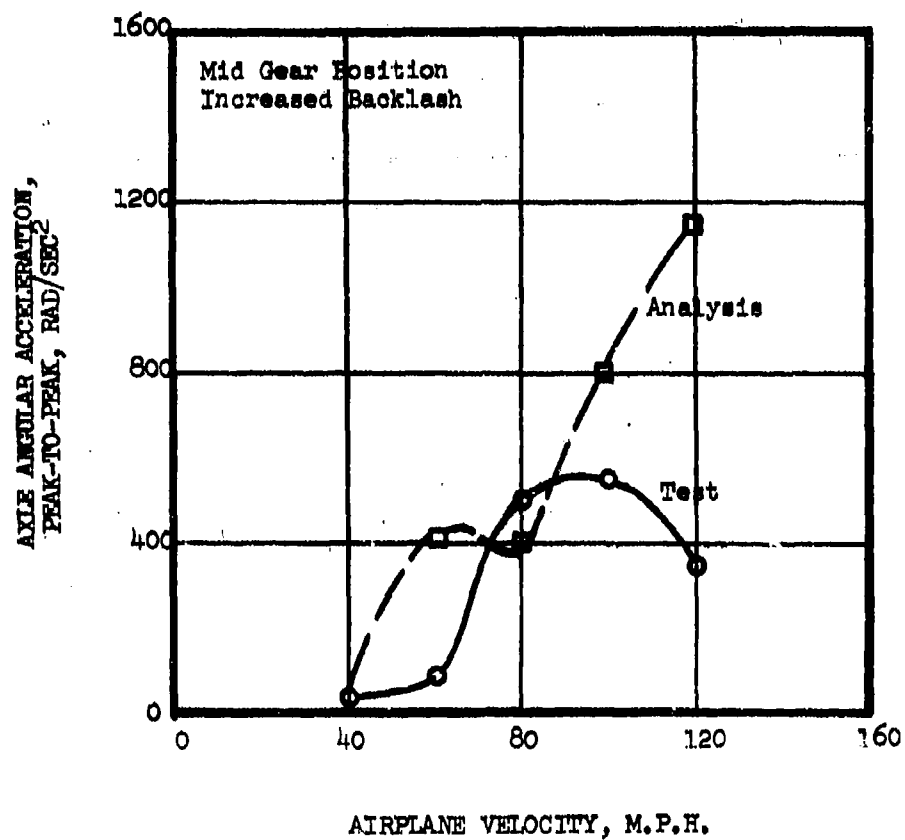
FIGURE 55 — COMPARISON OF TEST AND ANALYTICAL ACTIVE SYSTEM
RESPONSES WITH WHEEL IMBALANCE, MID GEAR POSITION

101

the passive system which currently correlates fairly well at 120 mph. In the passive system, the added energy absorption of the tire could be offset by lowering the actuator stiffness back to around 18000 in-#/rad, as estimated in Table 2. Thus, both the passive and active systems would correlate well at high velocity if the tire actually absorbs energy.

Another consideration relative to deterioration in correlation of the active system at the higher velocities is the use of wheel imbalance to induce torsional motions in the gear. Classically in shimmy analysis the fore and aft mode is neglected because the lateral and torsional modes dominate. Accordingly, the analysis used in the program does not include the fore and aft mode. Wheel imbalance imposes fore and aft loads on the gear, which result in torsional motions due to the lateral offset of the imbalance. Thus, the fore-aft and torsional gear motions are coupled via the wheel imbalance forcing function as well as any mechanical coupling that may exist in the gear. In the case of a passive system, this coupled response has a secondary effect on the onset of shimmy, since fore-aft gear motions are not as significant as lateral motions in producing tire forces. However, with the active system the torsional accelerometer will be exposed to the coupling which may result in altering the feedback signal by a shift in phasing over what would be expected from only the lateral and torsional modes. The change in signal can be either favorable or unfavorable in suppressing the response of the gear, and the effect should be more significant at high velocities. (This fore-aft gear loading could have been eliminated from the shimmy tests by using equal weights on opposite sides of the rim, located 180° apart).

The use of wheel imbalance as a means of providing data for correlation of analytical and test results of gear response in evaluating its shimmy characteristics does not provide stability margins as does the driven shimmy testing method, and also the analysis may require the inclusion of the fore-aft degree of freedom of the gear.

To aid in explaining some of the observed results of the active system tests, a simplified analysis of a linearized system was developed and is presented in Appendix E. In particular, the variation of the free shimmy response frequency with feedback gain and the creation of modes associated with the active system are discussed.

CONCLUSIONS AND RECOMMENDATIONS

Conclusions

1. The basic passive system shimmies at velocities above 80 mph in the extended gear position, as well as in the mid position with increased torsional backlash. This susceptibility to shimmy is the result of a shimmy damper which behaves as a soft spring with minimal damping at the shimmy frequency (22 Hz.).

2. The analytical model used in this program correctly predicts the shimmy tendencies of the passive system. Quantitative response comparisons between test and analytical results with wheel imbalance show good agreement in amplitude, but at 100 mph and above, the analytical response is at the driving frequency while the test response is at the shimmy frequency.

3. All versions of the active shimmy control system tested prevented shimmy even with wheel imbalance and more than twice the nominal torsional backlash.

4. Careful shaping of the feedback control signal is necessary to prevent undesired high frequency oscillations. This signal shaping, accomplished with a Bridged-T notch filter tuned to 180 Hz, must be done during the shimmy test program. The analytical model is not sufficiently precise to predict potential problems from higher frequency structural modes.

5. In addition to preventing shimmy, the active control system reduces the response of the gear to wheel imbalance relative to the passive system.

6. The active shimmy control system is stable at more than twice the nominal feedback gain employed; hence, the system as tested has 6 dB gain margin.

7. With zero feedback gain, the active control system still has positive shimmy damping, although its damping performance is quite poor.

8. The analytical model predicts the observed shimmy suppression capabilities of the active control system, but quantitative response comparisons

104

are only in fair agreement at velocities above 80 mph.

Recommendations

It is recommended that:

1. The active system analytical model be further refined to predict system responses more accurately. The refinements to be investigated include fore-aft gear response and separate fuselage fore-aft and lateral degrees-of-freedom.

2. Further testing and analysis be performed to assess the limitations of the present active control system. In particular, its performance with various signal failures should be determined over a wide range of operating conditions.

3. A fail safe concept be developed and incorporated into the breadboard system design to remove the operational limitations of the present system.

4. After the above has been completed, an active control system suitable as a flight test prototype for the T-37 be designed and built.

5. This system be flight tested with various degrees of degraded gear maintenance.

6. The feasibility of providing active shimmy control, in conjunction with electrical steering commands, for larger airplanes be investigated.

7. Wheel imbalance, if used as a means of inducing torsional response in single wheel shimmy tests, be installed such that fore and aft motions are not introduced.

APPENDIX A

OPERATION AND MAINTENANCE INSTRUCTIONS
ACTIVE SHIMMY DAMPER SYSTEM

A. Installation of Nose Gear Assembly in Airframe

1. Inflate tire to 35-50 psi.

2. Pre-pressurize shock strut air pressure to desired pressure (approximately 55 psi with strut extended/no load).

3. Remove 1" dia. trunnion pins from Gear Assembly.

4. Install 1/2" dia. bolts (installation tools) in trunnion pins from outboard ends.

5. Lift Gear Assembly into airframe. Push R.H. (side adjacent to steering actuator piston rod attachment to yoke) trunnion pin thru airframe bushing and gear yoke.

6. Start L.H. trunnion pin through airframe bushing and seven 1" I.D. washers between airframe and gear yoke, and into yoke.

7. Align the 3/16" diameter holes for retaining screws thru yoke and trunnion pin. Install 10-32 retaining screws into one side of trunnion pin, unscrew 1/2" diameter bolt (installation tool), and finish installing 10-32 retaining screw thru yoke and trunnion pin. (Two places).

8. Install Drag Link at upper end to airframe. Connect Drag Link at lower end to Gear Assembly.

9. Connect pressure and return hydraulic lines. (Note: Locate accumulators in pressure and return lines as close as practical to Gear Assembly. Pre-charge air pressure in accumulators as follows:

Pressure Accum. - 800 psi   Return Accum. - 25 psi

10. Connect electrical cable connectors.

NOTE: Hydraulic System Fluid MIL-H-5606
Hydraulic System Operating Pressure 1500 psi
Locate pressure line filter as close to test as possible

B. Changeover Procedure, Passive to Active Damper Configuration

(Note: If accessible, it should not be necessary to remove Gear Assembly from airframe to accomplish configuration changeover).

Figure A-1 is a layout drawing of the system showing the part numbers referred to herein.

1. Disconnect pressure and return flex lines from aircraft steering actuator. Cap pressure port, plug flex lines.

2. Disconnect connector to ΔP transducer.

3. Remove three allen head screws holding SL 1962 LVDT Bracket to SL 1960 Manifold and let Bracket hang on LVDT probe.

4. Remove jam nut holding SL 1963 Brace to bulkhead fitting in return port on aircraft actuator.

Remove four screws holding SL 1963 Brace to SL 1960 Manifold (3 Allen head, 1 slot head) (Note: Slot Head screw location required for clearance, left front.)

Remove SL 1963 Brace.

FIGURE A-1 - ACTIVE SIDEWAY CONTROL SYSTEM HARDWARE ARRANGEMENT

5. Remove lower bolt and drop Drag Link from gear.

6. Loosen two SL 1961 Bolts holding SL 1960 Manifold to aircraft actuator.

   Loosen two bolts evenly together 1/2 turn at a time. Do not remove bolts from SL 1960 Manifold, remove Manifold and Bolts as an assembly from aircraft actuator. Watch for loose springs and orifice poppet valves as Manifold and Bolts are removed.

7. Remove springs and aircraft orifice poppet valves.

8. Using #6-32 screw provided as tool, install SL 1966 plugs in place of orifice poppets.

9. Remove and replace two MS 28775-012 "O" Rings and Back-Up Rings forming face seal on SL 1961 Bolt between Manifold and aircraft actuator.

10. Re-install two aircraft springs and Manifold/Bolt Assembly. Tighten bolts evenly together 1/2 turn at a time to bolt SL 1960 Manifold to aircraft actuator.

11. Re-connect drag link to Gear Assembly.

12. Re-install SL 1963 Brace on SL 1960 manifold using bulkhead fitting jam nut and four screws. (Note: Location of one slot head screw required for clearance.) Cap return port on aircraft actuator.

13. Re-install SL 1962 LVDT Bracket and adjust LVDT Body position to center radially on probe.

14. Remove SL 1972 Cover Plate and install Model 31 Moog Servo valve.

15. Connect pressure and return lines to P & R ports on SL 1960 Manifold.

16. Remove aircraft feedback linkage as follows:

    (a) Remove cotter key and pivot pin from linkage connection to valve spool.

    (b) Remove phillips-head center pivot screw (watch for loose washer & bushing).

    (c) Slip feedback linkage fork off of pin on pilot input ring.

17. Connect electrical cable to Moog valve. Connect electrical cable to $\triangle$P transducer.

C. Parts Kit (Gear Assembly in Passive Configuration)

1 each Filter

2 each Accumulators - 1 Press
                         1 Return

2 each 1/4" Hoses

2 each 1/2" Bolts for Trunnion Pins

2 each 1/4" Hydraulic Fitting Caps

2 each 1/4" Hydraulic Fitting Plugs

2 each SL 1966 Plugs to replace orifice poppets

2 each Set SL Drawings

1 each Model 31 Moog Servo Valve with Dust Cover

4 Sets "O" rings and back-up rings for SL 1960 Manifold

2 each Drag Link Bolts (Attach to Steel Jig)

2 each Drag Link Bolts (for attaching upper end to real aircraft airframe)

2 each #6-32 Screws, approximately 2" long for installing SL 1966 Plugs

10 each 1" I.D. Washers (Use 7)

4 each Zip Plastic Bags

1 each 1/16" Safety Wire Hook

1 each Roll Tape

1 each Epoxy Kit

APPENDIX B

CIRCUIT DIAGRAM, ACTIVE SHIMMY CONTROL SYSTEM

Figure B-1 is an electrical circuit diagram for the final configuration
of the active shimmy control system. All test instrumentation electronics
are included. The Bridged-T notch filter added during the shimmy tests is
also shown. An explanation of the functions of the various circuits is con-
tained in the section entitled, "ACTIVE SHIMMY CONTROL SYSTEM DESCRIPTION".
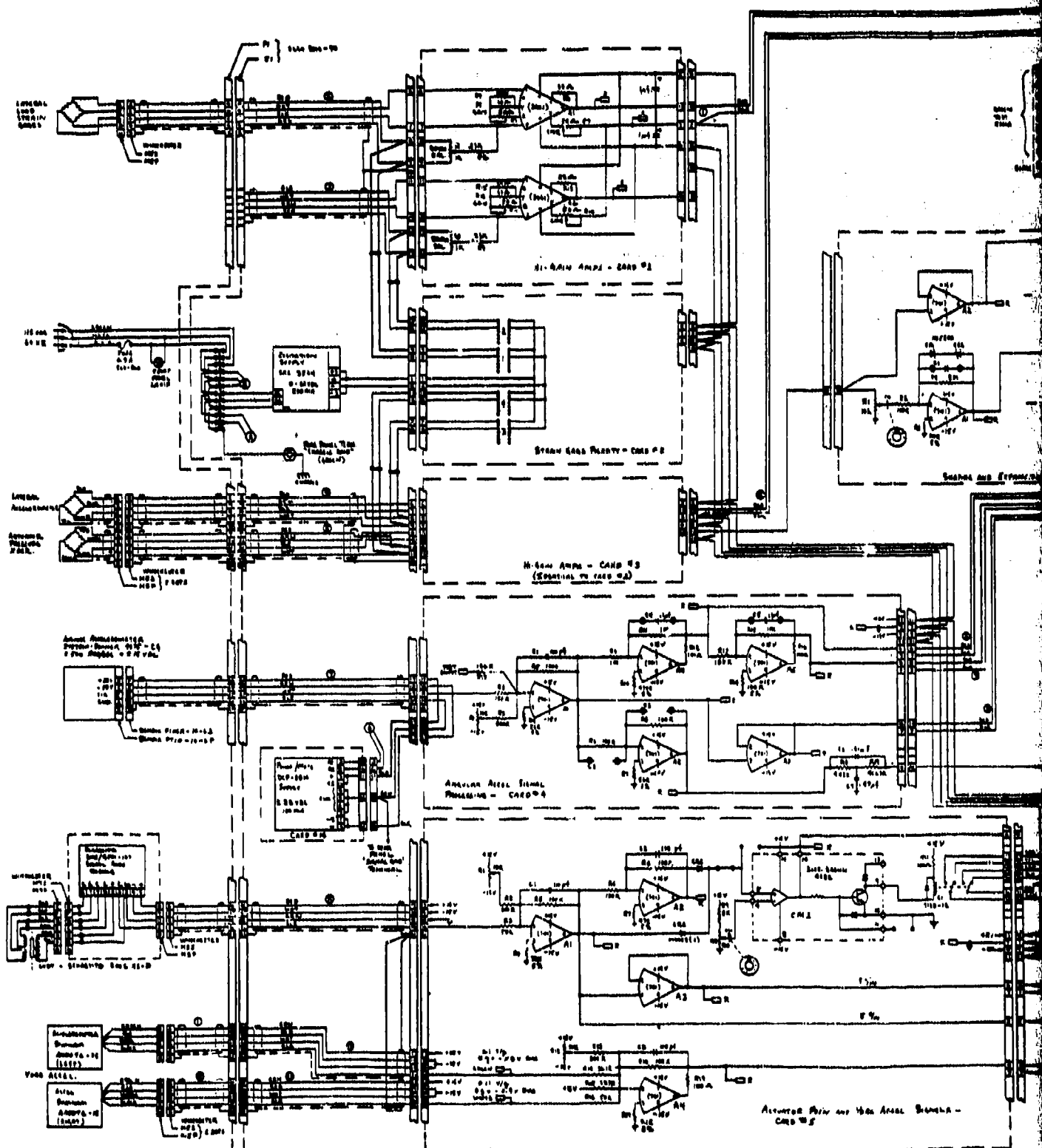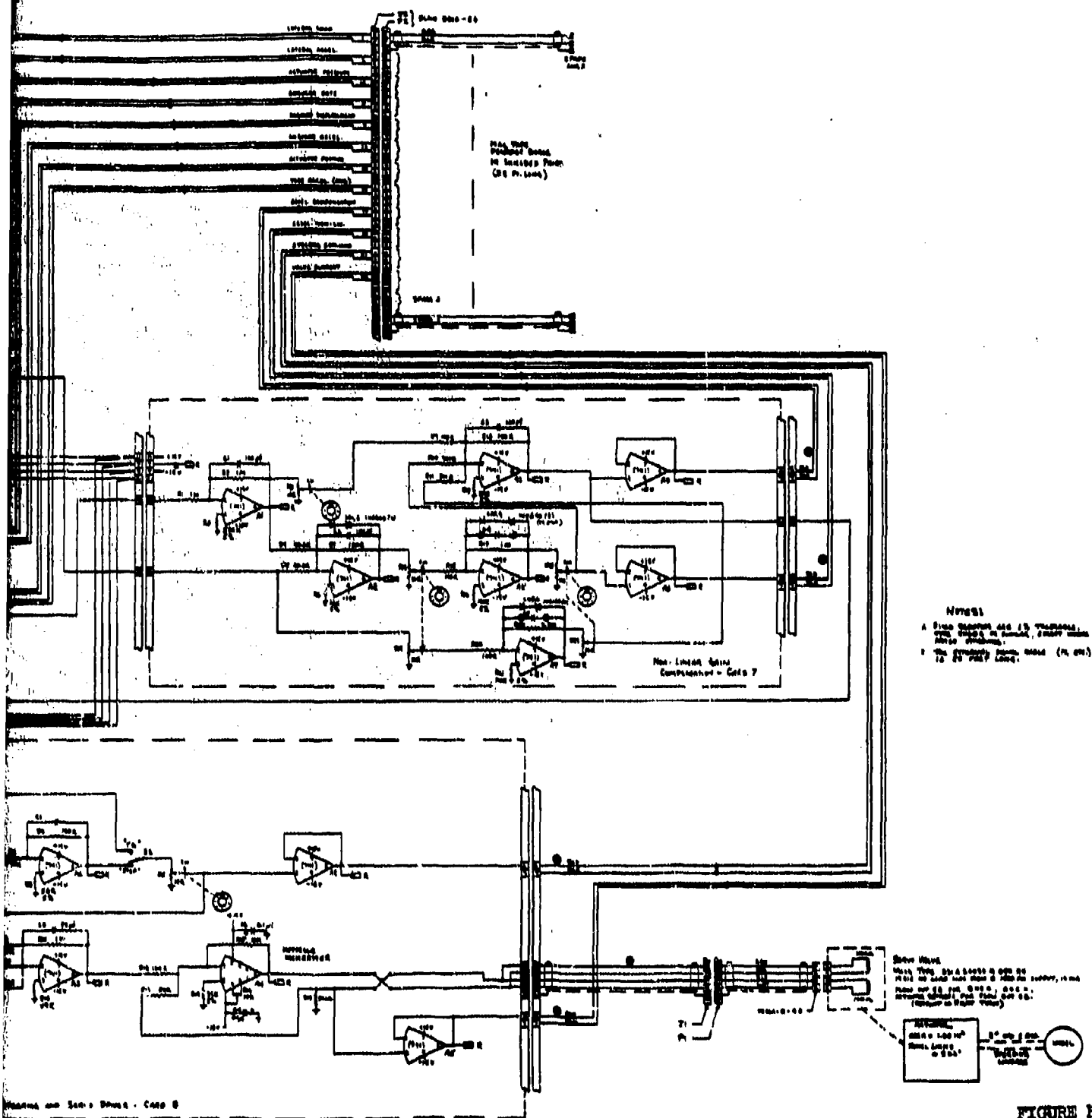
FIGURE B-1

CIRCUIT DIAGRAM,
ACTIVE SHIMMY
CONTROL SYSTEM   113

3

APPENDIX C

SHIMMY TEST TIME HISTORIES

Contained in this section are time history traces of selected portions of
the more pertinent shimmy tests. These plots were obtained by processing
the FM tape recording from the shimmy tests. Table C-1 summarizes the runs
presented. For the active system tests, only data for the final Bridged-T
notch filter configuration is shown, with the nominal feedback gain
(K_α = 0.7). Only velocities of 80 mph and above are presented. Table C-2
contains a description of the quantities that are plotted for each run.
On the time history plots, the expression "FIELD RUN XX" refers to the
shimmy test run number shown in Table C-1. The expression "RUN XX" is for
Lockheed reference only.

TABLE C-1

PLOT SUMMARY

Run No.	Gear Configuration	Gear Position	Backlash	Wheel Imbalance	Velocity, m.p.h.
27	Passive	Ext.	Nominal	10 in-oz	100
28					120
31					80
32				↓	100
33				0	80
34					100
35					120
39			Increased		80
40					100
41	↓	↓	↓	↓	120
153	Active	Ext.	Nominal	0	80
156				↓	100
159					120
162				10 in-oz	80
163				↓	100
164					120
167			Increased	0	80
168				↓	100
169					120
172				10 in-oz	80
173					100
174		↓			120
177		Middle			80
178					100
179				↓	120
182				0	80
183					100
184	↓	↓	↓	↓	120

TABLE C-2

PLOT TIME HISTORY DESCRIPTION

Quantity	Units	Description
CMD[*]	Inches	Electrical steering command signal expressed in terms of actuator displacement
Δx	Inches	Actuator displacement
$D^2 THETA/DT^2$	rad/sec^2	Axle angular acceleration about steering axis
D THETA/DT	rad/sec	Axle angular velocity about steering axis
THETA	rad	Axle angular position about steering axis
ΔP	p.s.i.	Actuator pressure differential

* This quantity plotted for active system runs only

116

ACTIVE AND PASSIVE SHIMMY TESTS
FIELD RUN 27 PASSIVE

TEST 26617   RUN 6   18 SEP 75

ΔX
0.05 INCHES/DIV

D°THETA/DT°
200 RAD/SEC° /DIV

D THETA/DT
.5 RAD/SEC/DIV

THETA
0.01 RADIANS/DIV

ΔP
50 PSID/DIV

SECONDS

117
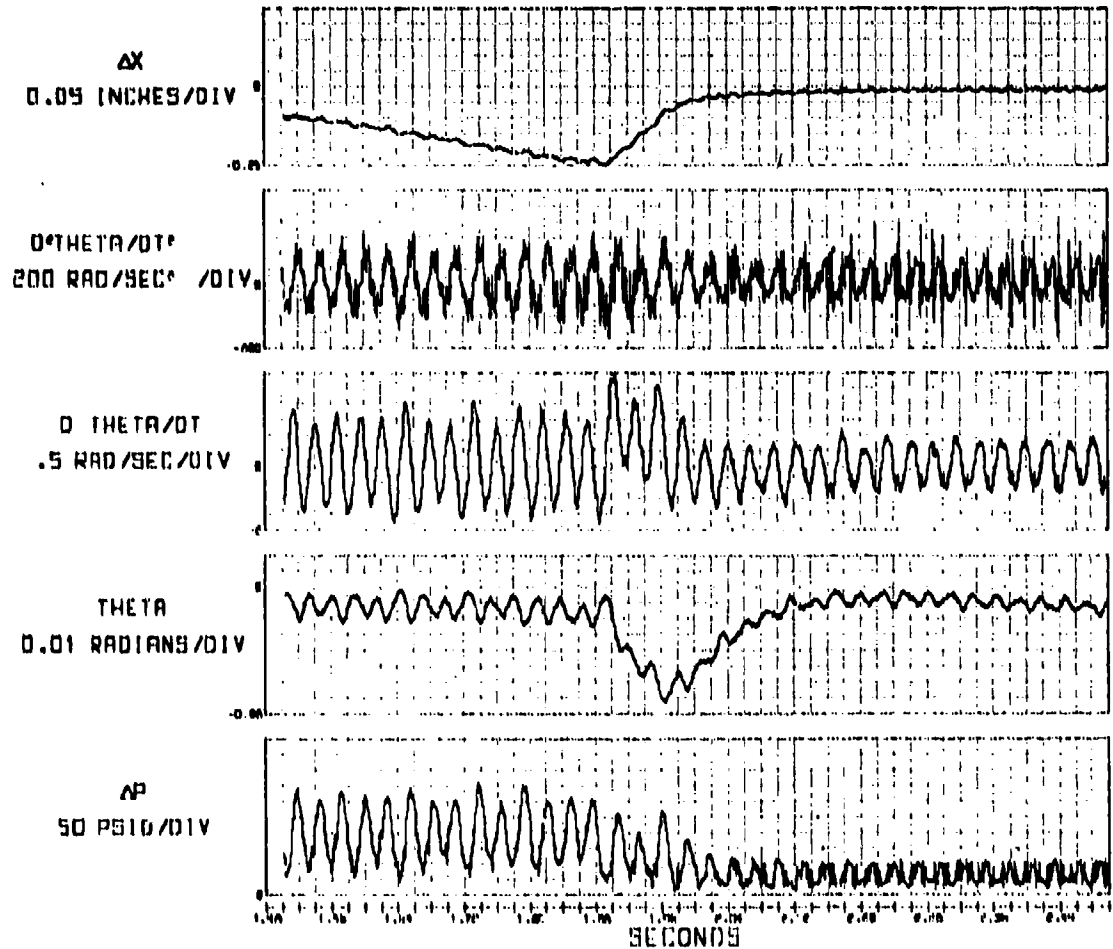
ACTIVE AND PASSIVE SHIMMY TESTS
FIELD RUN 26 PASSIVE

TEST 26617   RUN 7   18 SEP. 75
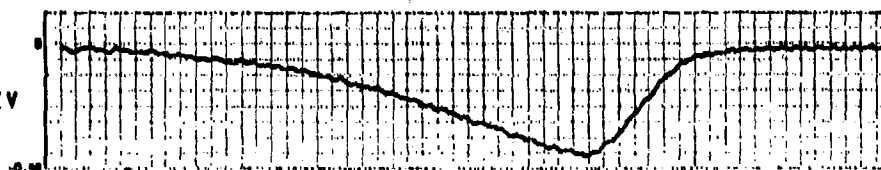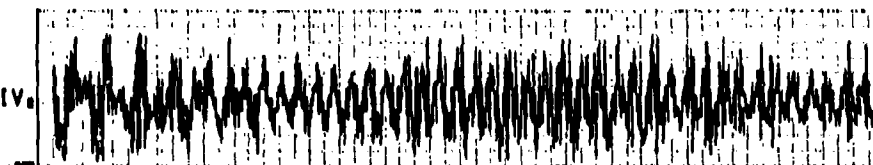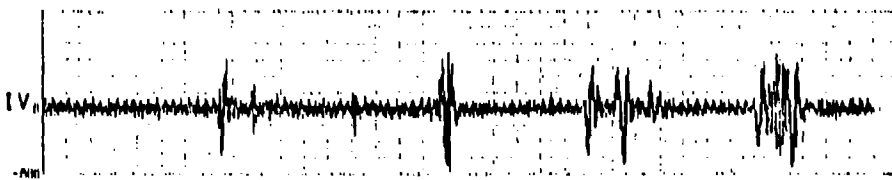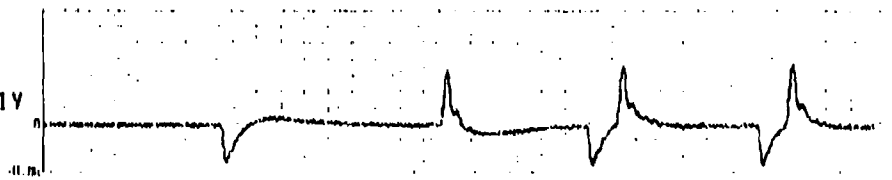
ΔX
0.05 INCHES/DIV

D²THETA/DT²
200 RAD/SEC² /DIV

D THETA/DT
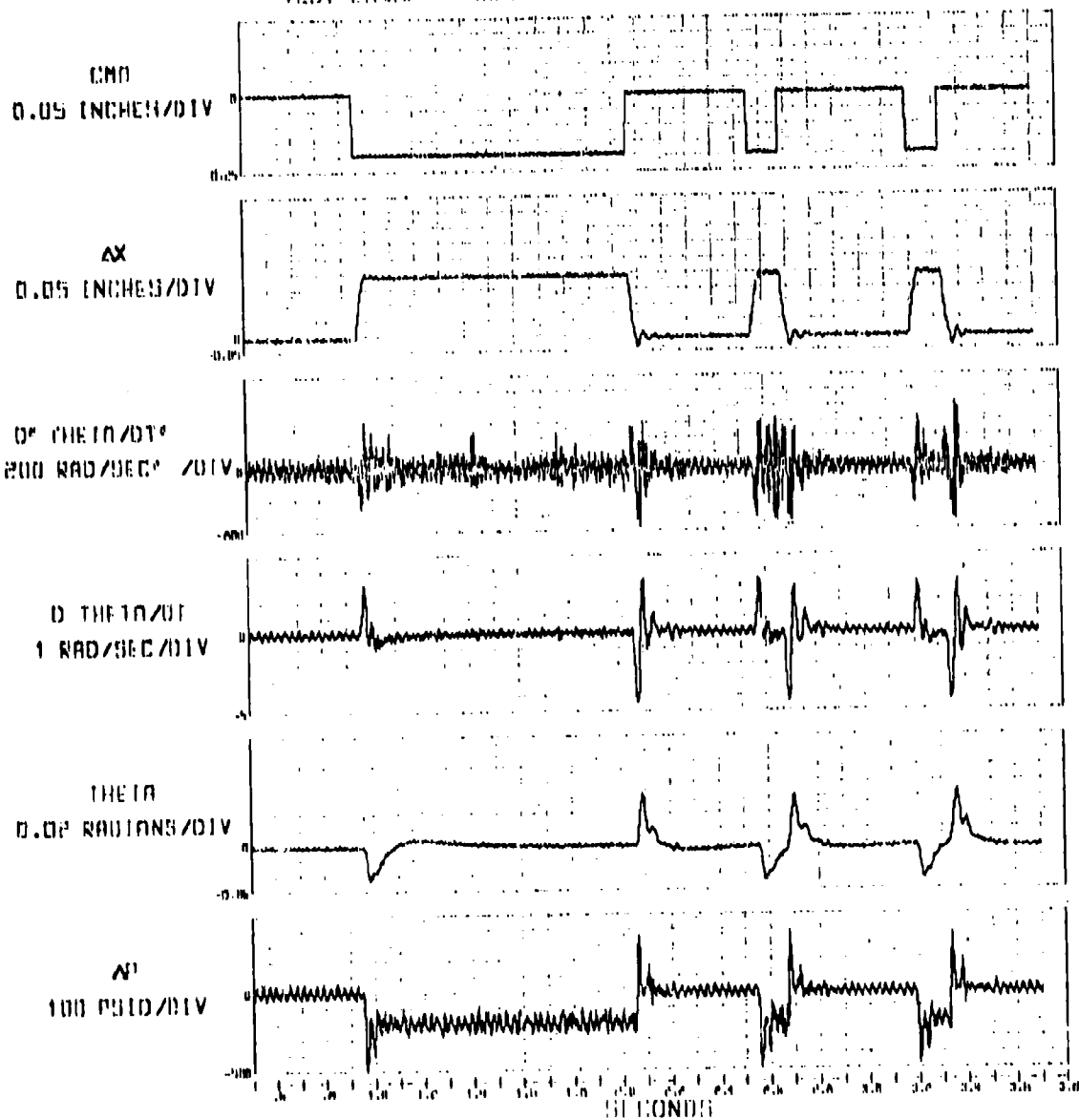1 RAD/SEC/DIV

THETA
0.02 RADIANS/DIV

ΔP
50 PSID/DIV

SECONDS

118
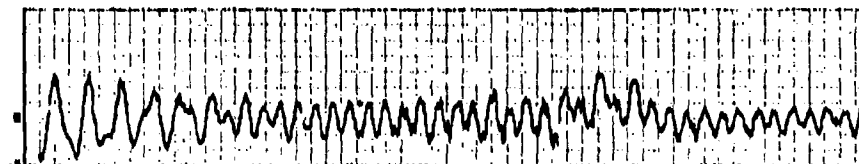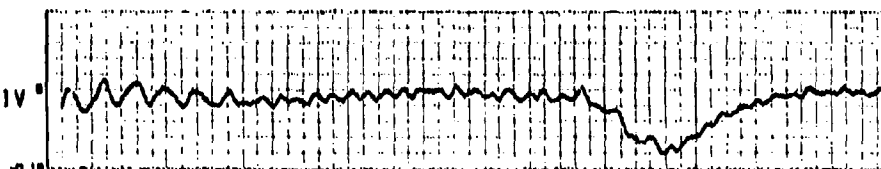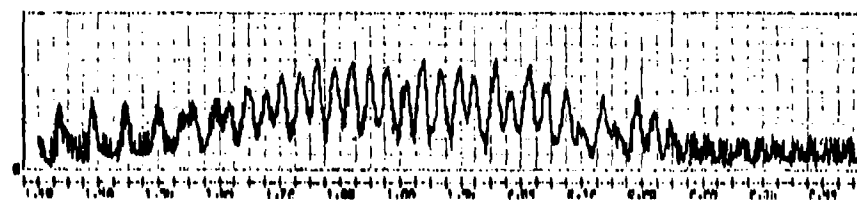
ACTIVE AND PASSIVE SHIMMY TESTS
FIELD RUN 31 PASSIVE

TEST 26617   RUN 8   18 SEP 75
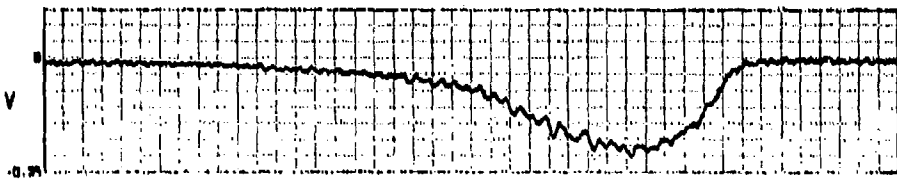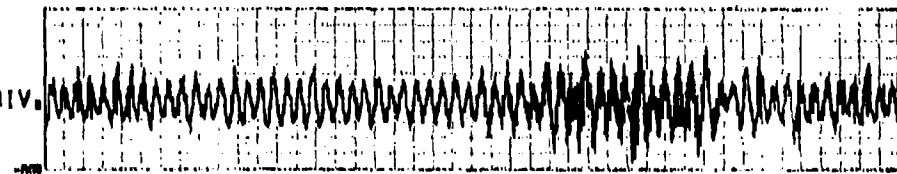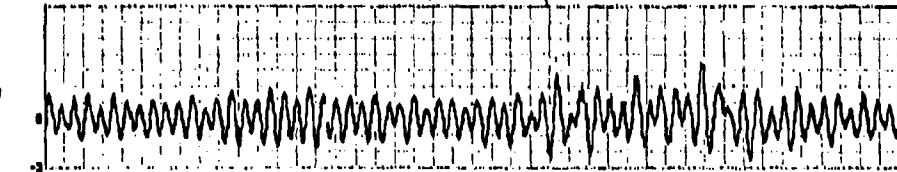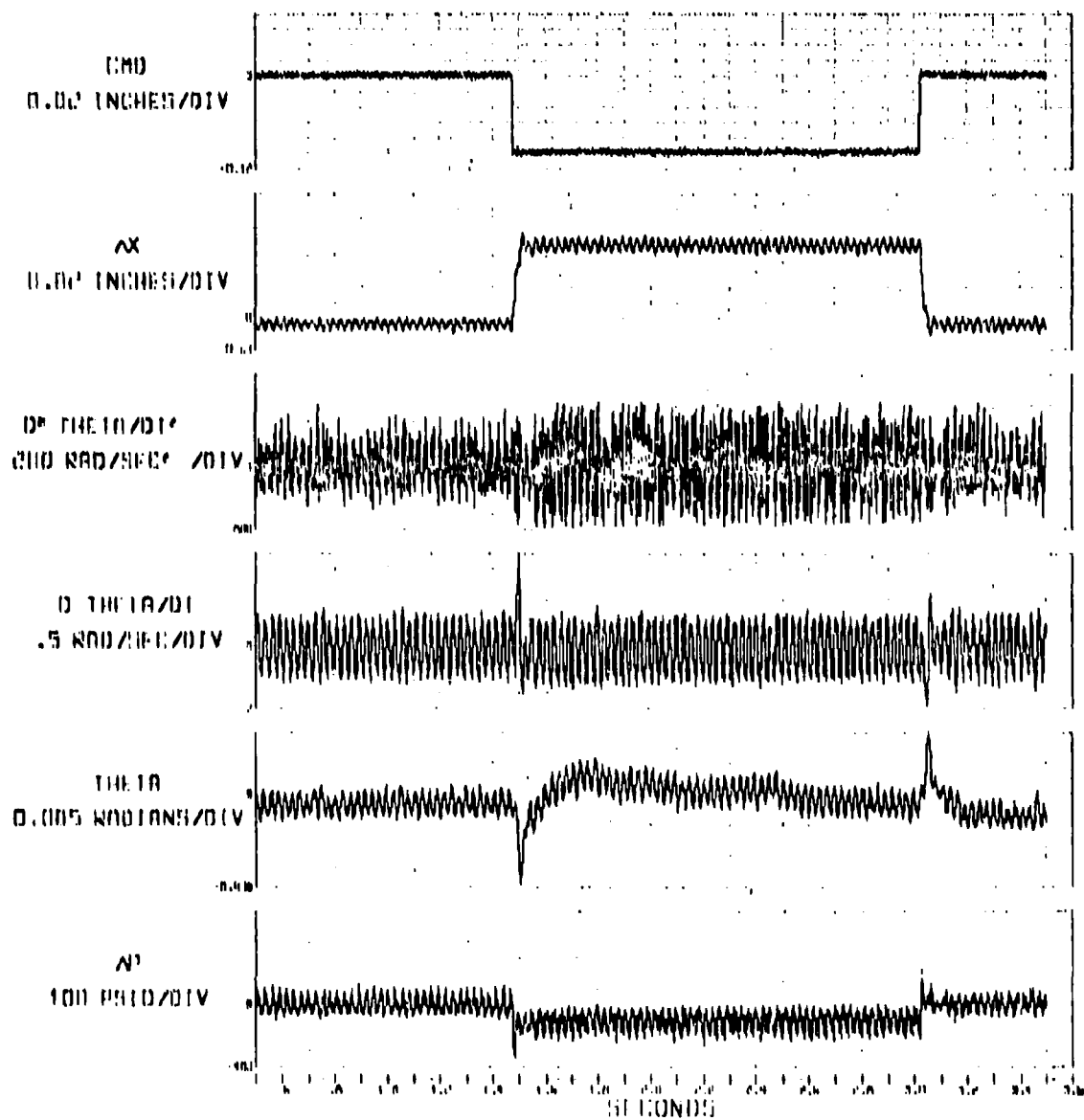
119

ACTIVE AND PASSIVE SHIMMY TESTS
FIELD RUN 32 PASSIVE

TEST 26617   RUN 9   18 SEP 75

120
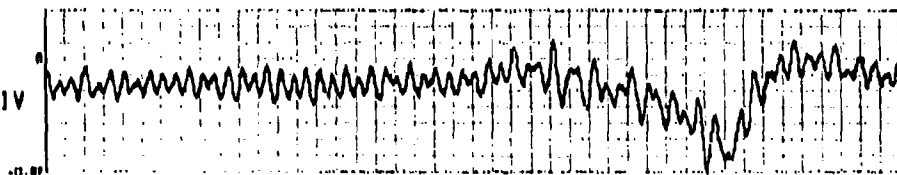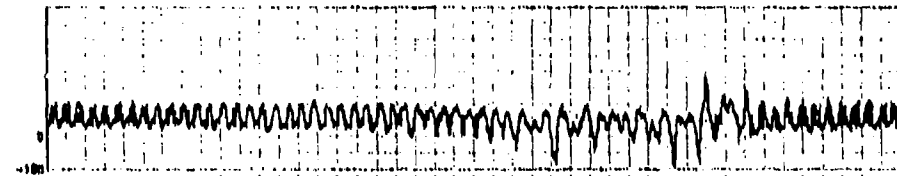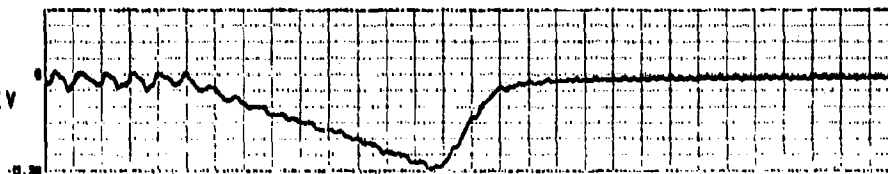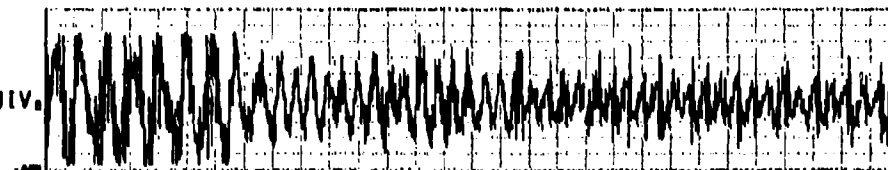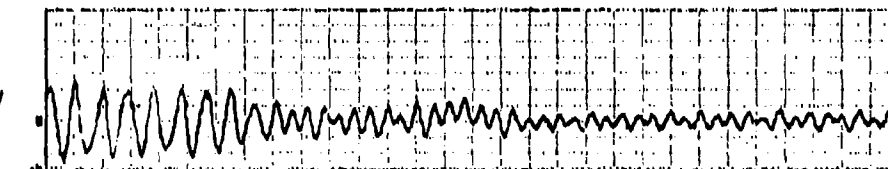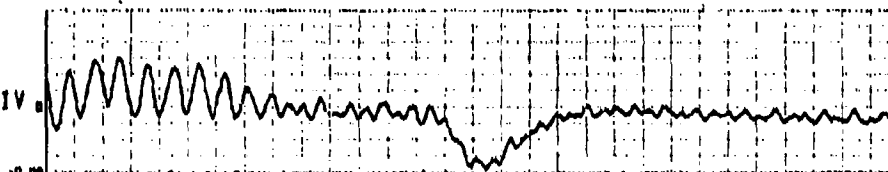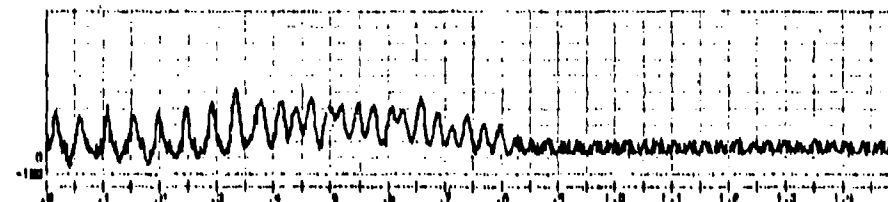
ACTIVE AND PASSIVE SHIMMY TESTS
FIELD RUN 33 PASSIVE

TEST 26617   RUN 16   18 SEP 75
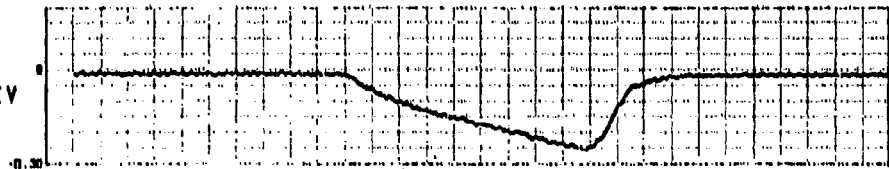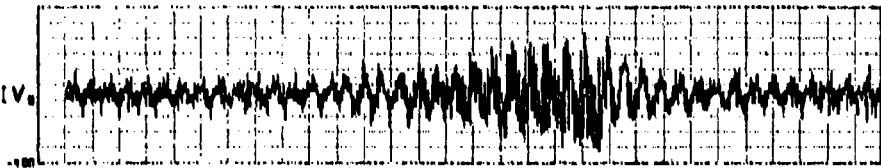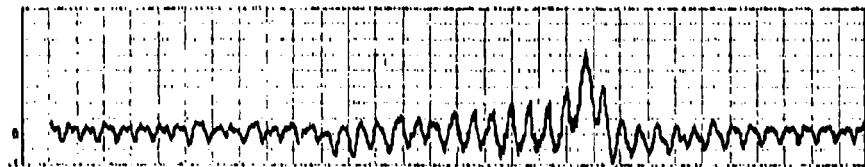
ΔX
0.05 INCHES/DIV

D'THETA/DT'
100 RAD/SEC' /DIV

D THETA/DT
.5 RAD/SEC/DIV

THETA
0.01 RADIANS/DIV

ΔP
50 PSID/DIV

SECONDS

121
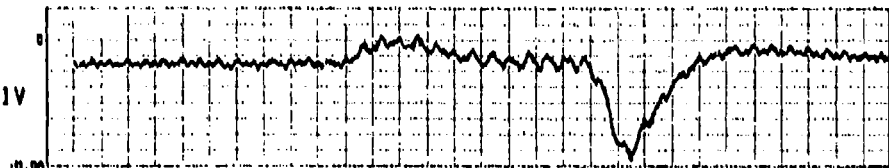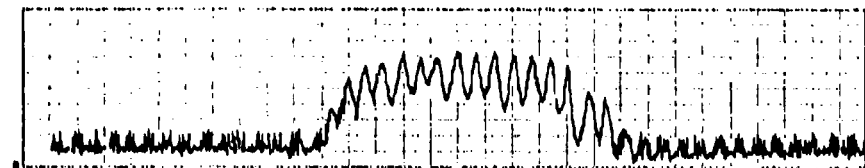
ACTIVE AND PASSIVE SHIMMY TESTS
FIELD RUN 34 PASSIVE

TEST 26617   RUN 15   10 SEP 75
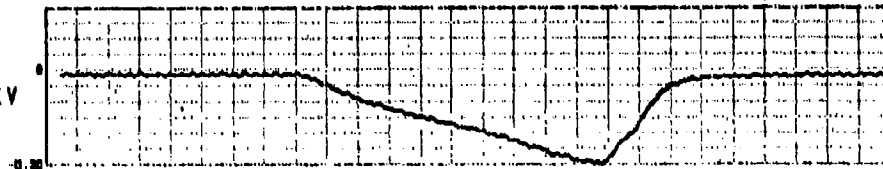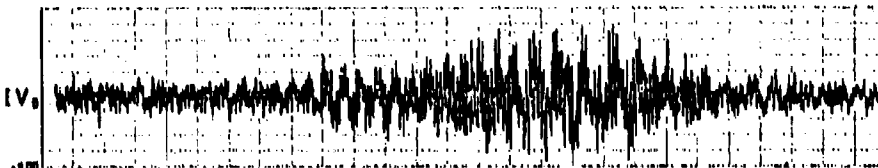
ΔX
0.05 INCHES/DIV

D"THETA/DT"
100 RAD/SEC" /DIV

D THETA/DT
.5 RAD/SEC/DIV

THETA
0.01 RADIANS/DIV

ΔP
50 PSID/DIV
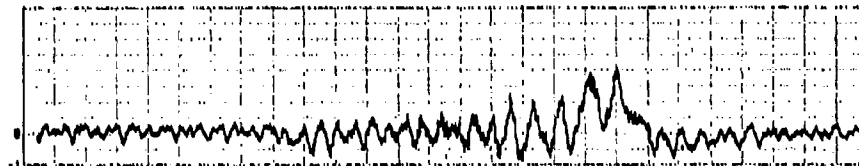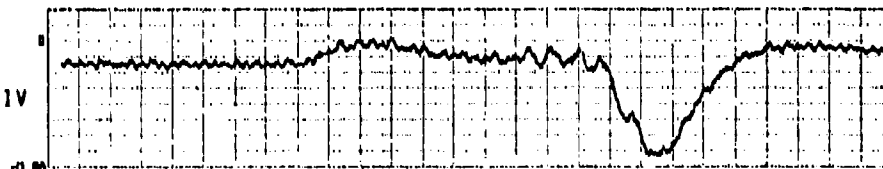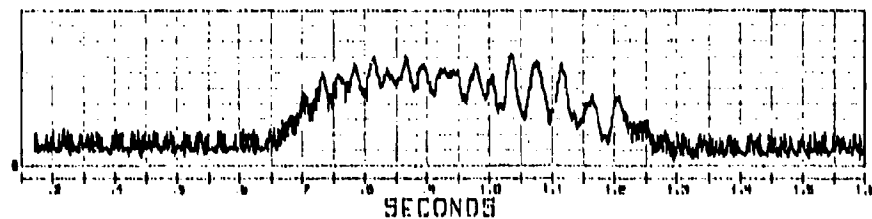
SECONDS

ACTIVE AND PASSIVE SHIMMY TESTS
FIELD RUN 39 PASSIVE

TEST 26617   RUN 14   18 SEP 75
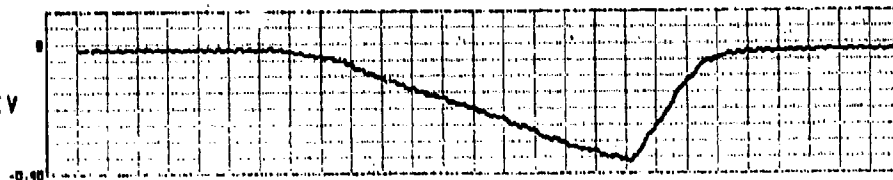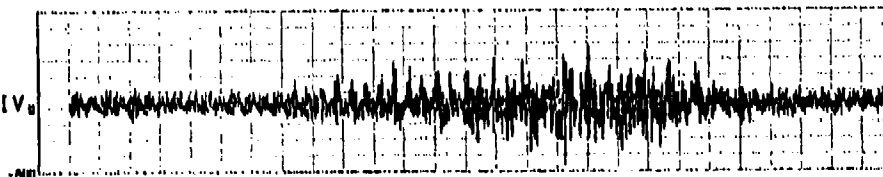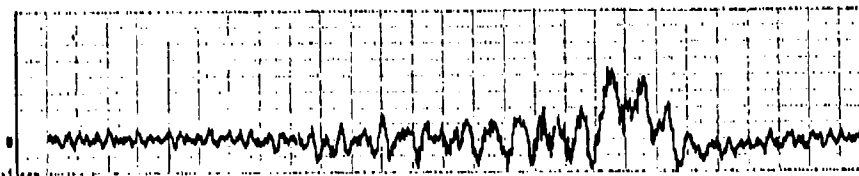
123
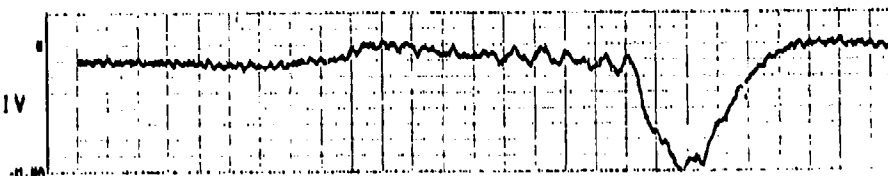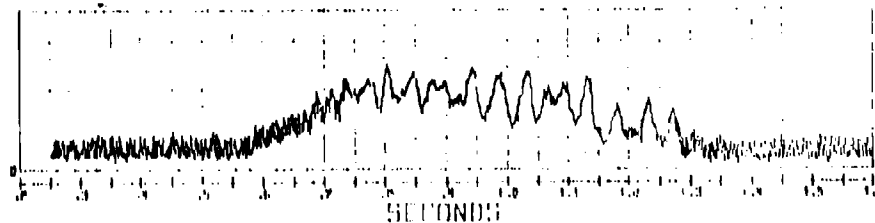
ACTIVE AND PASSIVE SHIMMY TESTS
FIELD RUN 34 PASSIVE

TEST 26591   RUN 1   17 SEP 75

124
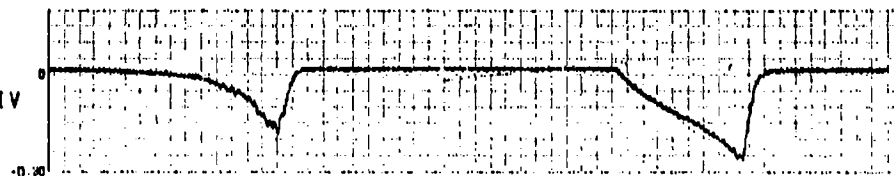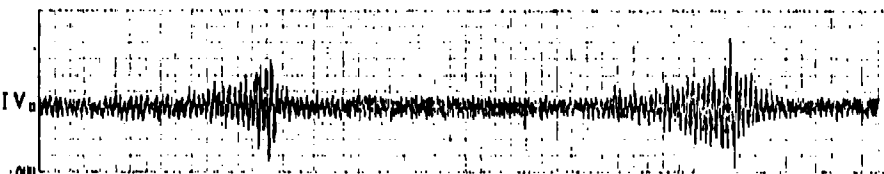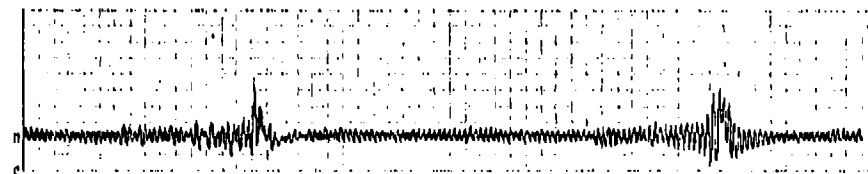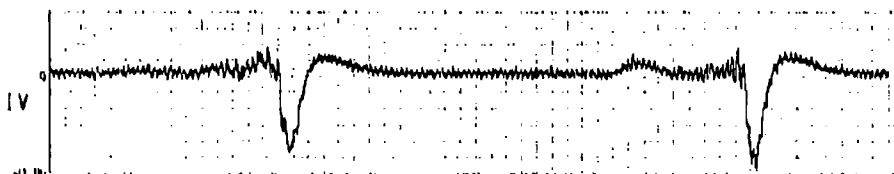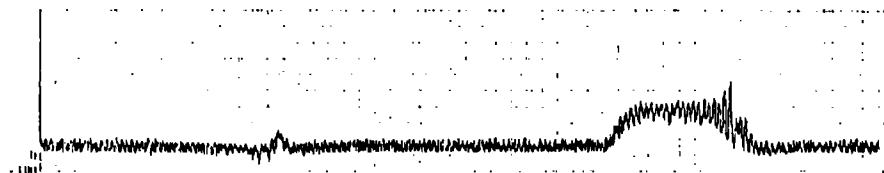
ACTIVE AND PASSIVE SHIMMY TESTS
FIELD RUN 40 PASSIVE

YEST 26617   RUN .17   18 SEP 75

ΔX
0.05 INCHES/DIV

D'THETA/DT'
200 RAD/SEC' /DIV

D THETA/DT
.5 RAD/SEC/DIV

THETA
0.01 RADIANS/DIV

ΛP
50 PSIO/DIV
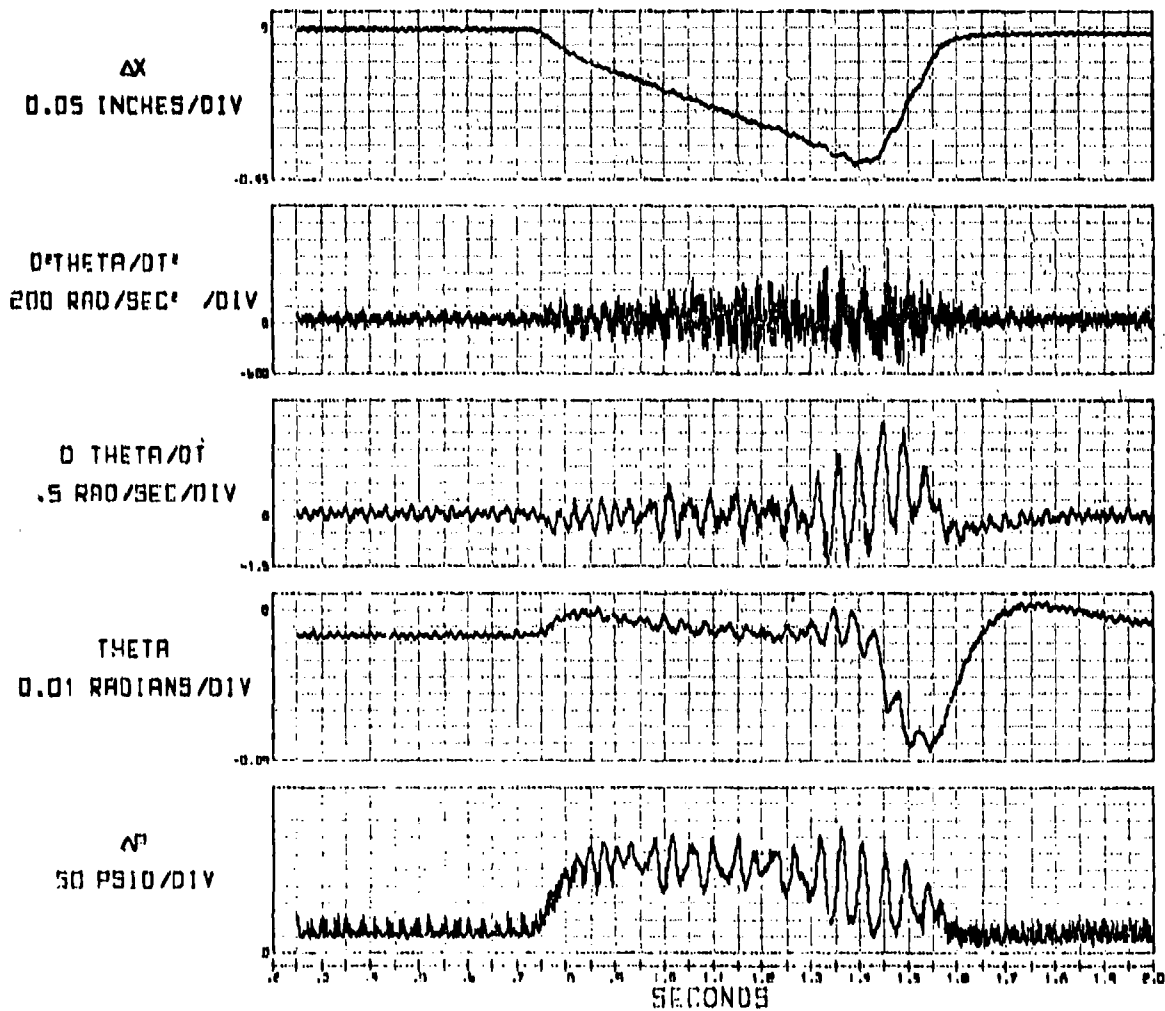
SECONDS

ACTIVE AND PASSIVE SHIMMY TESTS
FIELD RUN 41 PASSIVE

TEST 26617   RUN 19   18 SEP 75
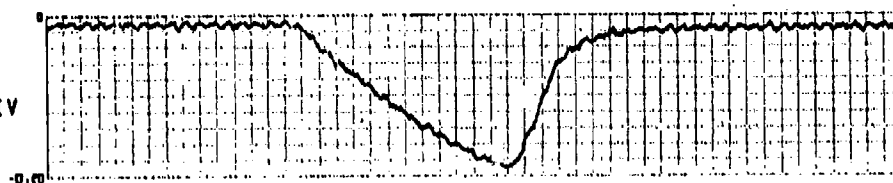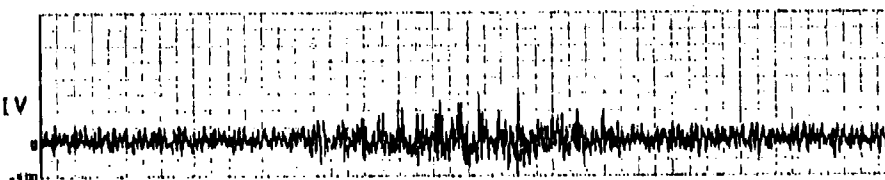
ΔX
0.02 INCHES/DIV

D"THETA/DT"
200 RAD/SEC" /DIV

D THETA/DT
.5 RAD/SEC/DIV

THETA
0.01 RADIANS/DIV

N'
50 PSID/DIV
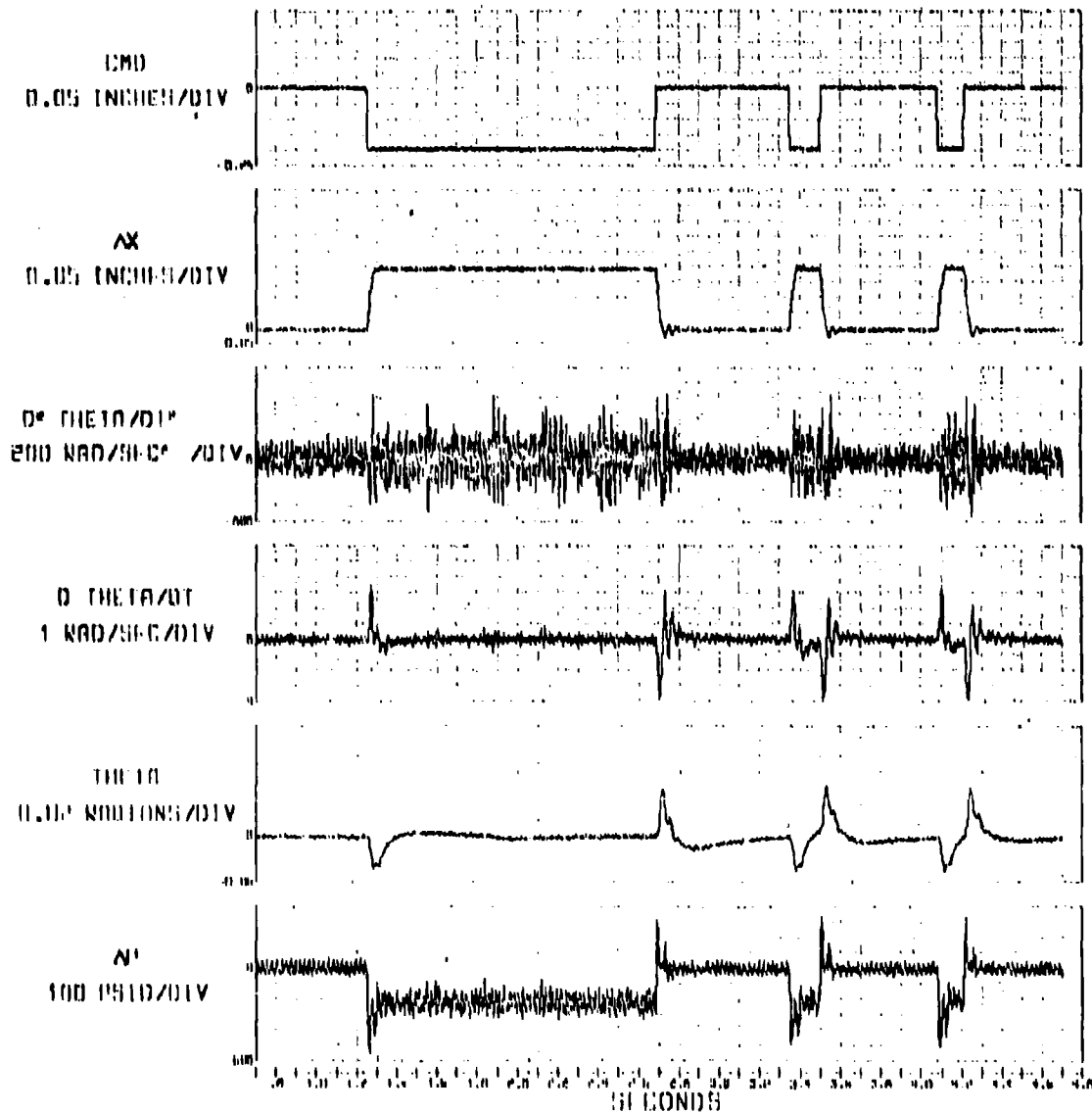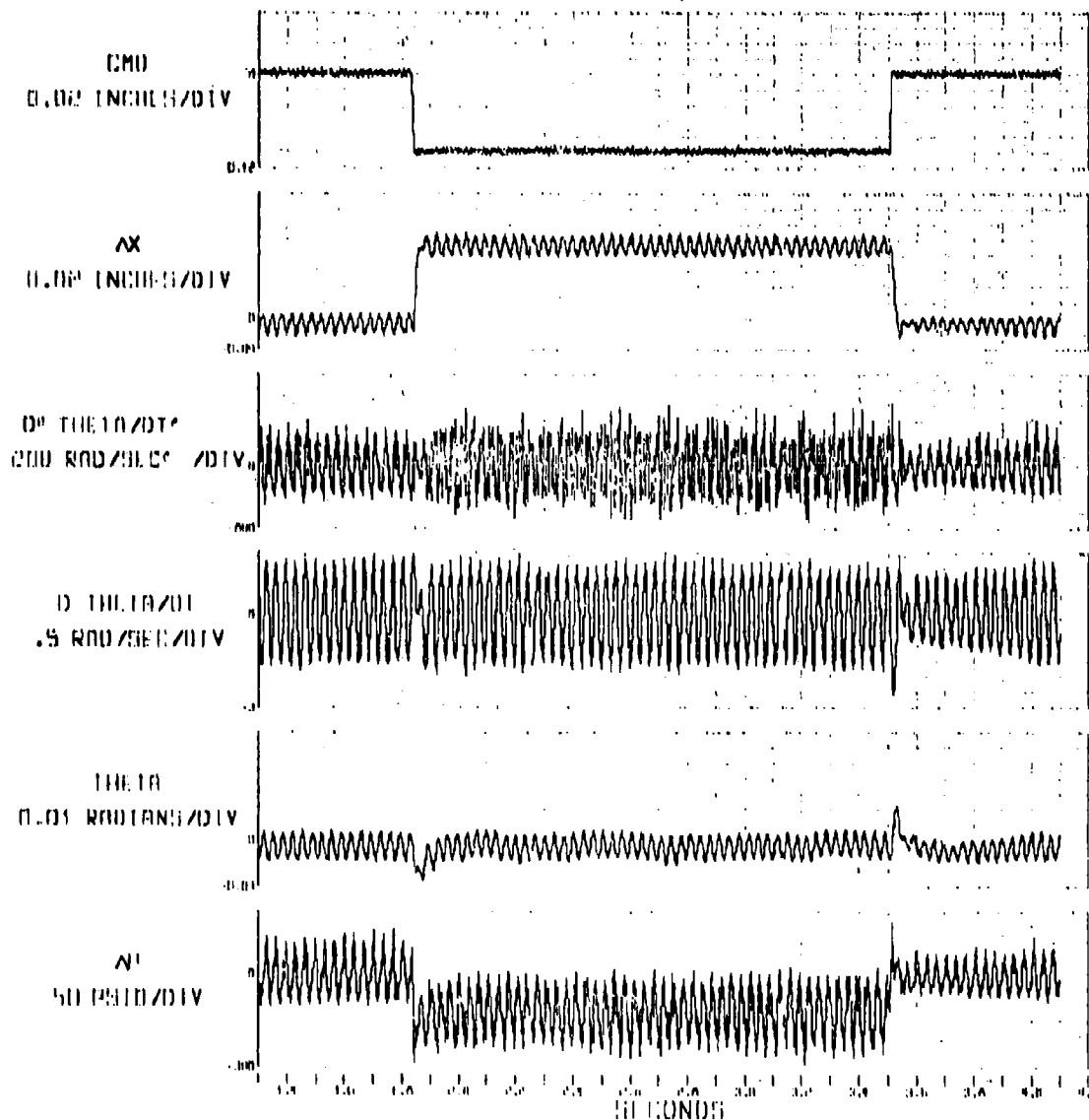
SECONDS

126
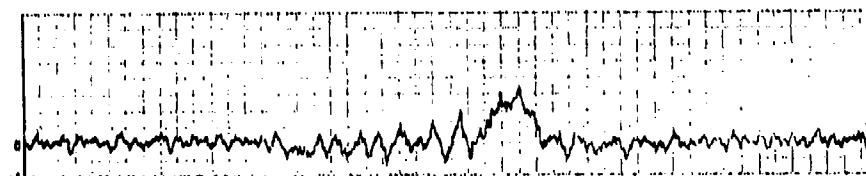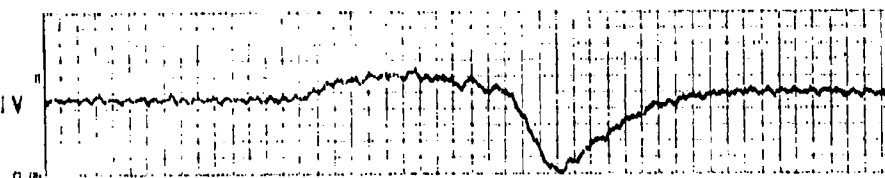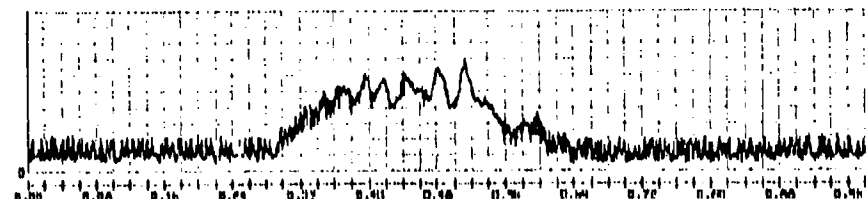
ACTIVE AND PASSIVE SHIMMY TESTS
FIELD RUN 150

TEST 265/12   RUN 3   16 SEP 75

127

ACTIVE AND PASSIVE SHIMMY TESTS
FIELD RUN 19b

TEST 2b5?b   RUN 4   16 SEP 75

128

ACTIVE AND PASSIVE SHIMMY TESTS
FIELD RUN 159

TEST P65/N°   RUN 5   16 SEP 75

CMD
0.05 INCHES/DIV

ΔX
0.05 INCHES/DIV

D² THETA/DT²
200 RAD/SEC² /DIV

D THETA/DT
1 RAD/SEC /DIV

THETA
0.02 RADIANS/DIV

N°
100 PSID/DIV

SECONDS

129

ACTIVE AND PASSIVE SHIMMY TESTS
FIELD RUN 162

TEST 26477   RUN 3   16 SEP 75

CMD
0.02 INCHES/DIV

ΛX
0.02 INCHES/DIV

DF THETA/DIV
200 RAD/SEC* /DIV

D THETA/DIV
.5 RAD/SEC/DIV

THETA
0.005 RADIANS/DIV

ΛP
50 PSID/DIV

SECONDS

130
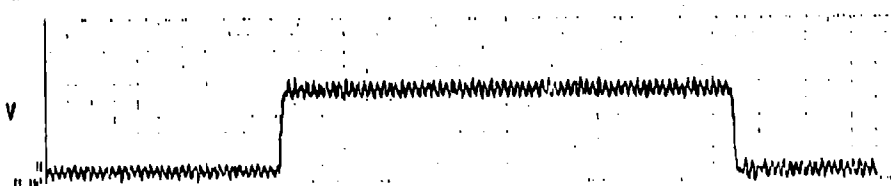
ACTIVE AND PASSIVE SHIMMY TESTS
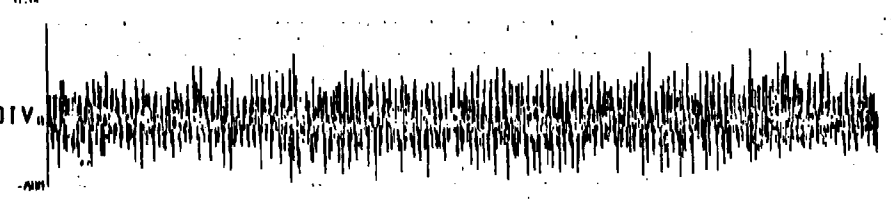FIELD RUN 163

TEST 265/N2   RUN 1   16 SEP 75

CMD
0.02 INCHES/DIV

X
0.02 INCHES/DIV

D² THETA/DT²
200 RAD/SEC²/DIV

D THETA/DT
.5 RAD/SEC/DIV

THETA
0.005 RADIANS/DIV

N'
100 PSID/DIV

SECONDS

131

ACTIVE AND PASSIVE SHIMMY TESTS
FIELD RUN 169

132

ACTIVE AND PASSIVE SHIMMY TESTS
FIELD RUN 167

133

ACTIVE AND PASSIVE SHIMMY TESTS
FIELD RUN 160

TEST 26SAP   RUN 7   16 SEP 75
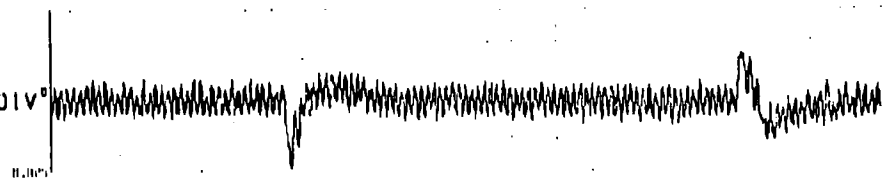
CMD
0.05 INCHES/DIV

AX
0.05 INCHES/DIV

D THETA/DT
200 RAD/SEC² /DIV

D THETA/DT
1 RAD/SEC/DIV

THETA
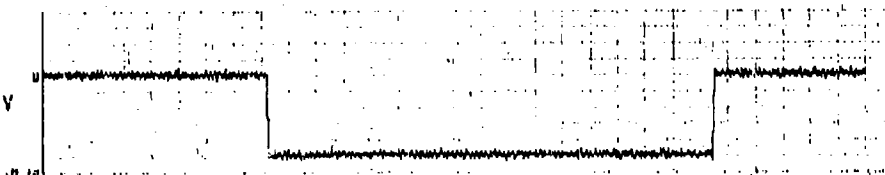0.02 RADIANS/DIV

N'
100 PSID/DIV

SECONDS

134

ACTIVE AND PASSIVE SHIMMY TESTS
FIELD RUN 160

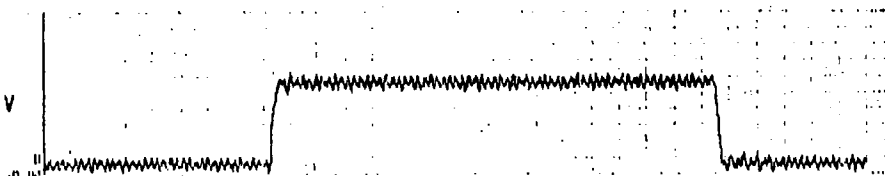TEST 25/42   RUN 8   16 SEP 75

CMD
0.05 INCHES/DIV

ΛX
0.05 INCHES/DIV

D" THETA/DT"
200 RAD/SEC" /DIV

D THETA/DT
1 RAD/SEC/DIV

THETA
0.10 RADIANS/DIV

N'
100 PSID/DIV

SECONDS

135

ACTIVE AND PASSIVE SHIMMY TESTS
FIELD RUN 120

TEST 26/30   RUN 9   16 SEP 75

ACTIVE AND PASSIVE SHIMMY TESTS
FIELD RUN 173

TEST 265/52   RUN 10   16 SEP 75
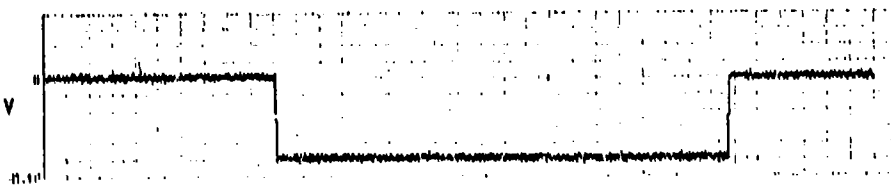
CMD
0.02 INCHES/DIV

ΛX
0.02 INCHES/DIV

D' THETA/DT'
200 RAD/SEC' /DIV

D THETA/DT
.5 RAD/SEC/DIV

THETA
0.005 RADIANS/DIV

N'
50 PSID/DIV

SECONDS

137

ACTIVE AND PASSIVE SHIMMY TESTS
FIELD RUN 120

TEST 265/2   RUN 11   16 SEP 75
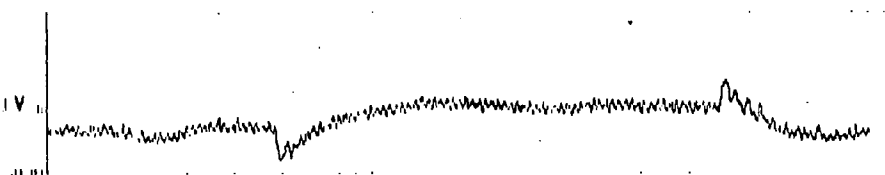
CMD
0.02 INCHES/DIV

ΛX
0.02 INCHES/DIV

D² THETA/DT²
200 RAD/SEC² /DIV

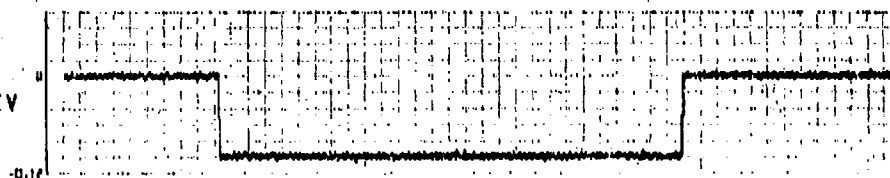D THETA/DT
.5 RAD/SEC/DIV

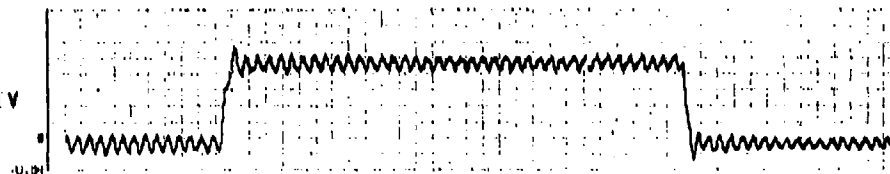THETA
0.01 RADIANS/DIV

N'
50 PSID/DIV

SECONDS

138

ACTIVE AND PASSIVE SHIMMY TESTS
FIELD RUN 177

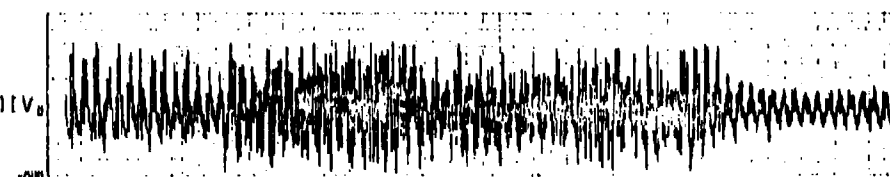TEST 26565   RUN 1   16 SEP 75

CMD
0.02 INCHES/DIV

ΛX
0.02 INCHES/DIV

D² THETA/DT²
200 RAD/SEC² /DIV

D THETA/DT
1 RAD/SEC/DIV

THETA
0.01 RADIANS/DIV

N'
100 PSID/DIV

SECONDS

ACTIVE AND PASSIVE SHIMMY TESTS
FIELD RUN 17A

TEST 26505   RUN P   16 SEP 75
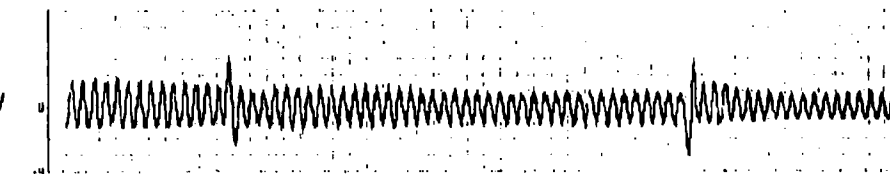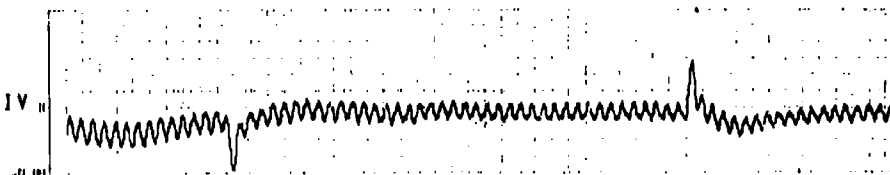

CMD
0.02 INCHES/DIV

AX
0.02 INCHES/DIV

D² THETA/DT²
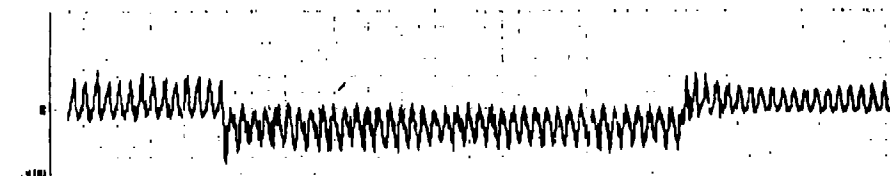200 RAD/SEC² /DIV

D THETA/DT
1 RAD/SEC/DIV

THETA
0.02 RADIANS/DIV

NP
100 PSID /DIV

SECONDS

ACTIVE AND PASSIVE SHIMMY TESTS
FIELD RUN 179

TEST 265/15   RUN 4   16 SEP 75

CMD
0.02 INCHES/DIV

ΛX
0.02 INCHES/DIV

D* THETA/DT*
200 RAD/SEC* /DIV

D THETA/DT
.5 RAD/SEC/DIV

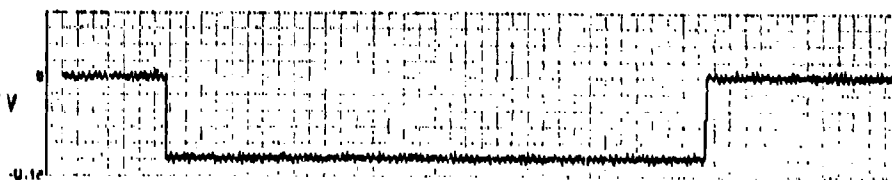THETA
0.01 RADIANS/DIV

ΛP
50 PSIO/DIV

SECONDS

141

ACTIVE AND PASSIVE SHIMMY TESTS
FIELD RUN 102

TEST 26585   RUN 5   16 SEP 75

CMD
0.05 INCHES/DIV

ΔX
0.05 INCHES/DIV

D² THETA/DT²
200 RAD/SEC² /DIV

D THETA/DT
1 RAD/SEC/DIV

THETA
0.02 RADIANS/DIV

ΔP
100 PSID/DIV

SECONDS

ACTIVE AND PASSIVE SHIMMY TESTS
FIELD RUN 1A3

TEST 26575   RUN 6   16 SEP 75
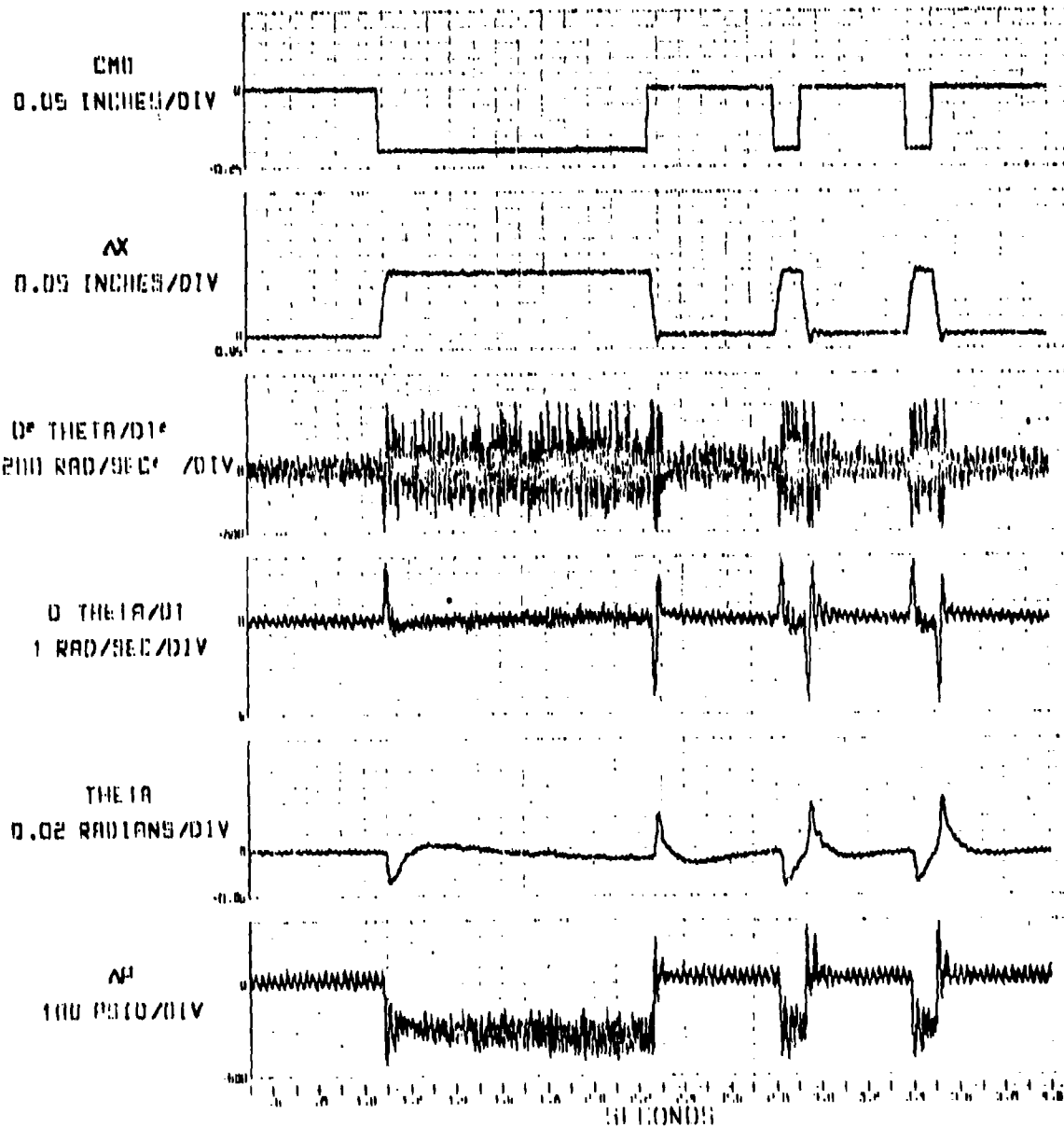
CMD
0.05 INCHES/DIV

AX
0.05 INCHES/DIV

D² THETA/DT²
200 RAD/SEC²/DIV

D THETA/DT
1 RAD/SEC/DIV

THETA
0.02 RADIANS/DIV

AP
100 PSIG/DIV

SECONDS

143

ACTIVE AND PASSIVE SHIMMY TESTS
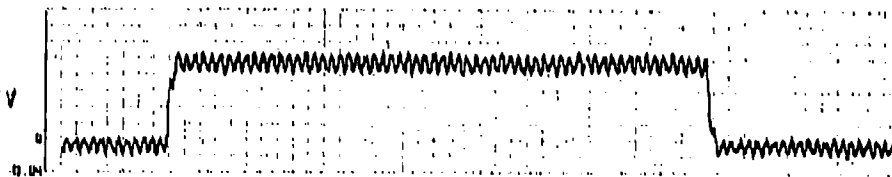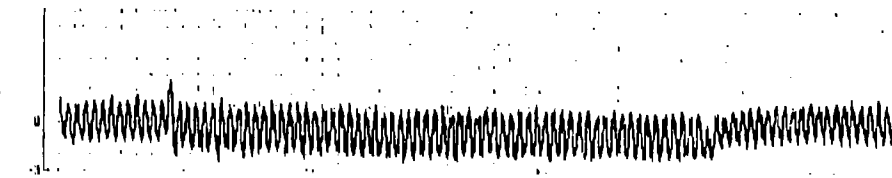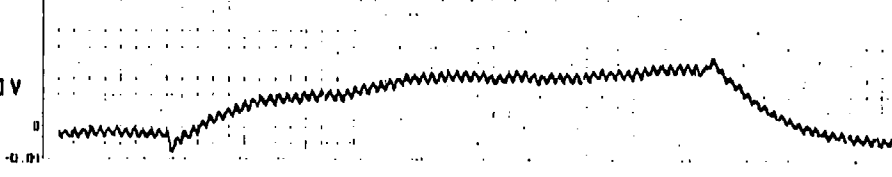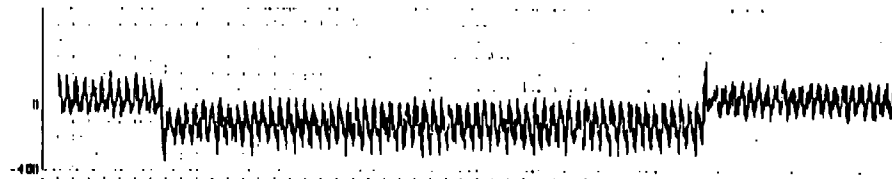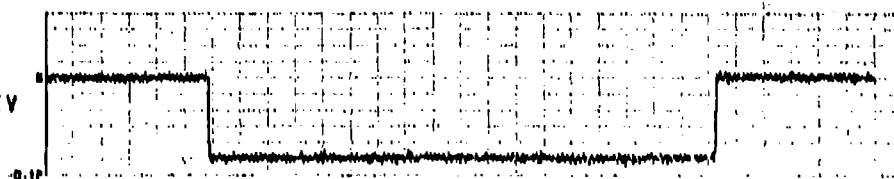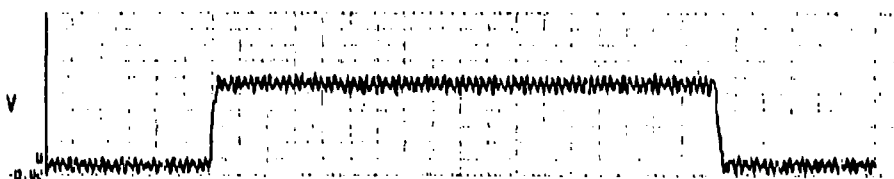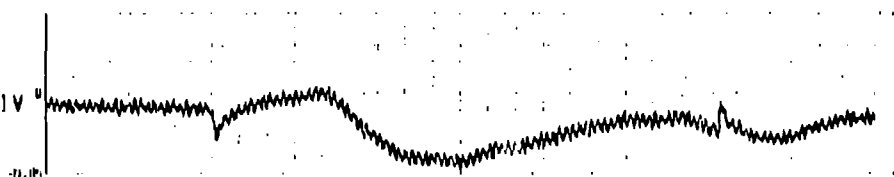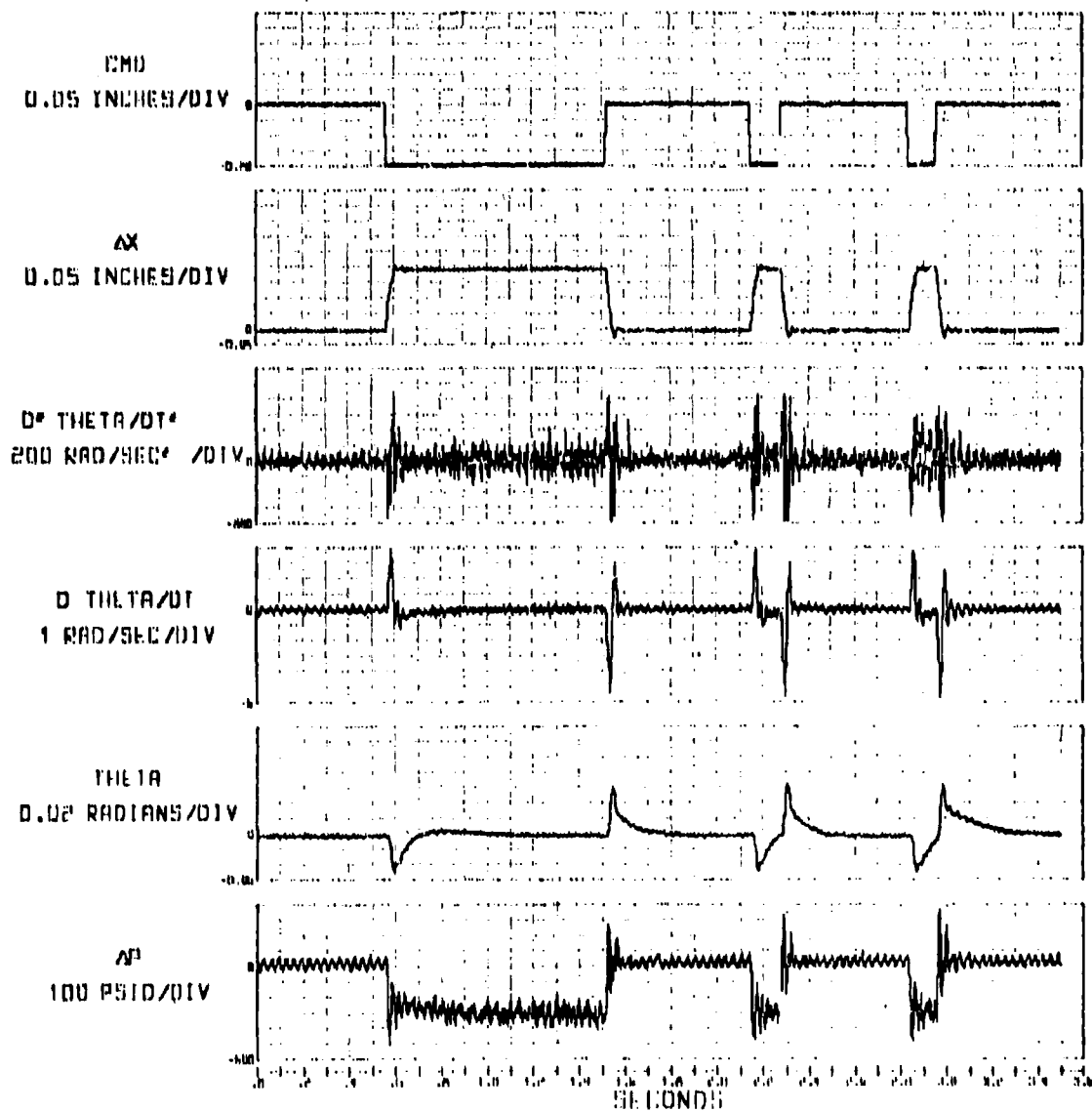FIELD RUN 154

TEST 26505   RUN 7   16 SEP 75

APPENDIX D
ANALYTICAL MODEL EQUATIONS

This appendix contains the equations of motion resulting from the analytical model of the Active Shimmy Control System described in the main body of the report. These equations are divided into two sections; initial conditions are the calculations performed only once per run involving quantities independent of time, and the time varying equations involve quantities that change with time.

With the Continuous System Modeling Program (CSMP) language used, the sequence of computations for the time varying equations is determined by the translator which translates the CSMP program into a FORTRAN program for compilation and execution. Therefore, the sequence of equations shown herein has no significance. It is appropriate to think of all these equations as being solved simultaneously as they are on an analog computer.

Table D-1 shows a description of the CSMP special functions used in the program. The nomenclature for the equations is the same as described in the section ANALYTICAL MODEL DESCRIPTION.

Initial Conditions

$$V = 88*12/60*VMPH$$

$$PI = 3.14159265$$

$$W1 = M*386$$

$$MLH = M*L*H$$

$$IIMM = ITH*IPH-MLH*MLH$$

Time Varying Equations

LATACC	=	H*PHDD/386
MUNB	=	UNBIO*RIMW*((V/R)**2)/32/386
MZUNBL	=	MUNB*SIN(V*TIME/R)
MXUNBL	=	MUNB*SIN(V*TIME/R-PI/2)

PHDS	=	DEADSP(-DPH,DPH,PH)
MPH	=	KPH*PHDS
MPHD	=	BPH*PHD
FS	=	MPH/H
YB	=	Y delayed by Z*HS/V
YD	=	(-Y+(SG+HS-L-LG)*TH+(H+R)*PH)*V/SG

FT	=	(Y+YB+2*(L+LG)*TH-2*(H+R)*PH)*KT
MT	=	(Y-YB-2*HS*TH)*KM

ALT2	=	AL-T2
ALT2D	=	ALD-T2D
TT	=	TH-T1
T1AL	=	T1-AL
T1ALDS	=	DEADSP(-DAL,DAL,T1AL)
TTDS	=	DEADSP(-DTH,DTH,TT)
TTD	=	THD-T1D

146

```
TT1      =  T1-T2

TT1D     =  T1D-T2D

AT       =  AL-AL1


THMDD    =  (OMEGA**2)*CMPXPL(0,0,ZETAA, OMEGAA, THDD)

THMD     =  .1*REALPL(0,.1, THMDD)

THM      =  .1*REALPL(0,.1, THMD)

XC       =  GISMAL*THMDD

ALT2PP   =  LEDLAG (P1,P2,XC)

ALT2C    =  ALT2PP


BETAD    =  (-BL+SQRT(ABS(BL*BL-4*BH*FKAL)))/(-2*BH)      FKAL ≤ 0

BETAD    =  (-BL+SQRT(ABS(BL*BL+4*BH*FKAL)))/(+2*BH)      FKAL > 0


BETA     =  AL1-T2

AL1D     =  BETAD+T2D

AL1      =  INTGRL(AL10,AL1D)


FK       =  KTH*TTDS

FKAL     =  KALP*AT                      Passive

FKAL     =  K3*INTGRL (0., X11)          Active

X11      =  X9-X10-K6*FKAL

X10      =  -K4*ALT2D

X9       =  X4*X8

X8       =  SIGN(X7)*SQRT (ABS(X7))

X7       =  X5-X6

X6       =  K5*FKAL

X5       =  K2*LIMIT(-1/K2, 1/K2, X2)

X4       =  ABS(X3)

X3       =  LIMIT (-1,1,X2)

X2       =  K1*OMEGAS**2*CMPXPL(0,0,ZETAS,OMEGAS,X1)

X1       =  ALT2C + K7*ALT2
```

147
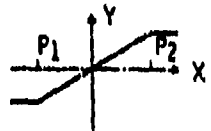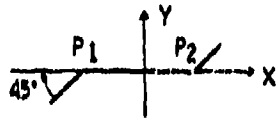
```
CP      =  CP1 + CP2*ABS(FS)

CF      =  CF1 + CF2*ABS(FS)


FCP     =  INSW(T1D,-CP,CP)

FCF     =  INSW(TT1D,-CF,CF)

FCA     =  INSW(ALT2D,-CA,CA)

FKOC    =  KOC*T1ALDS

FFUS    =  KF*T2 + BF*T2D


SPH     =  -I*V/R*THD-W1*L*TH+W*H*PH +MPH + MPHD
           -(H+R)*FT - (H+R)*FZ*PH+(L+LG)*FZ*TH-MXUNBL

STH     =  I*V/R*PHD +FK +FCP +(L+LG)*FT-MT-MZUNBL


PHDD    =  (-ITH*SPH-MLH*STH)/IIMM

THDD    =  (-IPH*STH-MLH*SPH)/IIMM

T1DD    =  (FCP+FK-FCF-FKOC)/ITH1

T2DD    =  (FCF+FCA+FKAL-FFUS)/ITH2

ALDD    =  (FKOC-FKAL-FCA)/IAL

PH      =  INTGRL(PHO,PHD)

PHD     =  INTGRL (PHDO,PHDD)

TH      =  INTGRL (THO, THD)

THD     =  INTGRL (THDO, THDD)

T1      =  INTGRL (T1O, T1D)

T1D     =  INTGRL (T1DO,T1DD)

T2      =  INTGRL (T2O, T2D)

T2D     =  INTGRL (T2DO, T2DD)

AL      =  INTGRL (ALO, ALD)

ALD     =  INTGRL (ALDO,ALDD)

Y       =  INTGRL (YO,YD)
```

148

GENERAL FORM	FUNCTION
$\dot{Y}$ = INTGRL (IC, X) Y (0) = IC INTEGRATOR	$Y = \int_0^t X \, dt + IC$ EQUIVALENT LAPLACE TRANSFORM: $\frac{1}{S}$
Y = REALPL (IC, P, X) Y (0) = IC 1ST ORDER LAG (REAL POLE)	$P\dot{Y} + Y = X$ EQUIVALENT LAPLACE TRANSFORM: $\frac{1}{PS + 1}$
Y = LEDLAG (P_1, P_2, X) LEAD - LAG	$P_2\dot{Y} + Y = P_1\dot{X} + X$ EQUIVALENT LAPLACE TRANSFORM: $\dfrac{P_1 S + 1}{P_2 S + 1}$
Y = CMPXPL $(IC_1, IC_2, P_1, P_2, X)$ Y (0) = IC_1 $\dot{Y}$ (0) = IC_2 2ND ORDER LAG (COMPLEX POLE)	$\ddot{Y} + 2P_1 P_2 \dot{Y} + P_2^2 Y = X$ EQUIVALENT LAPLACE TRANSFORM: $\dfrac{1}{S^2 + 2P_1 P_2 S + P_2^2}$
Y = INSW (X_1, X_2, X_3) INPUT SWITCH (RELAY)	$Y = X_2 \qquad X_1 < 0$ $Y = X_3 \qquad X_1 \geq 0$

Y = LIMIT (P_1, P_2, X) LIMITER	$Y = P_1 \qquad X < P_1$ $Y = P_2 \qquad X > P_2$ $Y = X \qquad P_1 \leq X \leq P_2$	
Y = DEADSP (P_1, P_2, X) DEAD SPACE	$Y = 0 \qquad P_1 \leq X \leq P_2$ $Y = X - P_2 \qquad X > P_2$ $Y = X - P_1 \qquad X < P_1$	

ACTIVE SHIMMY CONTROL SYSTEM LINEARIZED ANALYSIS

1. Control Law Definition

The following simplified schematic represents an electrohydraulic valve and actuator driving an undamped spring/inertia resonant system with acceleration feedback.
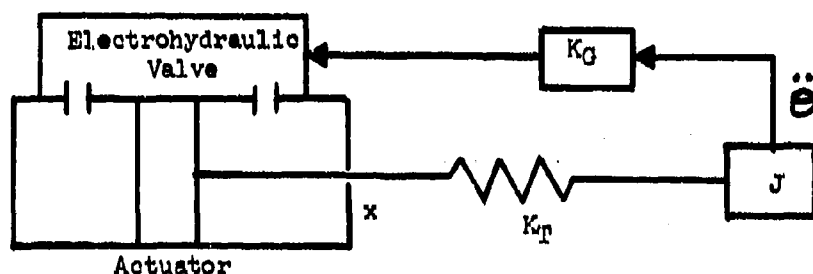
The block diagram for this system is the following
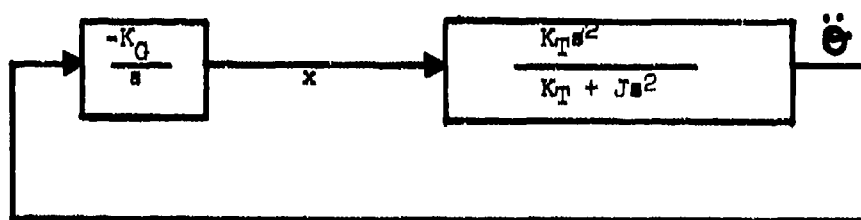
The parameters and variables are defined as follows:

K_G is the normalized Accelerometer-Electronics-Valve-Actuator

gain in rad/rad/sec^2

K_T is the torsional spring stiffness in in-lb/rad

J is the torsional inertia in in-lb/rad/sec^2

x is the actuator rotation in radians

θ is the spring - inertia mode rotation in radians

The characteristic equation for the system is

$$\left(\frac{-K_G}{s}\right) \frac{K_T s^2}{K_T + J s^2} = 1$$

$$J s^2 + K_T K_G s + K_T = 0$$

$$\frac{s^2}{K_T/J} + K_G s + 1 = 0$$

$$\frac{s^2}{\omega_n^2} + \frac{2\zeta s}{\omega_n} + 1 = 0$$

where

$$\omega_n^2 = \frac{K_T}{J}$$

$$\zeta = \frac{K_G \omega_n}{2}$$

From the characteristic equation, it is observed that the value of K_G directly controls the damping of the spring-inertia resonant mode. For the case of a resonant mode at 22 Hz or 138 radians, a K_G gain of 0.00725 provides a damping ratio of 0.50.

The above simplified model and analysis served as a basis for selection of the accelerometer feedback configuration employed in the active shimmy control system. Note that the tire dynamics are omitted from the model which alters the resonant frequency only slightly, and adds negative damping under certain conditions. The positive damping from gear friction is also ignored.

2. Expanded Model

The simplified model is expanded to include accelerometer and valve-actuator dynamics, position feedback on the actuator for electrical

151

steering and provisions for electronic compensation. This expanded block diagram is shown in Figure E-1. Again, tire and gear damping are not included in order to focus on the characteristics of the active system.

The lumped inertia of the torsional mode (J) is selected as 0.7 in-lb/rad/sec^2, based on laboratory measurements. The lumped spring rate of the torsional mode (K_T) is 1.51×10^4 in.lb./rad., producing an undamped torsional frequency of 23.4 Hz or 147 radians/sec in agreement with laboratory and dynamometer test results. The accelerometer transfer function is approximated by a second order system with an undamped resonant frequency (ω_{n_A}) of 1000 rad/sec and damping ratio (ζ_A) of 0.8 to match laboratory frequency response test results.

It is initially assumed that the actuator dynamically produces an actuator rate in proportion to valve flow so that the combined valve and actuator transfer function can be approximated by the valve response characteristics alone. This assumption ignores the valve flow rate degradation with load pressure, the fluid compressibility and leakage effects, all of which are of minor importance for the conditions tested. Using the supplier's data, the valve transfer function is approximated by a second order system with an undamped resonant frequency (ω_{nV}) of 1000 rad./sec. and a damping ratio (ζ_V) of 0.65.

The root locus for this system with no compensation and a nominal position loop gain (K_{fb}) of 82 is shown in Figure E-2. It is observed that a K_G of 0.0063 (corresponding to $K_\alpha = 1$, where K_α is the feedback gain parameter used during the shimmy tests) yields a modified torsional mode frequency of 16 Hz with a damping ratio of 0.42, while the next higher frequency mode created by the active system (7 Hz) has a damping ratio of 0.62. The system gain margin is 4 (at $K_G = 0.0252$, the 67 Hz mode has increased to 88 Hz with 0 damping). Excellent response and damping characteristics are obtained with this configuration.

Steering Command

Servovalve and Actuator

$$\frac{1}{s\left(\dfrac{s^2}{\omega_{NV}^2} + \dfrac{2\zeta_S}{\omega_{N_V}}s + 1\right)}$$

Structural Torsional Mode

$$\frac{K_T^2}{K_T + Js^2}$$

K_{Tb}

Accelerometer

$$\frac{1}{\dfrac{s^2}{\omega_{nA}^2} + \dfrac{2\zeta_A}{\omega_{nA}}s + 1}$$

Compensation Network

Gain

K_G
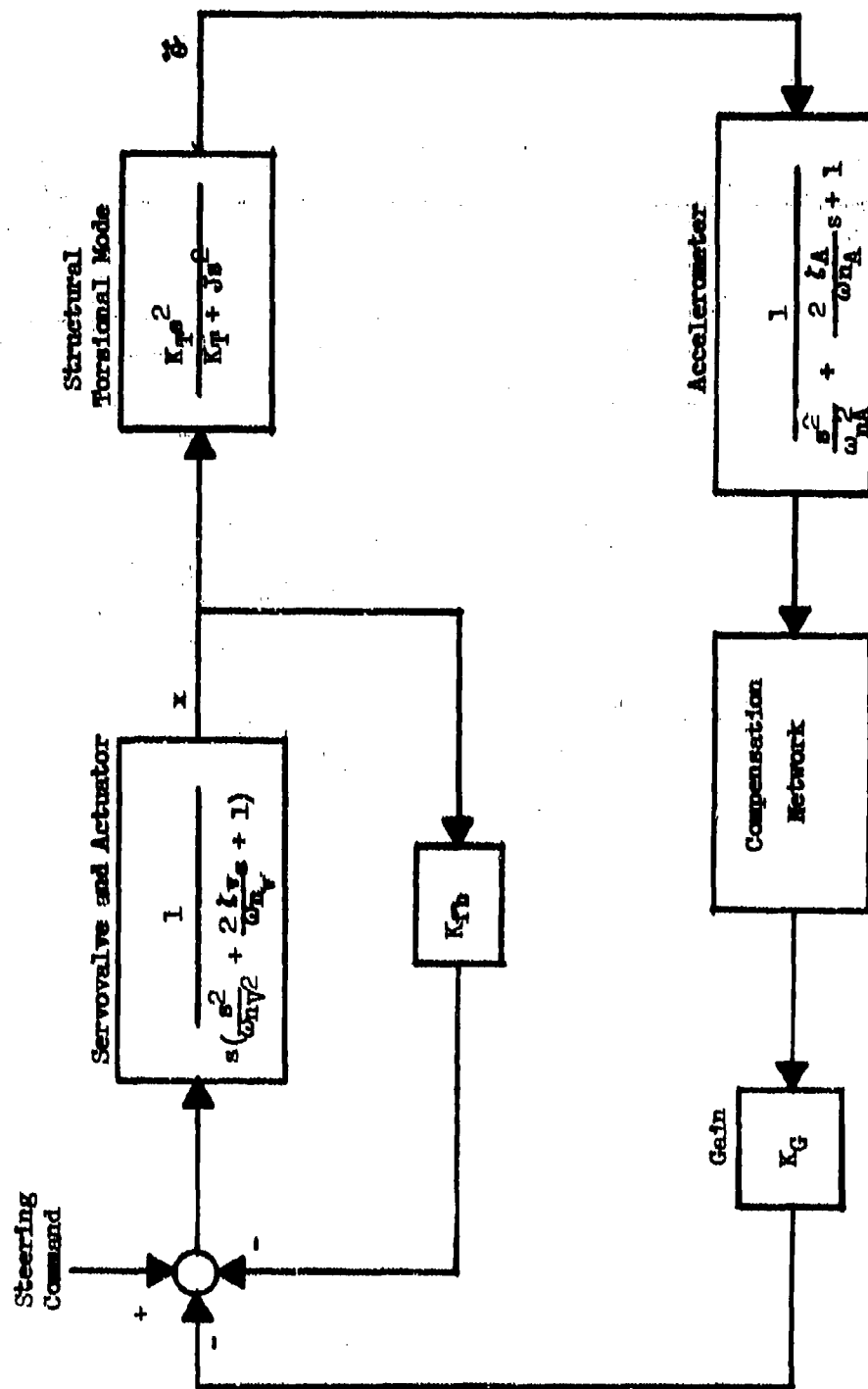
FIGURE E-1 - ACTIVE SHIMMY SYSTEM EXPANDED BLOCK DIAGRAM

153

Point	Gain K_Q
1	0
2	0.00315
3	0.0063
4	0.0126
5	0.0252

Servovalve and Actuator Quadratic

$\triangleright$ $f = 16$ Hz $\zeta = 0.42$

$\triangleright$ $f = 67$ Hz $\zeta = 0.62$

$\triangleright$ $f = 88$ Hz $\zeta = 0$

Mode Created by Active System

Accelerometer Quadratic

Structural Torsional Mode

Position Loop

1200

800

400

Imaginary Axis

Real Axis
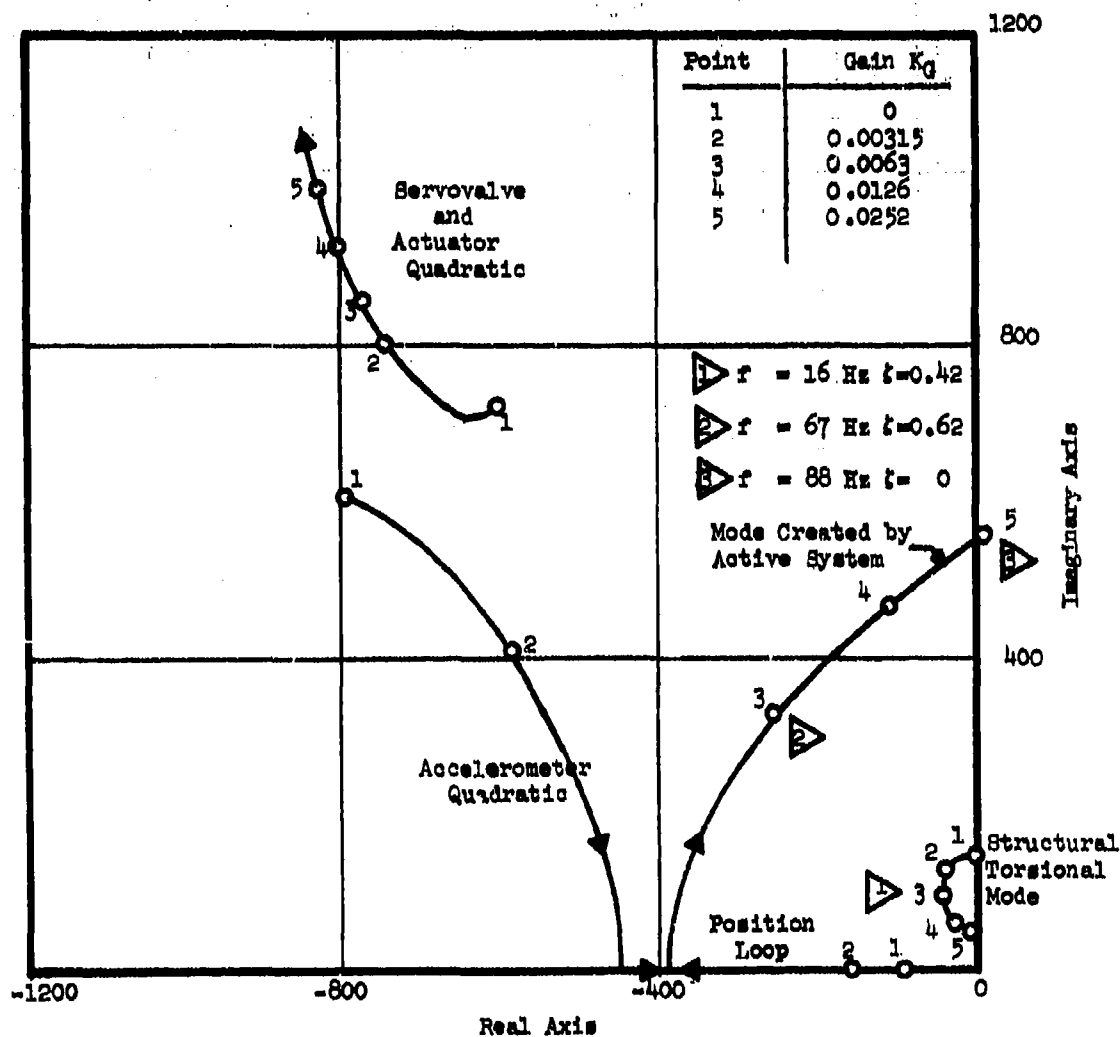
-1200   -800   -400   0

FIGURE E-2 — ROOT LOCUS OF LINEARIZED ACTIVE SHIMMY SYSTEM MODEL AS A FUNCTION OF K_Q

3. Model Refinement and Correlation with Experimental Test Results

Laboratory tests on the breadboard system indicated that the steering actuator characteristics produced some degradation in dynamic response of the combined valve and actuator as compared to the original estimates. The predominant sources of this degradation were not specifically identified but include such factors as dynamic seal leakage and stiffness, mounting stiffness, and hydraulic line and port characteristics. To approximate the high frequency dynamics measured in the laboratory, the valve and actuator quadratic in the active system model was modified to a resonant frequency (ω_{nv}) of 750 rad./sec. with a damping ratio (ζ_v) of 0.65.

During dynamometer testing at Wright Field, a structural mode at approximately 180 Hz was observed in the response data which was amplified by the active system with K_a gains as low 0.00189. A 5.14 to 1 bridged-T electronic compensation network was added to the active system to attenuate this mode by essentially replacing the mode by two real poles with the same undamped resonant frequency. This compensation network has the following transfer function, which is shown plotted in Figure E-3.

$$\frac{\dfrac{s^2}{\omega_{n_c}^2} + \dfrac{2\zeta_N}{\omega_{n_c}} s + 1}{\dfrac{s^2}{\omega_{n_c}^2} + \dfrac{2\zeta_D}{\omega_{n_c}} s + 1} \qquad \text{where} \quad \begin{aligned} \omega_{n_c} &= 1127 \text{ rad./sec.} \\ \zeta_N &= 0.257 \\ \zeta_D &= 1.32 \end{aligned}$$

The addition of these modifications to the block diagram shown in Figure E-1 produces a simplified linear approximation to the final configuration actually tested on the Wright Field dynamometer.

The root locus for this refined system model is shown in Figure E-4. The locus is based on the assumption that the compensation network numerator quadratic effectively cancels the structural mode quadratic leaving the compensation network denominator quadratic in the resulting
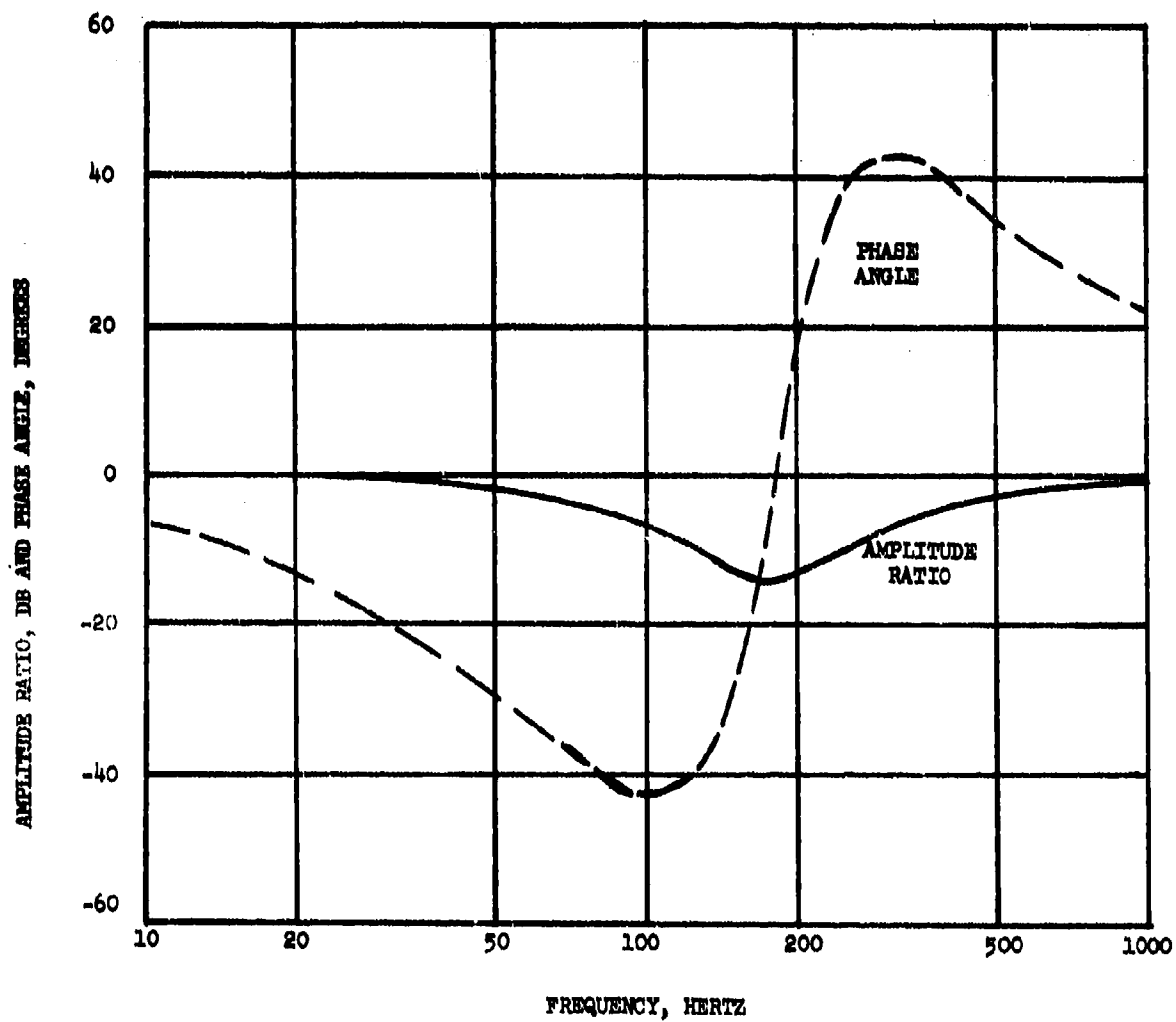
155

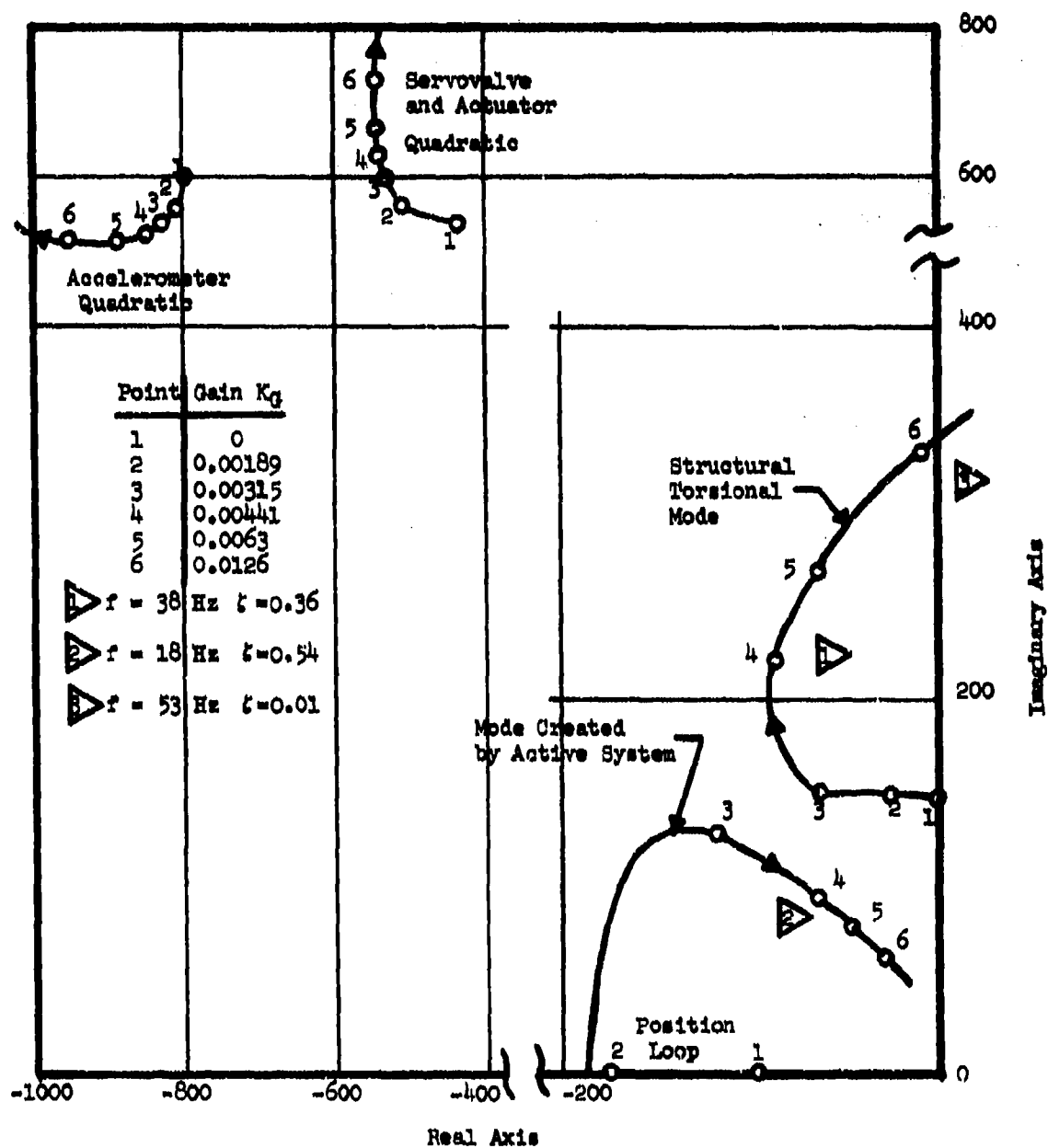FIGURE E-3 - BRIDGED-T NOTCH FILTER TRANSFER FUNCTION

Real Axis

FIGURE E-4 — ROOT LOCUS OF REFINED ACTIVE SHIMMY SYSTEM MODEL AS A FUNCTION OF K_G

800

6 Servovalve
   and Actuator
5
   Quadratic
4

3
2
1

6   5   4 3 2 1

Accelerometer
Quadratic

600

400

6

Structural
Torsional
Mode

5

4

200

Point	Gain K_G
1	0
2	0.00189
3	0.00315
4	0.00441
5	0.0063
6	0.0126

$\triangleright$ 1 $f = 38$ Hz $\zeta = 0.36$

$\triangleright$ 2 $f = 18$ Hz $\zeta = 0.54$

$\triangleright$ 3 $f = 53$ Hz $\zeta = 0.01$

Mode Created
by Active System

3

3   2 1

4
5
6

Position
2 Loop 1

-1000   -800   -600   -400   -200

Imaginary Axis

0

157

system model.

The locus indicates that the K_G selected for the final dynamometer runs (0.00441) is near optimum (maximum damping) and modifies the torsional mode to a damped natural frequency of approximate 38 Hz (compared to about 32 Hz observed in tests) with a damping ratio of 0.36. The lower frequency mode created by the active system for this value of K_G has a damped natural frequency of 18 Hz (16 Hz observed) with a damping ratio of 0.54. The locus further indicates that the system has a gain margin of slightly greater than 3 and will go unstable at a frequency of approximately 53 Hz. All of these results correlate well with the actual dynamometer test results, particularly considering the degree of simplification associated with the linearized analytical model.

REFERENCES

1.   NACA TM-1365   "Shimmy of a Pneumatic Wheel", B. Von Schlippe, August 1954

2.   NASA TR-R-64   "Mechanical Properties of Pneumatic Tires with Special Reference to Modern Aircraft Tires", R.F. Smiley and W. B. Horne, 1960

3.   318B-7305-008   "T-37 Shimmy Investigation Final Report", Cessna Aircraft Co., 1973